Smouldering to Treat PFAS in Sewage Sludge

T. Fournie[a*], T.L. Rashwan[a,b], C. Switzer[c], J.I. Gerhard[a,‡]

[a] *Department of Civil and Environmental Engineering, Western University, N6A 5B9 London, ON, Canada, tfourni4@uwo.ca, jgerhard@uwo.ca*

[b] *School of Engineering & Innovation, The Open University, Milton Keynes, MK7 6AA, UK [1], tarek.rashwan@open.ac.uk*

[c] *Department of Civil and Environmental Engineering, University of Strathclyde, G1 1XQ Glasgow, UK, christine.switzer@strath.ac.uk*

[1] *Current address*

** Corresponding author*

[‡] *Deceased*

This is a peer reviewed, accepted author manuscript of the following research article: Fournie, T., Rashwan, T. L., Switzer, C., & Gerhard, J. I. (2023). Smouldering to treat PFAS in sewage sludge. *Waste management*, 164, 219-227. https://doi.org/10.1016/j.wasman.2023.04.008

Abstract

Wastewater treatment plants are accumulation points for per- and polyfluoroalkyl substances (PFAS) facilitating treatment. This study explores using smouldering combustion to treat PFAS in sewage sludge. Base case experiments at the laboratory scale (LAB) used dried sludge mixed with sand. High moisture content (MC) LAB tests, 75% MC sludge by mass, explored impacts of MC on treatment and supplemented with granular activated carbon (GAC) to achieve sufficient temperatures for thermal destruction of PFAS. Additional LAB tests explored using calcium oxide (CaO) to support fluorine mineralization. Further tests performed at an oil-drum scale (DRUM) assessed scale on PFAS removal. Pre-treatment sludge and post-treatment ash samples from all tests were analyzed for 12 PFAS (2C-8C). Additional emissions samples were collected from all LAB tests and analyzed for 12 PFAS and hydrogen fluoride.

Smouldering removed all monitored PFAS from DRUM tests, and 4-8 carbon chain length PFAS from LAB tests. For base case tests, PFOS and PFOA were completely removed from sludge; however, high content in the emissions (79-94% of total PFAS by mass) shows volatilization without degradation. Smouldering high MC sludge at ~900 °C (30 g GAC/kg sand) improved PFAS degradation compared to treatment below 800 °C (<20 g GAC/kg sand). Addition of CaO before smouldering reduced PFAS content in emissions by 97-99% by mass; with minimal PFAS retained in the ash and minimal HF production, the fluorine from the PFAS was likely mineralized in the ash. Co-smouldering with CaO had dual benefits of removing PFAS while minimizing other hazardous emission by-products.

Keywords

Smouldering combustion; Sewage sludge; PFAS; Remediation; Wastewater treatment

List of Abbreviations

BDL	Below detection limit
CaF_2	Calcium fluoride
CaO	Calcium oxide
DI	Deionized water
DRUM	Oil-drum reactor scale experiments (0.3 m radius)
GAC	Granular activated carbon
HF	Hydrofluoric acid
H_2SO_4	Sulfuric acid
LAB	Laboratory scale reactor experiments (0.08 m radius)
LC-MS/MS	Liquid chromatography with tandem mass spectrometry
MC	Moisture content
PFAS	Per- and polyfluoroalkyl substances
PFBA	Perfluorobutanoic acid
PFBS	Perfluorobutanesulfonic acid
PFHpA	Perfluoroheptanoic acid
PFHpS	Perfluoroheptanesulfonic acid
PFHxA	Perfluorohexanoic acid
PFHxS	Perfluorohexanesulfonic acid
PFPA	Perfluoropropanoic acid
PFPeA	Perfluoropentanoic acid
PFPeS	Perfluoropentanesulfonic acid
PFOA	Perfluorooctanoic acid

PFOS	Perfluorooctane sulfonate
ppb	Parts per billion
TFA	Trifluoroethylene
TISAB	Total Ionic Strength Adjustment Buffer
USEPA	United States Environmental Protection Agency
WWTP	Wastewater treatment plant

1.0 Introduction

Endocrine disrupting per- and polyfluoroalkyl substances (PFAS) are compounds of concern that accumulate in sewage sludge and other organic environments (Clarke and Smith, 2011). PFAS are a group of thousands of chemicals, with the most common being perfluorooctane sulfonate (PFOS) and perfluorooctanoic acid (PFOA)(Buck et al., 2011). Due to their toxicity and persistence in the environment, both PFOS and PFOA production have been restricted around the world (UNEP, 2019; USEPA, 2020). The properties of PFAS, including chemical and thermal stability, made them useful in a wide range of materials and applications (Kissa, 2001); however, these same properties also make PFAS widespread in the environment and challenging to remediate.

Wastewater treatment plants (WWTPs) are key accumulation points for PFAS, and are therefore valuable opportunities for intervention technologies (Arvaniti et al., 2014, 2012; Gómez-Canela et al., 2012; Moodie et al., 2021; Sindiku et al., 2013; Sun et al., 2011; Venkatesan and Halden, 2013; Yan et al., 2012). Sources of PFAS to WWTPs include industrial discharge (Kunacheva et al., 2011; Washington et al., 2010); landfill leachate (Gallen et al., 2016); and domestic sources (Pan et al., 2010). Since conventional wastewater treatment methods are ineffective at treating PFAS, WWTPs tend to be a sink for these compounds (Ahrens et al., 2009). Additionally, WWTPs are potential sources of PFAS since they can be formed via precursor degradation (Houtz et al., 2018; Lakshminarasimman et al., 2021; Pan et al., 2010; Sepulvado et al., 2011). Within WWTPs, most PFAS tends to be concentrated in sewage sludge (Clarke and Smith, 2011; Milinovic et al., 2016; Zhang et al., 2013). Therefore, sewage sludge management needs to consider the fate of these compounds. Landfilling sewage sludge can result in PFAS entering the environmental via leachate

(Ahrens et al., 2011; Gallen et al., 2016). A common alternative to landfilling sewage sludge is direct land application as a soil amendment. Land applied sludges can be a significant source of PFAS contamination to the environment through surface runoff or infiltration (Sepulvado et al., 2011), or circulation in the environment via plant uptake (Blaine et al., 2013). With increasing regulations, especially for PFOS and PFOA (USEPA, 2021), there is significant interest in developing methods to remove and degrade PFAS from sewage sludge. For example, various thermal treatment methods demonstrate good potential to remove PFAS from sewage sludge though their application is relatively limited. Current thermal methods being explored include pyrolysis (Kim et al., 2015; Kundu et al., 2021), hydrothermal treatments (Yu et al., 2020; Zhang and Liang, 2021), and incineration (Wang et al., 2013). In particular, incineration shows strong potential destroying contaminants present in sewage sludge (Ross et al., 2018), but it is also energy intensive and expensive (Werther and Ogada, 1999). Incineration of dried sludge amended with hydrated lime has been shown to effectively mineralize >70% of fluorine at treatment temperatures >600°C (Wang et al., 2013). While demonstrating a highly effective method of treating PFAS contaminated sludge, the long residence times, and the high sludge to calcium ratio (0.43 g $Ca(OH)_2$: 1 g sludge) may make scaling this treatment method challenging and expensive. Pyrolysis has shown mixed results in its ability to remove PFAS from sewage sludge, with one study finding insignificant reductions in the biochar following pyrolysis (Kim et al., 2015), and another study showing effective removal (>90%) of PFOS and PFOA using pyrolysis at 500°C while sequestering other PFAS in produced biochar by adsorption (Kundu et al., 2021). Similarly, hydrothermal treatments have also shown mixed results in their ability to treat PFAS. One study reported that reductions in PFAAs were often coupled with increases in PFAA

precursors (Zhang and Liang, 2021), while another showed reductions of ~35-45% PFOS and ~100% PFOA from sludge at temperatures between 260-350°C with mobilization to produced biocrude oil noted (Yu et al., 2020). Characterization of gaseous emissions was not included and PFAS may have been present there, too. Also, these studies used spiked rather than native PFAS; results with aged PFAS may be different. Ultrasound (Zhang et al., 2022), and acid-microwave assisted persulfate digestion (Hamid and Li, 2018) have shown to be ineffective to treat PFAS in sewage sludge; however, these studies do provide valuable information that can help advance thermal and other treatment technologies. Overall, more work is needed to advance effective treatment of PFAS in wastewater treatment systems.

Smouldering combustion was recently shown to be an effective method of treating PFAS contaminated soils (Duchesne et al., 2020). Smouldering is a flameless form of burning that occurs on the surface of a fuel within a porous medium (Torero et al., 2020). This exothermic reaction produces heat from the heterogenous oxidation of the fuel (i.e., oxygen directly attacks the fuel surface) (Ohlemiller, 1985). Smouldering has the potential to be self-sustaining with no additional energy input required after ignition if the oxidation reactions release sufficient energy to overcome heat losses (Ohlemiller, 1985). Smouldering combustion has been demonstrated to be an effective, energy efficient remediation strategy for contaminated soils (Gerhard et al., 2020; Grant et al., 2016; Pironi et al., 2009; Scholes et al., 2015; Switzer et al., 2009), wastewater sludges (Rashwan et al., 2016), and faeces (Yermán et al., 2015). In this context, the organic contaminants and/or wastes are the fuel embedded within a soil mixture, and self-sustained smouldering destroys virtually all of it by oxidation; typically, only inert soil grains (e.g., quartz sand) and inorganic ash remain after treatment. To treat PFAS contaminated soil, a supplemental

fuel was added (i.e., granular activated carbon (GAC)) to achieve sufficient temperature for PFAS degradation (~900 °C) (Duchesne et al., 2020). While smouldering sewage sludge has been explored in the context of process optimization (Rashwan et al., 2016), scaling (Feng et al., 2021; Rashwan et al., 2021a), landfilling potential (Feng et al., 2020), resource recovery potential (Fournie et al., 2022a), and the behaviour of dioxins and furans (Fournie et al., 2022b), the fate of PFAS during sewage sludge smouldering is unknown.

The aim of this study is to evaluate the use of smouldering to treat PFAS in sewage sludge. This was done in three phases: (I) evaluating PFAS removal, (II) assessing methods of improving degradation of PFAS, and (III) exploring the impact of scaling on PFAS removal. Phases I and II consisted of a series of laboratory smouldering experiments that evaluated PFAS fate in varied input and operating conditions, including high moisture content sludge, as well as CaO addition, which has been shown to improve PFAS mineralization during thermal treatment of sewage sludge (Wang et al., 2013). Finally, Phase III explored how scale impacts PFAS removal. This work presents the first comprehensive evaluation of PFAS fate during smouldering treatment of sewage sludge.

2.0 Materials and Methods

2.1 Waste collection and preparation:

Sewage sludge was obtained from a wastewater treatment plant in Ontario, Canada. Complete details on wastewater processing and sludge generation at Greenway can be found elsewhere (Fournie et al., 2021; Rashwan et al., 2016). The sewage sludge was produced from a dewatered slurry of primary and secondary sludge and had an average moisture content (MC) of 74.3% on a wet-mass basis, determined using USEPA Method 1684 (Telliard, 2001). All sewage sludge utilized for the LAB tests was collected in a single batch (~40 kg) in April 2021 to minimize variability between tests. Sewage sludge utilized for the DRUM tests was collected in individual batches (~30 kg) immediately ahead of each test. DRUM tests were performed between February and June 2018.

Sewage sludge storage and preparation followed a modified procedure developed by Rashwan et al. (2016). Virgin sewage sludge was batch dried in an oven at 105 °C to achieve a MC of <1%. The samples were dried until there were no measurable changes in sludge mass. To homogenize the material, the dried sludge was pulverized using an immersion blender and sieved to ensure all material was <1 cm. The homogenized, dried sludge was then stored in 19 L sealed containers at 5 °C until use.

Preliminary analysis of sewage sludge samples collected between February and June 2018 showed that concentrations of PFOS ranged from 224 – 2230 ng/g and PFOA was below the detection limit for all samples (Table S1-1, Supplementary Materials, Section S1). The high variability in sewage sludge PFAS concentrations could be due to temporal changes which has

been recently explored (Thompson et al., 2022). The sewage sludge contained similarly high PFOS compared to treatment studies that have spiked their sewage sludge (Hamid and Li, 2018; Yu et al., 2020); therefore, the sewage sludge was used without additional PFAS spiking. Furthermore, not spiking the sludge can improve our understanding of treating PFAS bound within the sludge matrix.

2.2 Smouldering reactor set-up and procedure:

Cylindrical reactors fabricated from stainless steel were used for all laboratory experiments (LAB: 0.08 m radius, 0.008 m^3 volume) and larger scale tests in oil-drum sized reactors (DRUM: 0.3 m radius, 0.27 m^3 volume). The reactors were wrapped in 0.051 m thick insulation (LAB: MinWool®, Johns Manville; DRUM: FyreWrap® Elite® Blanket, Unifrax). The reactor set-up and instrumentation are shown for LAB tests in Figure 1 and DRUM tests in Supplementary Materials, Section S3.

Seven LAB and three DRUM tests were conducted, summarized in Table 1. The LAB tests were separated into two phases. Phase I consisted of three repeat LAB base case tests (I-1, I-2, and I-3) using dried sewage sludge (MC <1%) mixed with silica sand in a ratio of 6.5:1 sand-to-dried sludge (g/g). This ratio is higher than what has been used in previous studies smouldering dried sludge (Fournie et al., 2022a, 2022b; Rashwan et al., 2021a) to increase the fuel loading and therefore the ability to quantify PFAS products in the emissions and post-treatment materials (herein referred to as 'ash'). Phase II consisted of four LAB tests: two with higher MC sludge (75% by mass) combined with GAC (CAS: 7440-44-0, PTI Process Chemicals, 100 mesh size, mean particle size < 0.15 mm) at 20 g GAC/kg sand (II-1-1) and 30 g GAC/kg sand (II-1-2) and two with

CaO (CAS: 1305-788, Carmeuse Lime & Stone) (II-2-1: 5 g CaO/kg sand; II-2-2: 10 g CaO/kg sand). In the high MC tests, sludge was combined with sand in a ratio of 4.5:1 sand-to-sludge (g/g) on a wet-mass basis and GAC was added to these higher MC tests to achieve smouldering temperatures >900 °C by supplementing the low calorific value sludge. These concentrations were chosen based on previous research involving PFAS-contaminated soils (Duchesne et al., 2020). The other two tests were similar to the base case, 6.5:1 sand-to-dried sludge, with the addition of CaO to react with the PFAS in the sludge and mineralize fluorine at treatment temperatures <900 °C (Wang et al., 2015, 2013). Concentrations were selected to explore how CaO content impacted mineralization without significantly reducing the fuel bed permeability, which can deteriorate smouldering performance (Wang et al., 2021). Phase III consisted of three DRUM tests, the first with dried sludge (III-1), and the other two with high MC sludge (III-2: 72.3% by mass; III-3: 74.4% by mass). The sand-to-sludge ratios for III-1 and III-2 were 6.5:1, and III-3 was 4.5:1, all on a wet-mass basis. No CaO or GAC was added for these tests.

Sludge was mechanically mixed with coarse silica sand (CAS: 14808-60-7, 1.18 ≤ mean grain diameter ≤ 2.36 mm, WP #2, K & E) to achieve the target sand-to-sludge ratio (Table 1), and create a smoulderable mixture (Rashwan et al., 2016). For the higher MC LAB tests (II-1-1 and II-1-2), water was added to the dried sludge and sand to reconstitute the sludge back to 75% MC following a method developed by (Rashwan et al., 2016). For the higher MC DRUM tests (III-2 and III-3), sludge was collected just prior to experimentation and, therefore, did not require any drying or rewetting prior to treatment. A clean sand cap (~5-10 cm thick) was added on top of the fuel bed to lower the exiting temperatures when the smouldering front approached the top of the reactor.

Reactors were placed on load cells (LAB: KCC150, Metler Toledo; DRUM: KD1500, Mettler Toledo) to measure each experiment's fuel destruction rate. Thermocouples (LAB: Type K, 0.0032 m diameter, Omega Ltd; DRUM: Type K, 0.0064 m diameter; Kelvin Technologies) were installed along the full height of the reactors to record process temperatures throughout each test. For the LAB tests, centreline (8 cm) and half-radius (5 cm) thermocouples were installed to better understand the temperature evolutions throughout the reactor, which has shown to vary more significantly at smaller scales (Rashwan et al., 2021b).

The DRUM test set-up and procedure using convective ignition is described in detail elsewhere (Fournie et al., 2022a, 2022b; Rashwan, 2020; Rashwan et al., 2021c) and can be found in Supplementary Materials, Section S3. The LAB test set-up and procedure using conductive ignition followed established methods (Duchesne et al., 2020; Rashwan et al., 2016), and is described briefly below (Figure 1).

The LAB reactor was ignited using a coiled resistive heater (450 W, 120 V, Watlow Ltd.), with no air flow. When the first thermocouple reached 200 °C, air was injected into the reactor base at a Darcy flux of 5.0 cm/s – via a mass flux controller (FMA5400/5500 Series, Omega Ltd.) – for the remainder of the test until the fuel bed cooled to ambient temperature. Smouldering was confirmed when the first thermocouple within the fuel bed peaked (3.5 cm from the base). The heater was then turned off and the airflow supported the self-sustaining smouldering propagation. The end of each experiment was identified when the smouldering front reached the end of the fuel bed.

2.3 Emissions and sample collection:

For every experiment, rigorous cleaning procedures were conducted based on (Duchesne et al., 2020). Ahead of each experiment, all glassware and tubing used in the emissions sampling train and sample bottles were rinsed three times with deionized (DI) water, isopropanol (CAS 67-63-0, Fisher Chemical), and methanol (CAS 67-56-1, Fisher Chemical).

During experiments, an NDIR infrared gas analyzer measured oxygen, carbon dioxide, and carbon monoxide data from the LAB tests every two seconds (Model: 7500ZA, Teledyne Analytical Instruments). Two emissions sampling trains (Figure 1) were used in the LAB tests to subsample the emissions exiting the reactor for (1) PFAS and (2) hydrofluoric acid (HF). The PFAS sampling train was adapted from (Duchesne et al., 2020), and the HF sampling train from EPA Method 26 (2019). These methods have been shown to effectively collect PFAS and HF in emissions from LAB smouldering tests (Duchesne et al., 2020). Each PFAS emissions sample was collected using a vacuum pump (DOA-P704-AA, Gast) pulling sample at ~3 L/min. The emissions passed through two sorption tubes containing 50 g GAC aligned in series to prevent PFAS breakthrough and topped with 1 – 3 g glass wool to secure the GAC. The HF emissions sample was similarly collected using a vacuum pump pulling sample at ~3 L/min. Emissions from the HF train passed through 4 glass impingers within an ice bath (4.0 °C). Impingers 1 and 4 were empty and impingers 2 and 3 contained 15 mL of 1% H_2SO_4. The total volume of emissions sample collected from each sampling train were quantified using flow totalizers (PFAS train: FMA6616 Series, Omega Ltd.; HF train: FMA4316 Series, Omega Ltd.). More details on emissions sampling can be found in Supplementary Materials, Section S2. Leakage of ambient air into each sampling train was quantified and minimized to <5% (see Supplementary Materials, Section S2 for procedure).

Following emissions capture, GAC from each sorption tube was collected in full and stored in PFAS free polypropylene bottles (VWR®). Additional PFAS samples included the glass wool, tubing rinse, and sorption tube rinses. The liquid from (1) the first and second impingers, and (2) the third and fourth impingers were combined into two HF samples. The tubing ahead of the HF emissions sampling train was rinsed using DI water and the rinse was also collected for analysis.

Representative samples of 100-200 g of post-treatment material (i.e., ash mixed with sand) were collected from three locations within the reactor, the sand cap (~38 – 48 cm from reactor base), the top of the fuel bed (~27 – 31 cm from reactor base), and the bottom of the fuel bed (~13 – 20 cm from reactor base) (see Supplementary Materials, Section S2 for sample photos). Samples were stored in 250 mL jars at 5 °C. Since samples collected at the top and bottom of the fuel bed had similar concentrations, these values were averaged to approximate the concentration in the fuel bed following smouldering treatment (herein referred to as 'ash'). The concentrations in the sand cap were presented separately (Supplementary Materials, Section S5).

2.4 Emissions and Solids Analyses

Solid samples were extracted with basic methanol (0.1% ammonium hydroxide (CAS: 1336-21-6, Fisher Scientific) v/v) using 5:1 extractant-to-sample (g/g). Samples were vortexed for 30 seconds, then placed on a shaker table at 30 RPM for 48 hours. Samples were then centrifuged at 4000 RPM for 10 minutes, and a sub-sample transferred to a PFAS-free HPLC vial for analysis.

All PFAS analyses were conducted by the Environmental Sciences Group at the Royal Military College of Canada. These analyses were completed following a modified EPA 8327 method using liquid chromatography with tandem mass spectrometry (LC-MS/MS). Full details on the analyses,

including quality assurance and quality control can be found in Supplementary Materials, Section S4.

The HF collected in the impinger liquids were analyzed using an ion probe (HQ30d-flexi, Hach). The analysis followed EPA Method 9214 (1996). Briefly, the probe was calibrated using standards between 0.5 – 2 mg/L (BDH Chemicals, VWR®). Samples were prepared with 1:1 (v/v) sample-to-TISAB solution (Supelco, Sigma Aldrich) to neutralize the sample. Samples were analyzed in triplicates and an internal standard was run between each sample.

A combination of X-ray diffractometer (XRD) analysis and Scanning electron microscopy with energy dispersive X-ray spectroscopy (SEM/EDX) analysis were performed on the post-treatment ash from I-1, II-2-1, II-2-2, and III-1 tests to evaluate the use of CaO to mineralize fluorine from the sludge. These analyses were performed by Surface Science Western using a Rigaku SmartLab XRD, and a Hitachi SU8230 Regulus Ultra High-Resolution Field Emission SEM. Full specifications of the instrumentation and operating conditions can be found in the Supplementary Materials, Section S9.

3.0 Results and Discussion

3.1. Overview of smouldering experiments

Smouldering destroyed more than 90% of the initial sludge biomass under all experimental conditions, leaving <10% as residual inorganic ash in the reactor. Peak temperatures ranged between 700 – 926 °C in LAB tests and 461 – 550 °C in DRUM tests (Table 1).

Smouldering of dry sewage sludge in base case tests had an average peak centreline temperature of 808 °C ± 65 °C and average propagation velocity of 0.44 ± 0.13 cm/min (Table 1). The base case tests had the most consistent temperature distributions across the radius of the reactor (Supplementary Materials, Section S2). Higher MC is a source of heat losses that typically reduces peak temperatures in the reactor (Fournie et al., 2022a; Rashwan et al., 2021a). These heat losses were offset by the addition of 20 g/kg GAC (centreline: 746 °C ± 21 °C) and exceeded by the addition of 30g/kg GAC (centreline: 905 °C ± 21 °C) (Phase II; Table 1). Both high MC/GAC tests had similar average propagation velocities (II-1-1: 0.52 ± 0.13 cm/min; II-1-2: 0.50 ± 0.09 cm/min). This aligns with previous research exploring the relationship between GAC content and smouldering temperature (Duchesne et al., 2020). The temperature profiles, sampling times, and heating rates can be found in the Supplementary Materials, Section S2 for LAB tests, and Section S3 for DRUM tests.

Addition of CaO at 5 and 10 g/kg did not alter the smouldering temperature, which remained consistent with base case tests, but it did impact the propagation velocities (Table 1) and heating rates of the tests (Supplementary Materials, Section S2). Increasing the CaO content in the fuel mixture reduced the propagation velocity from 0.53 ± 0.11 cm/min with 5 g CaO/kg sand to 0.30

± 0.14 cm/min with 10 g CaO/kg sand. Additionally, both CaO tests had slower heating rates than all other tests, consistently lower than 125 °C/min (Supplementary Materials, Section S2). In comparison, the base case and high MC/GAC tests had heating rates between 125 – 300 °C/min. The lower heating rates were likely driven by physical and chemical processes. The addition of CaO may have reduced the permeability of the fuel mixture. Reductions in permeability have been shown to slow the propagation velocity of smouldering; however, they should not impact robustness (Wang et al., 2021). Furthermore, although the system is net exothermic, some aspect of the fluorine mineralization may require energy input. The presence of these additional processes may have slowed energy transfer to adjacent fuel in the system resulting in decreased heating rates during these tests.

The DRUM scale tests (Phase III) had lower treatment temperatures and slower propagation velocities than were observed in any of the LAB tests. The dry sludge DRUM test, III-1, had average peak centreline temperatures between 534 – 550 °C (Table 1). The two higher MC DRUM tests (i.e., III-2 and III-3) had average peak centreline temperatures between 461 – 477 °C reflecting the additional energy to vaporize water ahead of smouldering.

For the LAB tests, the average peak half-radius temperatures varied, sometimes significantly, from the average peak centreline temperatures. These differences in temperatures across the radius of the reactor have important implications for treating PFAS since high temperatures (>900 °C) are required for effective degradation of these compounds (Duchesne et al., 2020; Mahinroosta and Senevirathna, 2020). Temperature gradients will likely not influence the removal of PFAS from the ash since it has been shown previously that PFAS volatilize at low

temperatures, <400 °C (Crownover et al., 2019; Winchell et al., 2021). However, temperature gradients will impact degradation, resulting in longer chain compounds in the emissions that would still need to be treated. The temperature differences across the reactor are likely due to a combination of heterogeneities in the fuel mixtures and heat losses (Rashwan et al., 2021b). Smouldering sludge at a larger scale – closer to what could be implemented at a WWTP – could minimize these heat losses and foster more persistent high temperature regions (Rashwan et al., 2021b), and thereby improve treatment.

3.2. PFAS in virgin sludge and post-treatment solids

Figure 2 outlines the initial concentrations of 12 PFAS in the sewage sludge prior to smouldering compared to the post-treatment ashes from both LAB and DRUM tests. For all tests, there was complete removal of >3C PFAS from the solids.

3.2.1. LAB Experiments (Phase I and Phase II)

In the base case and high MC/GAC tests, TFA (2C) was the primary compound measured in the ash. Traces of PFPA (3C) were also measured in the ash from one of the base case tests, I-2 (Supplementary Materials, Section S5). Increases of TFA were measured in the ash during the base case tests (3.1 – 15 ng/g-dry sludge) compared to what was originally present in the dried sludge (0.0 – 8.9 ng/g-dry sludge), which suggests some degradation of larger PFAS during smouldering. Some retention of PFAS, primarily TFA, PFPA, and/or PFHpS, was observed in the sand cap, likely due to re-condensation (1.6 – 53 ng/g-dry sludge; Supplementary Materials, Section S5). The high MC tests had the lowest relative temperatures (Supplementary Materials, Section S2) and highest PFAS retentions in the sand cap (II-1-1: 190 ng/g-dry sludge; II-1-2: 110 ng/g-dry sludge). The presence of only TFA in the sand cap of higher GAC test compared to a distribution of TFA (2C), PFPA (3C), and PFHpS (7C) in the lower GAC test suggests that the higher temperature/energy smouldering improved degradation of PFAS, breaking down the larger chains into smaller compounds. This same result was found for smouldering PFAS contaminated soils (Duchesne et al., 2020). Understanding the smouldering conditions under which significant PFAS degradation is possible for higher moisture content sludge is important because treating

87 higher moisture content sludge can help reduce energy requirements for dewatering at
88 wastewater treatment plants.

89 Similar to the high MC/GAC tests, both CaO tests only had retention of TFA in the ash (II-2-1: 8.9
90 ng/g-dry sludge; II-2-2: 19 ng/g-dry sludge). In addition to TFA, the top sand cap from both CaO
91 tests contained PFCA (Supplementary Materials, Section S5). The top sand cap retained more
92 total PFAS than remained in the ash for both CaO tests (II-2-1: 47 ng/g-dry sludge; II-2-2: 29 ng/g-
93 dry sludge), likely reflecting recondensation of PFAS in the top sand cap.

94 3.2.2. DRUM Experiments (Phase III)

95 While the LAB tests had some retention of short-chained PFAS in the ash, primarily TFA, the
96 DRUM tests had complete removal of all PFAS from the ash (Figure 2). The removal was
97 irrespective of the initial PFAS content in the sludge, which varied between sludge batches
98 collected for each DRUM test (Figure 2). The DRUM tests had lower smouldering front
99 propagation velocities than the LAB tests (Table 1). The slower front movement means that every
100 location was exposed to elevated treatment temperatures for longer times, which likely
101 facilitated complete removal of all PFAS from the solids. This presents an advantage of
102 smouldering over other thermal treatment methods for removing PFAS. Smouldering is able to
103 remove and potentially destroy PFAS as the smouldering front propagates through the fuel bed,
104 as opposed to long residence times which have been required in other studies that do not
105 typically destroy all PFAS (Hamid and Li, 2018; Wang et al., 2013; Yu et al., 2020; Zhang et al.,
106 2022; Zhang and Liang, 2021).

107

3.3. PFAS in emissions

Figure 3 outlines the initial contents of 12 PFAS in the sewage sludge prior to smouldering compared to the content measured in the emissions from the LAB tests.

The emissions from the base case tests contained primarily PFOS (4.8 – 440 ng/g-dry sludge) and PFOA (23 – 73 ng/g-dry sludge), both 8C. With complete removal of PFOS from the ash and only somewhat lower PFOS in the emissions compared to the initial content in the sludge (52 – 907 ng/g-dry sludge), the higher PFOS in the emissions suggests release into the emissions without much degradation. Emissions under base case smouldering conditions would require further treatment for PFAS. Since low quantities of PFOA were originally present in the sewage sludge (0.13 – 0.79 ng/g-dry sludge), its elevated presence in the emissions is evidence of formation during smouldering, possibly through precursors (Zhang and Liang, 2021). Precursor formation of PFOS is also possible and could be another explanation for some of the elevated content in the emissions. Future work could explore PFAS degradation and formation during smouldering.

Both higher MC/GAC tests had similar total PFAS in the emissions (II-1-1: 490 ng/g-dry sludge; II-1-2: 470 ng/g-dry sludge) but the compounds differed. Of the PFAS analyzed, II-1-1 contained primarily PFOS (430 ng/g-dry sludge; 88%) while II-1-2 comprised primarily TFA (340 ng/g-dry sludge; 72%), suggesting improved degradation with higher treatment temperatures.

The total PFAS content in the emissions from the CaO tests was significantly lower than all other tests (II-2-1: 15 ng/g-dry sludge; II-2-2: 10 ng/g-dry sludge). The treatment temperatures observed during both CaO tests (centreline: 760 – 880 °C; half-radius: 670 – 810 °C) were likely sufficient to support mineralization of fluorine from PFAS in the presence of adequate calcium

(Wang et al., 2013). The primary PFAS found in the emissions following the CaO tests was TFA (II-2-1: 8.9 ng/g-dry sludge; II-2-2: 7.7 ng/g-dry sludge). The presence of calcium to mineralize fluorine from PFAS has been shown to prevent the release of short and longer-chained PFAS (>3C) in emissions (Wang et al., 2013) and reduces the production of secondary fluorinated compounds (Riedel et al., 2021). Higher concentration of CaO (10 g CaO/kg sand) reduced the total PFAS content in the emissions by 33% (relative to 5 g CaO/kg sand). In particular, PFOS was not detected in the emissions.

With DRUM tests achieving treatment temperatures between 460 – 550 °C (Table 1), we hypothesize that most of the PFAS originally present in the sludge was released in the emissions with minimal degradation, similar to the LAB base case tests (I-1, I-2, & I-3) and lower concentration GAC test (II-1-1). The only other semi-pilot scale study assessing PFAS treatment of sewage sludge also found near complete removal of PFAS from the bottom solids via pyrolysis (Zhang and Liang, 2021). Future work could examine the PFAS emissions by-products from smouldering sludge at larger scales and work to optimize treatment via operating conditions and amendments (e.g., GAC and/or CaO).

3.4. Defluorination

Minimal HF was measured in the emissions during the base case tests (1500 – 3800 ng HF/g-dry sludge) and the lower GAC test (II-2-1: 608 ng HF/g-dry sludge) (Figure 4). The lower relative temperatures (724 – 860 °C), slower heating rates, and lower propagation velocities likely supported release of longer chained PFAS in the emissions (Figure 3) rather than destroying these compounds.

The higher GAC test had the highest production of HF (II-1-2: 43000 ng HF/g-dry sludge), further evidence of improved degradation during the higher energy/temperature smouldering. Moreover, the faster heating rates (Supplementary Materials, Section S2) and smouldering propagation (Table 1) may reduce the time for the PFAS to volatilize ahead of being oxidized by the smouldering front. A faster heating rate may also be favourable to improve degradation when thermal destruction alone is used. Future work could explore the role of heating rates on PFAS destruction via smouldering.

Based on low HF emissions (3100 – 5800 ng HF/g-dry sludge) and low PFAS in emissions (10 – 15 ng/g-dry sludge), ash (8.9 – 19 ng/g-dry sludge), and sand cap (27 – 47 ng/g-dry sludge), smouldering with CaO likely mineralized some of the fluorine with the calcium, forming new compounds that remained sequestered in the ash. This potential mineralization required significantly less calcium amendment (0.005 – 0.01 g CaO : 1 g sludge for this study) than other studies using calcium amendments (i.e., 0.43 g $Ca(OH)_2$: 1 g sludge (Wang et al., 2013), and 0.037 g $Ca(OH)_2$: 1 g sludge (Zhang and Liang, 2021)). Lower calcium requirements make scaling the process more economically viable. Both elemental and mineral analyses were conducted

(Supplementary Materials, Section S9); however, the concentrations of fluorine and fluorine containing minerals were below the instrument detection limits, likely due to the low quantity relative to other constituents in the sewage sludge. More work is needed to understand the fate of fluorine during sewage sludge smouldering and how to optimize treatment, particularly mineralization of fluorine, with calcium amendment and/or GAC. Smouldering offers key process advantages, effectively treating high MC sludge at lower treatment temperatures (Rashwan et al, 2016; Fournie et al, 2021), while fluorine mineralization has been observed at temperatures as low as 400 °C (Wang et al., 2015, 2013).

4.0 Conclusion

Smouldering combustion can be used to treat PFAS effectively in high moisture content (MC) sewage sludge with complete removal of PFAS compounds 4C – 8C. The most effective treatment of PFAS-laden sewage sludge involved the use of calcium oxide (CaO) to sequester fluorine in the resulting ash. Addition of 5 – 10 mg CaO per kg of dried sludge ahead of smouldering treatment achieved complete removal of PFAS 4C – 8C without significant PFAS or HF release in emissions. The low ratio of CaO to fuel used in this study makes scaling the process more economically viable and further optimization is likely possible. In contrast, smouldering of sludge bulked with only sand volatilized most of the PFAS. Some PFAS recondensed downstream in cooler regions in the reactor and the rest released via emissions. Supplementing the sludge and sand mixture with higher calorific value fuel (30 g GAC / kg sand) increased the energy of the system, fostering peak temperatures of ~900 °C, and improved PFAS degradation. Other high calorific value fuels such as wood chips could achieve similar conditions. While higher energy smouldering supports thermal degradation of PFAS, it also generates HF emissions, which require further treatment. In contrast, CaO addition achieved similar PFAS 4C – 8C degradation at temperatures between 670 – 880 °C, which were lower than required to degrade PFAS by other thermal treatments and avoided HF production. Smouldering with calcium amendment had the dual benefits of removing PFAS without producing other hazardous emission by-products. Overall, smouldering is a promising, lower energy alternative for treating PFAS in sewage sludge, even considering high MC sludge. The improved treatment at increasing scale demonstrates high potential for full-scale implementation at WWTPs.

This research explored the mineral phases formed in the ash with calcium and fluorine when a calcium amendment was added to sewage sludge. As the concentrations of fluorine and fluorine containing compounds were below detection limits of the methods used, the ultimate fluorine fate after sewage sludge smouldering is still uncertain. Future work could seek to address this question. Other areas for further investigation include optimizing smouldering treatment of PFAS-laden sewage sludge with calcium amendments, including high MC sludges, and investigating the long-term stability of mineralized fluorine sequestered in residual ash. Based on the process improvements noted in this work, calcium amendment may also be beneficial to explore in other sewage treatment processes for PFAS.

5.0 Acknowledgements

Funding was provided by the Ontario Ministry of Research, Innovation and Science; the Government of Canada through the Federal Economic Development Agency for Southern Ontario through the Ontario Water Consortium's Advancing Water Technologies Program (Grant SUB02392) with in-kind support from: 1) the Ontario Ministry of the Environment, Conservation and Parks and 2) Savron, a wholly owned subdivision of Geosyntec Consultants Ltd; and the Natural Sciences and Engineering Research Council of Canada (Postgraduate Scholarships-Doctoral [PGS D 3 - 535379 – 2019 and PGSD 3 - 489978 – 2016] and Grant Nos. CREATE 449311-14, RGPIN 2018-06464, and RGPAS-2018-522602), the Government of Ontario (Ontario Graduate Scholarship 2018), and the Water Environment Association of Ontario's Residuals and Biosolids Research Fund Award (2018 and 2019). The identification and quantification of the PFAS were performed in collaboration with the Royal Military College, Environmental Science Group in Kingston, Ontario, with analyses performed by David Patch. We gratefully acknowledge the assistance and valuable input of Alex Duchesne and Brian Harrison in creating the PFAS and HF glass sampling train, experimental set-up and procedure, experimental set-up and sampling assistance provided by Anna Duong and Madeleine Hooper, HF probe assistance provided by Natalie Connors, London Ontario's Greenway Wastewater Treatment Centre (especially from Chris McKenzie), and additional project support from Gudgeon Thermfire International (especially from Justin Barfett and Randy Adamski), Jiahao Wang, Gillian Wilton, Cody Murray, Megan Green, Dr. Marco Zanoni, Joshua Brown, Brendan Evers, Thomas Mathias, Dillon McIntyre, Jordan Teeple, Jad Choujaa, Maxwell Servos, Reid Clementino, Kia Barrow, Nick Rogowski, and Christopher Kwan.

Supplementary Materials

Supplementary data associated with this article can be found online at:

5.0 References

Ahrens, L., Felizeter, S., Sturm, R., Xie, Z., Ebinghaus, R., 2009. Polyfluorinated compounds in waste water treatment plant effluents and surface waters along the River Elbe, Germany. Mar. Pollut. Bull. 58, 1326–1333. https://doi.org/10.1016/j.marpolbul.2009.04.028

Ahrens, L., Shoeib, M., Harner, T., Lee, S.C., Guo, R., Reiner, E.J., 2011. Wastewater treatment plant and landfills as sources of polyfluoroalkyl compounds to the atmosphere. Environ. Sci. Technol. 45, 8098–8105. https://doi.org/10.1021/es1036173

Arvaniti, O.S., Andersen, H.R., Thomaidis, N.S., Stasinakis, A.S., 2014. Sorption of Perfluorinated Compounds onto different types of sewage sludge and assessment of its importance during wastewater treatment. Chemosphere 111, 405–411. https://doi.org/10.1016/j.chemosphere.2014.03.087

Arvaniti, O.S., Ventouri, E.I., Stasinakis, A.S., Thomaidis, N.S., 2012. Occurrence of different classes of perfluorinated compounds in Greek wastewater treatment plants and determination of their solid-water distribution coefficients. J. Hazard. Mater. 239–240, 24–31. https://doi.org/10.1016/j.jhazmat.2012.02.015

Blaine, A.C., Rich, C.D., Hundal, L.S., Lau, C., Mills, M.A., Harris, K.M., Higgins, C.P., 2013. Uptake of perfluoroalkyl acids into edible crops via land applied biosolids: Field and greenhouse studies. Environ. Sci. Technol. 47, 14062–14069. https://doi.org/10.1021/es403094q

Buck, R.C., Franklin, J., Berger, U., Conder, J.M., Cousins, I.T., Voogt, P. De, Jensen, A.A., Kannan, K., Mabury, S.A., van Leeuwen, S.P.J., 2011. Perfluoroalkyl and polyfluoroalkyl substances

296 in the environment: Terminology, classification, and origins. Integr. Environ. Assess.
297 Manag. 7, 513–541. https://doi.org/10.1002/IEAM.258

298 Clarke, B.O., Smith, S.R., 2011. Review of 'emerging' organic contaminants in biosolids and
299 assessment of international research priorities for the agricultural use of biosolids.
300 Environ. Int. 37, 226–247. https://doi.org/10.1016/J.ENVINT.2010.06.004

301 Crownover, E., Oberle, D., Kluger, M., Heron, G., 2019. Perfluoroalkyl and polyfluoroalkyl
302 substances thermal desorption evaluation. Remediat. J. 29, 77–81.
303 https://doi.org/10.1002/REM.21623

304 Duchesne, A.L., Brown, J.K., Patch, D.J., Major, D., Weber, K.P., Gerhard, J.I., 2020. Remediation
305 of PFAS-Contaminated Soil and Granular Activated Carbon by Smoldering Combustion.
306 Environ. Sci. Technol. 54, 12631–12640. https://doi.org/10.1021/acs.est.0c03058

307 Feng, C., Cheng, M., Gao, X., Qiao, Y., Xu, M., 2020. Occurrence forms and leachability of
308 inorganic species in ash residues from self-sustaining smouldering combustion of sewage
309 sludge. Proc. Combust. Inst. 000, 1–8. https://doi.org/10.1016/j.proci.2020.06.008

310 Feng, C., Huang, J., Yang, C., Li, C., Luo, X., Gao, X., Qiao, Y., 2021. Smouldering combustion of
311 sewage sludge: Volumetric scale-up, product characterization, and economic analysis. Fuel
312 305, 121485. https://doi.org/10.1016/J.FUEL.2021.121485

313 Fournie, T., Rashwan, T.L., Switzer, C., Gerhard, J.I., 2022a. Phosphorus recovery and reuse
314 potential from smouldered sewage sludge ash. Waste Manag. 137, 241–252.
315 https://doi.org/10.1016/J.WASMAN.2021.11.001

316 Fournie, T., Rashwan, T.L., Switzer, C., Grant, G.P., Gerhard, J.I., 2022b. Exploring PCDD/Fs and
317 potentially toxic elements in sewage sludge during smouldering treatment. J. Environ.
318 Manage. 317, 115384. https://doi.org/10.1016/J.JENVMAN.2022.115384

319 Fournie, T., Switzer, C., Gerhard, J.I., 2021. USEPA LEAF methods for characterizing phosphorus
320 and potentially toxic elements in raw and thermally treated sewage sludge. Chemosphere
321 275, 130081. https://doi.org/10.1016/j.chemosphere.2021.130081

322 Gallen, C., Drage, D., Kaserzon, S., Baduel, C., Gallen, M., Banks, A., Broomhall, S., Mueller, J.F.,
323 2016. Occurrence and distribution of brominated flame retardants and perfluoroalkyl
324 substances in Australian landfill leachate and biosolids. J. Hazard. Mater. 312, 55–64.
325 https://doi.org/10.1016/J.JHAZMAT.2016.03.031

326 Gerhard, J.., Grant, G.P., Torero, J.L., 2020. STAR: A Uniquely Sustainable In Situ and Ex Situ
327 Remediation Process, in: Sustainable Remediation of Contaminated Soil and Groundwater:
328 Materials, Processes, and Assessment. Butterworth-Heinemann, pp. 221–245.

329 Gómez-Canela, C., Barth, J.A.C., Lacorte, S., 2012. Occurrence and fate of perfluorinated
330 compounds in sewage sludge from Spain and Germany. Environ. Sci. Pollut. Res. 19, 4109–
331 4119. https://doi.org/10.1007/s11356-012-1078-7

332 Grant, G.P., Major, D., Scholes, G.C., Horst, J., Hill, S., Klemmer, M.R., Couch, J.N., 2016.
333 Smoldering Combustion (STAR) for the Treatment of Contaminated Soils: Examining
334 Limitations and Defining Success. Remediat. J. 26, 27–51.
335 https://doi.org/10.1002/rem.21468

Hamid, H., Li, L.Y., 2018. Fate of perfluorooctanoic acid (PFOA) in sewage sludge during microwave-assisted persulfate oxidation treatment. Environ. Sci. Pollut. Res. 25, 10126–10134. https://doi.org/10.1007/s11356-018-1576-3

Houtz, E., Wang, M., Park, J.S., 2018. Identification and Fate of Aqueous Film Forming Foam Derived Per- and Polyfluoroalkyl Substances in a Wastewater Treatment Plant. Environ. Sci. Technol. 52, 13212–13221. https://doi.org/10.1021/acs.est.8b04028

Kim, J.H., Ok, Y.S., Choi, G.H., Park, B.J., 2015. Residual perfluorochemicals in the biochar from sewage sludge. Chemosphere 134, 435–437. https://doi.org/10.1016/j.chemosphere.2015.05.012

Kissa, E., 2001. Fluorinated surfactants and repellents, Vol. 97. ed. CRC Press.

Kunacheva, C., Tanaka, S., Fujii, S., Boontanon, S.K., Musirat, C., Wongwattana, T., Shivakoti, B.R., 2011. Mass flows of perfluorinated compounds (PFCs) in central wastewater treatment plants of industrial zones in Thailand. Chemosphere 83, 737–744. https://doi.org/10.1016/J.CHEMOSPHERE.2011.02.059

Kundu, S., Patel, S., Halder, P., Patel, T., Hedayati Marzbali, M., Pramanik, B.K., Paz-Ferreiro, J., De Figueiredo, C.C., Bergmann, D., Surapaneni, A., Megharaj, M., Shah, K., 2021. Removal of PFASs from biosolids using a semi-pilot scale pyrolysis reactor and the application of biosolids derived biochar for the removal of PFASs from contaminated water. Environ. Sci. Water Res. Technol. 7, 638–649. https://doi.org/10.1039/d0ew00763c

Lakshminarasimman, N., Gewurtz, S.B., Parker, W.J., Smyth, S.A., 2021. Removal and formation

of perfluoroalkyl substances in Canadian sludge treatment systems – A mass balance approach. Sci. Total Environ. 754. https://doi.org/10.1016/j.scitotenv.2020.142431

Mahinroosta, R., Senevirathna, L., 2020. A review of the emerging treatment technologies for PFAS contaminated soils. J. Environ. Manage. https://doi.org/10.1016/j.jenvman.2019.109896

Milinovic, J., Lacorte, S., Rigol, A., Vidal, M., 2016. Sorption of perfluoroalkyl substances in sewage sludge. Environ. Sci. Pollut. Res. 23, 8339–8348. https://doi.org/10.1007/s11356-015-6019-9

Moodie, D., Coggan, T., Berry, K., Kolobaric, A., Fernandes, M., Lee, E., Reichman, S., Nugegoda, D., Clarke, B.O., 2021. Legacy and emerging per- and polyfluoroalkyl substances (PFASs) in Australian biosolids. Chemosphere 270, 129143. https://doi.org/10.1016/J.CHEMOSPHERE.2020.129143

Ohlemiller, T.J., 1985. Modeling of smoldering combustion propagation. Prog. Energy Combust. Sci. 11, 277–310. https://doi.org/10.1016/0360-1285(85)90004-8

Pan, Y., Shi, Y., Wang, J., Cai, Y., 2010. Evaluation of perfluorinated compounds in seven wastewater treatment plants in Beijing urban areas. Sci. China Chem. 2011 543 54, 552–558. https://doi.org/10.1007/S11426-010-4093-X

Pironi, P., Switzer, C., Rein, G., Fuentes, A., Gerhard, J.I., Torero, J.L., 2009. Small-scale forward smouldering experiments for remediation of coal tar in inert media. Proc. Combust. Inst. 32 II, 1957–1964. https://doi.org/10.1016/j.proci.2008.06.184

376 Rashwan, T., 2020. Sustainable Smouldering for Waste-to-Energy: Scale, Heat Losses, and
377 Energy Efficiency. Electron. Thesis Diss. Repos.

378 Rashwan, T.L., Fournie, T., Torero, J.L., Grant, G.P., Gerhard, J.I., 2021a. Scaling up self-sustained
379 smouldering of sewage sludge for waste-to-energy. Waste Manag. 135, 298–308.
380 https://doi.org/10.1016/J.WASMAN.2021.09.004

381 Rashwan, T.L., Gerhard, J.I., Grant, G.P., 2016. Application of self-sustaining smouldering
382 combustion for the destruction of wastewater biosolids. Waste Manag. 50, 201–212.
383 https://doi.org/10.1016/j.wasman.2016.01.037

384 Rashwan, T.L., Torero, J.L., Gerhard, J.I., 2021b. The improved energy efficiency of applied
385 smouldering systems with increasing scale. Int. J. Heat Mass Transf. 177, 121548.
386 https://doi.org/10.1016/J.IJHEATMASSTRANSFER.2021.121548

387 Rashwan, T.L., Torero, J.L., Gerhard, J.I., 2021c. Heat losses in a smouldering system: The key
388 role of non-uniform air flux. Combust. Flame 227, 309–321.
389 https://doi.org/10.1016/j.combustflame.2020.12.050

390 Riedel, T.P., Wallace, M.A.G., Shields, E.P., Ryan, J. V., Lee, C.W., Linak, W.P., 2021. Low
391 temperature thermal treatment of gas-phase fluorotelomer alcohols by calcium oxide.
392 Chemosphere 272, 129859. https://doi.org/10.1016/J.CHEMOSPHERE.2021.129859

393 Ross, I., Mcdonough, J., Miles, J., Storch, P., Kochunarayanan, P.T., Kalve, E., Hurst, J., Dasgupta,
394 S.S., Burdick, J., 2018. A review of emerging technologies for remediation of PFASs.
395 Remediation 28, 101–126. https://doi.org/10.1002/rem.21553

Scholes, G.C., Gerhard, J.I., Grant, G.P., Major, D.W., Vidumsky, J.E., Switzer, C., Torero, J.L., 2015. Smoldering Remediation of Coal-Tar-Contaminated Soil: Pilot Field Tests of STAR. Environ. Sci. Technol. 49, 14334–14342. https://doi.org/10.1021/ACS.EST.5B03177

Sepulvado, J.G., Blaine, A.C., Hundal, L.S., Higgins, C.P., 2011. Occurrence and fate of perfluorochemicals in soil following the land application of municipal biosolids. Environ. Sci. Technol. 45, 8106–8112. https://doi.org/10.1021/es103903d

Sindiku, O., Orata, F., Weber, R., Osibanjo, O., 2013. Per- and polyfluoroalkyl substances in selected sewage sludge in Nigeria. Chemosphere 92, 329–335. https://doi.org/10.1016/j.chemosphere.2013.04.010

Sun, H., Gerecke, A.C., Giger, W., Alder, A.C., 2011. Long-chain perfluorinated chemicals in digested sewage sludges in Switzerland. Environ. Pollut. 159, 654–662. https://doi.org/10.1016/j.envpol.2010.09.020

Switzer, C., Pironi, P., Gerhard, J.I., Rein, G., Torero, J.R., 2009. Self-sustaining smoldering combustion: A novel remediation process for non-aqueous-phase liquids in porous media. Environ. Sci. Technol. 43, 5871–5877. https://doi.org/10.1021/es803483s

Telliard, W., 2001. Method 1684: Total, fixed, and volatile solids in water, solids, and biosolids. Washington.

Thompson, K.A., Mortazavian, S., Gonzalez, D.J., Bott, C., Hooper, J., Schaefer, C.E., Dickenson, E.R.V., 2022. Poly- and Perfluoroalkyl Substances in Municipal Wastewater Treatment Plants in the United States: Seasonal Patterns and Meta-Analysis of Long-Term Trends and

Average Concentrations. ACS Environ. Sci. Technol. Water 2, 690–700. https://doi.org/10.1021/ACSESTWATER.1C00377/ASSET/IMAGES/LARGE/EW1C00377_0005.JPEG

Torero, J.L., Gerhard, J.I., Martins, M.F., Zanoni, M.A.B., Rashwan, T.L., Brown, J.K., 2020. Processes defining smouldering combustion: Integrated review and synthesis. Prog. Energy Combust. Sci. https://doi.org/10.1016/j.pecs.2020.100869

UNEP, 2019. SC-9/12: Listing of perfluorooctanoic acid (PFOA), its salts and PFOA- related compounds. Geneva.

USEPA, 2021. Contaminants on the Fourth Drinking Water Contaminant Candidate List. Environmental Protection Agency.

USEPA, 2020. Significant New Use Rule: Long-Chain Perfluoroalkyl Carboxylate and Perfluoroalkyl Sulfonate Chemical Substances. Environmental Protection Agency.

Venkatesan, A.K., Halden, R.U., 2013. National inventory of perfluoroalkyl substances in archived U.S. biosolids from the 2001 EPA National Sewage Sludge Survey. J. Hazard. Mater. 252–253, 413–418. https://doi.org/10.1016/j.jhazmat.2013.03.016

Wang, F., Lu, X., Li, X.Y., Shih, K., 2015. Effectiveness and mechanisms of defluorination of perfluorinated alkyl substances by calcium compounds during waste thermal treatment. Environ. Sci. Technol. 49, 5672–5680. https://doi.org/10.1021/es506234b

Wang, F., Shih, K., Lu, X., Liu, C., 2013. Mineralization Behavior of Fluorine in Perfluorooctanesulfonate (PFOS) during Thermal Treatment of Lime-Conditioned Sludge.

436 Environ. Sci. Technol. 47, 2621–2627. https://doi.org/10.1021/es305352p

437 Wang, J., Grant, G.P., Gerhard, J.I., 2021. The influence of porous media heterogeneity on
438 smouldering remediation. J. Contam. Hydrol. 237, 103756.
439 https://doi.org/10.1016/J.JCONHYD.2020.103756

440 Washington, J.W., Yoo, H., Ellington, J.J., Jenkins, T.M., Libelo, E.L., 2010. Concentrations,
441 distribution, and persistence of perfluoroalkylates in sludge-applied soils near Decatur,
442 Alabama, USA. Environ. Sci. Technol. 44, 8390–8396.
443 https://doi.org/10.1021/ES1003846/SUPPL_FILE/ES1003846_SI_001.PDF

444 Werther, J., Ogada, T., 1999. Sewage sludge combustion. Prog. Energy Combust. Sci.
445 https://doi.org/10.1016/S0360-1285(98)00020-3

446 Winchell, L.J., Ross, J.J., Wells, M.J.M., Fonoll, X., Norton, J.W., Bell, K.Y., 2021. Per- and
447 polyfluoroalkyl substances thermal destruction at water resource recovery facilities: A
448 state of the science review. Water Environ. Res. 93, 826–843.
449 https://doi.org/10.1002/WER.1483

450 Yan, H., Zhang, C.J., Zhou, Q., Chen, L., Meng, X.Z., 2012. Short- and long-chain perfluorinated
451 acids in sewage sludge from Shanghai, China. Chemosphere 88, 1300–1305.
452 https://doi.org/10.1016/j.chemosphere.2012.03.105

453 Yermán, L., Hadden, R.M., Carrascal, J., Fabris, I., Cormier, D., Torero, J.L., Gerhard, J.I.,
454 Krajcovic, M., Pironi, P., Cheng, Y.L., 2015. Smouldering combustion as a treatment
455 technology for faeces: Exploring the parameter space. Fuel 147, 108–116.

https://doi.org/10.1016/j.fuel.2015.01.055

Yu, J., Nickerson, A., Li, Y., Fang, Y., Strathmann, T.J., 2020. Fate of per- and polyfluoroalkyl substances (PFAS) during hydrothermal liquefaction of municipal wastewater treatment sludge. Environ. Sci. Water Res. Technol. 6, 1388–1399. https://doi.org/10.1039/c9ew01139k

Zhang, C., Yan, H., Li, F., Hu, X., Zhou, Q., 2013. Sorption of short- and long-chain perfluoroalkyl surfactants on sewage sludges. J. Hazard. Mater. 260, 689–699. https://doi.org/10.1016/j.jhazmat.2013.06.022

Zhang, W., Liang, Y., 2021. Effects of hydrothermal treatments on destruction of per- and polyfluoroalkyl substances in sewage sludge. Environ. Pollut. 285, 117276. https://doi.org/10.1016/J.ENVPOL.2021.117276

Zhang, W., Zhang, Q., Liang, Y., 2022. Ineffectiveness of ultrasound at low frequency for treating per- and polyfluoroalkyl substances in sewage sludge. Chemosphere 286, 131748. https://doi.org/10.1016/J.CHEMOSPHERE.2021.131748

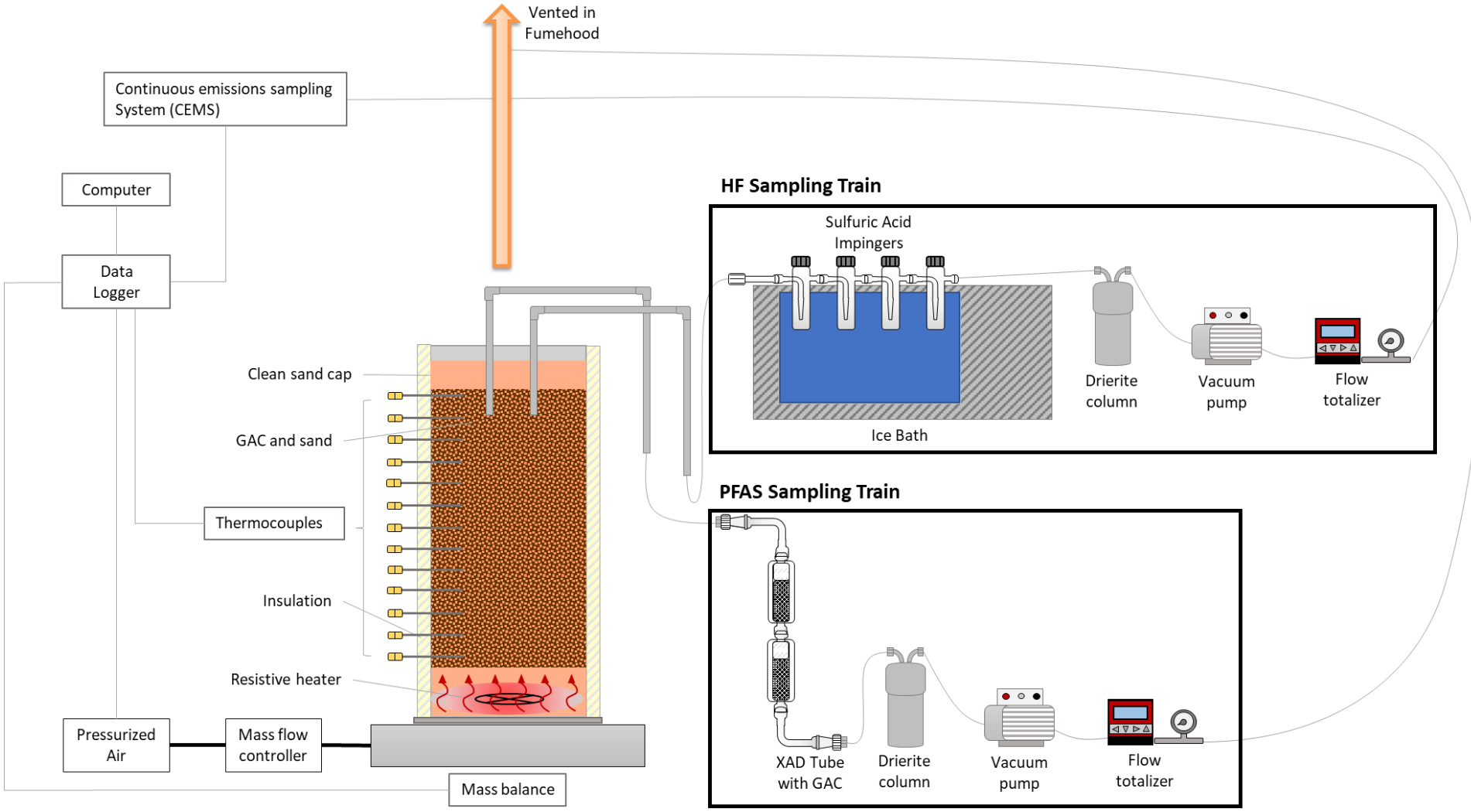

Figure 1: Experimental set-up and sampling for LAB tests.

Table 1: Summary of smouldering experiments

Experiment	Experimental Conditions						Results	
	Moisture Content	Sand/Sludge	GAC Concentration	CaO Added	Pack Height	Air Flux	Average Centreline Peak Temperature ± S.E. [a]	Smouldering Velocity ± S.E. [a]
	(%)	(g/g)	(g GAC/kg sand)	(g CaO/kg sand)	(cm)	(cm/s)	(°C)	(cm/min)
PHASE I: LAB Base case								
I-1	0	6.5 [b]	-	-	31.1	5.0	856 ± 34	0.44 ± 0.07
I-2	0	6.5 [b]	-	-	34.3	5.0	737 ± 37	0.42 ± 0.08
I-3	0	6.5 [b]	-	-	34.9	5.0	831 ± 41	0.46 ± 0.08
PHASE II: LAB High MC and Amendments								
II-1-1	75 [c]	4.5 [d]	20	-	29.2	5.0	746 ± 21	0.52 ± 0.13
II-1-2	75 [c]	4.5 [d]	30	-	29.2	5.0	905 ± 21	0.50 ± 0.09
II-2-2	0	6.5 [b]	-	5	28.6	5.0	818 ± 57	0.53 ± 0.11
II-2-1	0	6.5 [b]	-	10	29.2	5.0	824 ± 54	0.30 ± 0.14
PHASE III: DRUM								
III-1	3.2	6.5 [d] (25.5 [b])	-	-	53.5	5.0	542 ± 7.7	0.34 ± 0.04
III-2	72.3 [e]	6.5 [d]	-	-	61.6	5.0	473 ± 1.7	0.23 ± 0.01
III-3	74.4 [e]	4.5 [d]	-	-	61.9	5.0	469 ± 7.8	0.23 ± 0.03

[a] Standard error calculated as $\frac{\sigma}{\sqrt{n}}$

[b] Measured on a dry-mass basis

[c] Moisture content of virgin sludge after drying and rehydrating

[d] Measured on a wet-mass basis

[e] Moisture content of virgin sludge, no drying occurred for these tests

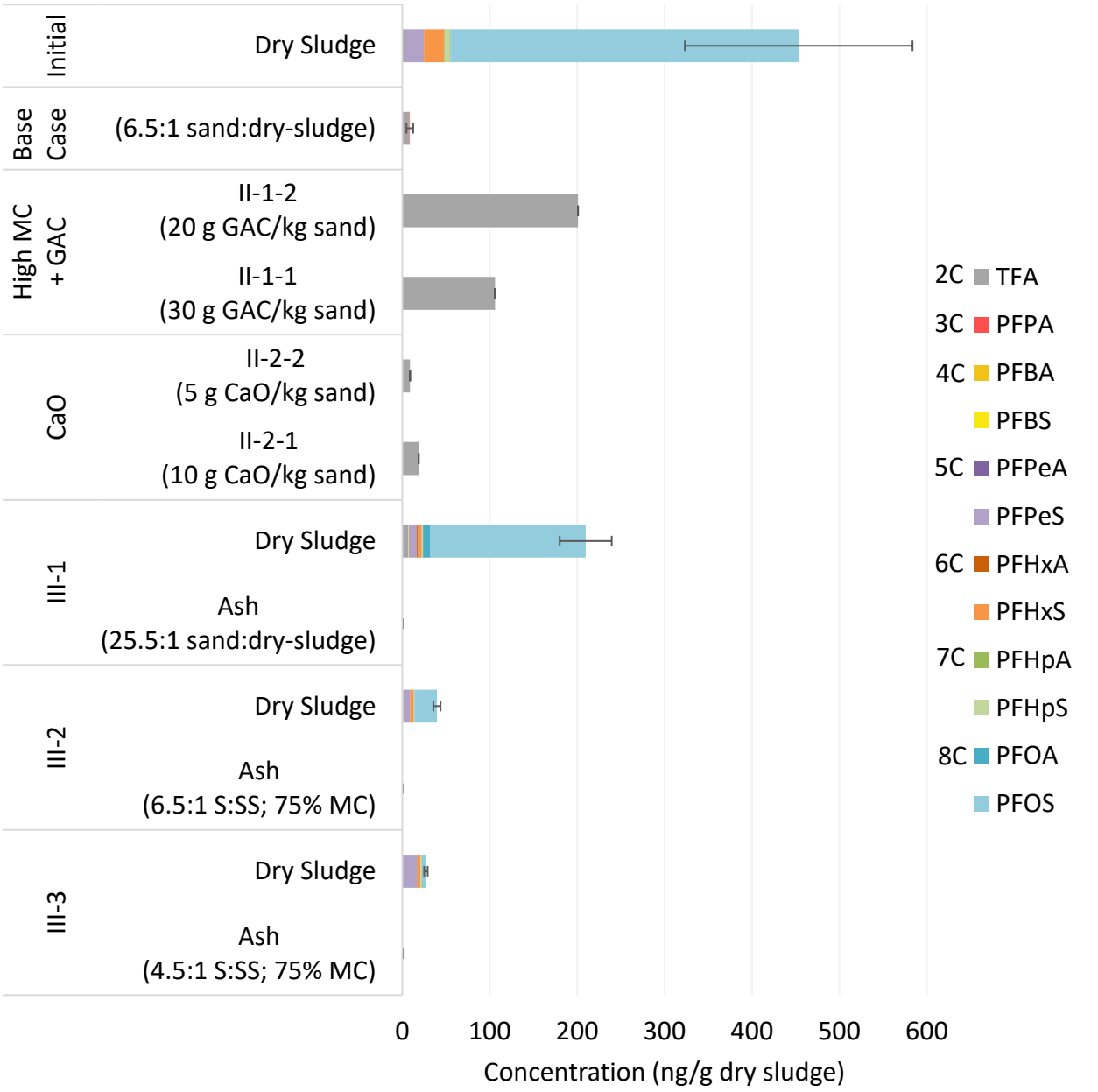

Figure 2: Content of 12 PFAS originally present in sludges and post-treatment solids following smouldering treatment from a) LAB Phase I: base cases and Phase II: high MC (75%) and GAC, and CaO tests, and b) DRUM Phase III. Error bars represent standard error of the cumulative PFAS concentration determined from replicate samples.

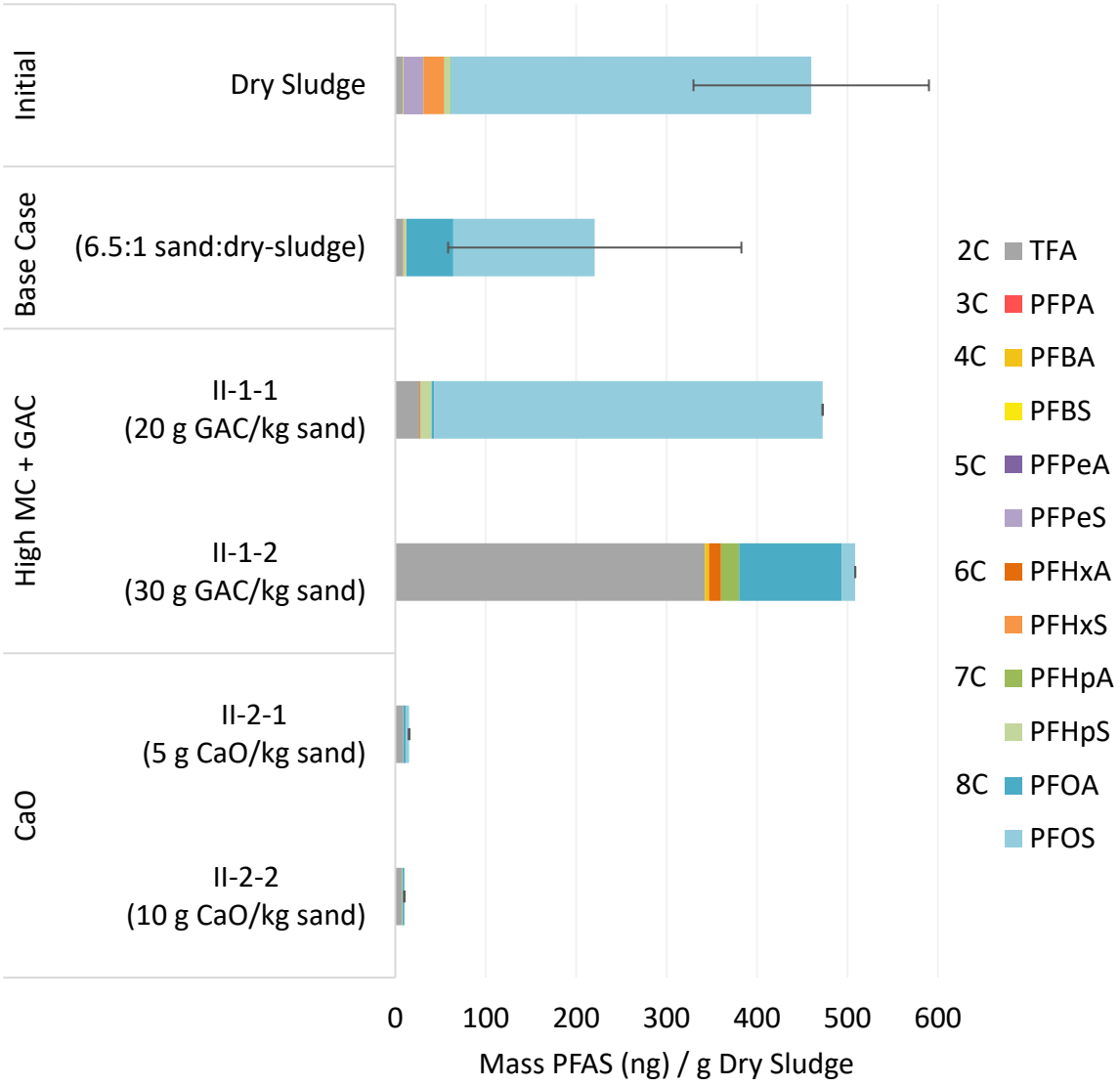

Figure 3: Content of 12 PFAS in the emissions during smouldering compared to the content originally present in the dried sludge. The content in the emissions has been normalized to account for differences between the experiments.

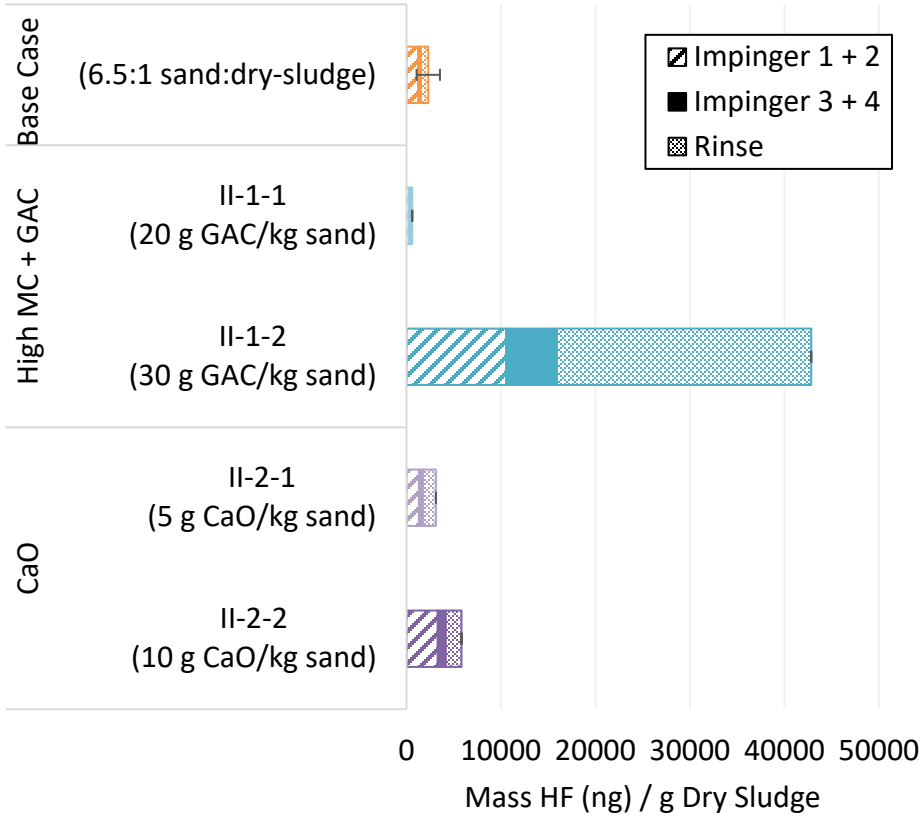

Figure 4: HF content measured in the emissions from each laboratory smouldering experiment. The contents collected from two sections of the glassware sampling train and additionally the glassware rinse have been presented separately. The contents in the emissions have been normalized to account for differences between the experiments.

Supplementary Materials

Smouldering to Treat PFAS in Sewage Sludge

T. Fournie[a*], T. Rashwan[a,b], C. Switzer[c], J. Gerhard[a,ǂ]

[a] *Department of Civil and Environmental Engineering, Western University, N6A 5B9 London, Ontario, Canada*
[b] *School of Engineering & Innovation, The Open University, Milton Keynes, MK7 6AA, UK* [1]
[c] *Department of Civil and Environmental Engineering, University of Strathclyde, G1 1XQ Glasgow, UK*
[1] *Present address*
[*] *Corresponding author*
[ǂ] *Deceased*

S1. Preliminary PFAS Analysis

Table S1-1: Preliminary PFAS Analysis on Sewage Sludge Collected between February 2018 and June 2018

PFAS Concentration (ng/g)	Dried Sludge Sample			
	1 [a]	2 [a, b]	3 [c]	4 [d]
PFBA	1580 ± 862	553 ± 37.1	1060 ± 641	1940 ± 160
PFPeA	3320 ± 282	2390 ± 507	1720 ± 578	2310 ± 5.43
PFBS	*B.Q.L.*	*B.Q.L.*	*B.Q.L.*	*B.Q.L.*
PFHxA	1110 ± 73.1	657 ± 14.0	882 ± 429	863 ± 60.0
PFHpA	6190 ± 1580	3450 ± 1140	3420 ± 568	5720 ± 234
PFOA	*B.D.L.*	*B.D.L.*	*B.D.L.*	*B.D.L.*
PFHxS	*B.D.L.*	*B.D.L.*	*B.D.L.*	*B.D.L.*
PFNA	*B.D.L.*	*B.D.L.*	*B.D.L.*	*B.D.L.*
PFDA	*B.D.L.*	*B.D.L.*	*B.D.L.*	*B.D.L.*
PFOS	1590 ± 638	449 ± 224	458 ± 229	*B.D.L.*
PFUnA	*B.D.L.*	*B.D.L.*	*B.D.L.*	*B.D.L.*
PFDoA	*B.D.L.*	*B.D.L.*	*B.D.L.*	*B.D.L.*
PFOSA	*B.D.L.*	*B.D.L.*	*B.D.L.*	*B.D.L.*

[a] Sludge had a MC of 3.23%, ash content of 26.7%, and was collected in February, 2018

[b] Secondary batch of sludge

[c] Sludge had a MC of 72.3%, ash content of 26.9%, and was collected in May, 2018

[d] Sludge had a MC of 74.4%, ash content of 24.8%, and was collected in June, 2018

S2. Supplemental Information on Smouldering Experiments

Table S2-1: Additional experimental data and results from LAB scale Phase I & II

Experiment	Experimental Conditions					Results			
	Moisture Content		Sand/ Sludge	GAC Concentration	CaO Added	Average Peak Temperature			
	After drying (%)	After rehydrating (%)	(g/g)	(g GAC/ kg sand)	(g CaO/ kg sand)	Centreline (°C)	Half Radius (°C)	Sand Cap (°C)	Air Phase (°C)
PHASE I: LAB Base case									
I-1	<1	-	6.5 [a]	-	-	856 ± 34	805 ± 67	499 ± 63	186 ± 10
I-2	<1	-	6.5 [a]	-	-	737 ± 37	818 ± 34	- [c]	175 ± 10
I-3	<1	-	6.5 [a]	-	-	831 ± 41	877 ± 37	562 ± 60	181 ± 17
PHASE II: LAB High MC and Amendments									
II-1-1	<1	75	4.5 [b]	20	-	746 ± 21	573 ± 89	434 ± 13	151 ± 13
II-1-2	<1	75	4.5 [b]	30	-	905 ± 21	749 ± 89	521 ± 24	210 ± 3
II-2-1	<1	-	6.5 [a]	-	5	818 ± 57	721 ± 48	550 ± 6	235 ± 36
II-2-2	<1	-	6.5 [a]	-	10	824 ± 54	741 ± 72	661 ± 62	263 ± 55

[a] Measured on a dry-mass basis

[b] Measured on a wet-mass basis

[c] No thermocouples were present in the sand cap during this test

Emissions Sampling Train

Leak Test Procedure

Both the PFAS and HF emissions sampling trains were leak tested prior to each experiment and contribution of ambient air to the system was minimized to <5%. To do this, nitrogen was injected through one sampling train at a time and the emissions exiting were analyzed using a CEMS. A vacuum pump (DOA-P704-AA, Gast) pulled nitrogen through the system at ~3 L/min. The system ran for several minutes to allow the emissions reading to stabilize. An oxygen measurement of <1% is ideal; however, due to complexities of the emissions sampling train, a measurement of <5% was deemed acceptable and the test would proceed as planned. If a measurement >5% was obtained, each joint of the sampling train would be cleaned, greased, and resecured and the leak test would be repeated.

Sampling

Emissions sampling was initiated after the first thermocouple in the fuel bed peaked. Typically, the emissions sample should be collected until long after the smouldering front exits the fuel bed to capture any end-effects. However, the sampling windows were sometimes shortened to prevent breakthrough of bio-oil (during dry sludge smouldering) and water (during high MC sludge smouldering), which would damage equipment.

Temperature Profiles

Peak temperatures in the clean sand cap ranged from 434 – 661 °C (Table S2-1). Longer smouldering tests (i.e., CaO and DRUM tests) tended to have higher temperatures in the sand cap than the faster tests. This is likely because the sand cap had a longer period of exposure to higher temperatures and was therefore able to retain more of the heat energy from smouldering.

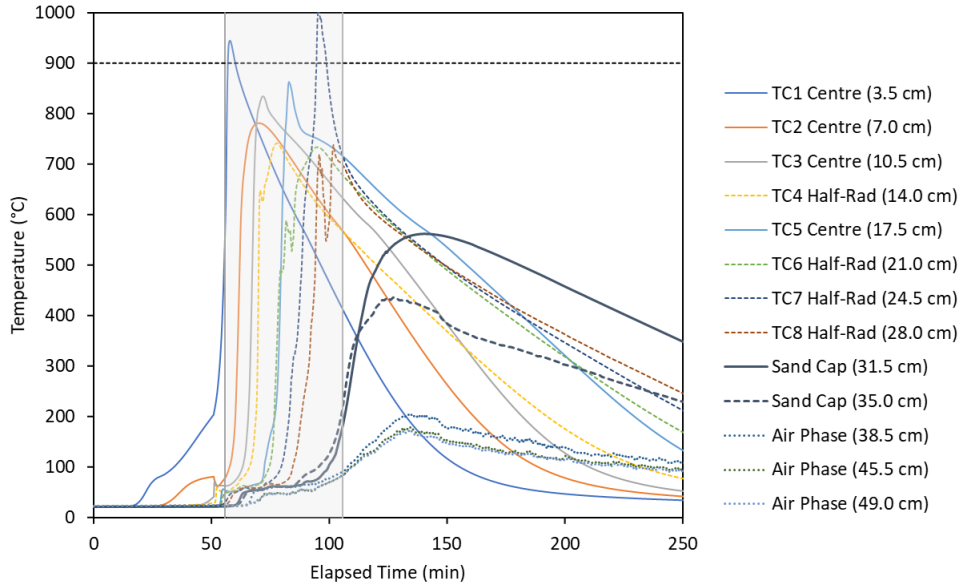

Figure S2-1: Test I-1, the first of 3 base case tests where dried sludge was mixed with sand at a ratio of 6.5:1 sand:dried sludge. The sampling period from 56 – 106 min is shaded in grey. The lower temperature range for significant PFAS degradation (as determined for incineration) is shown as a dotted line.

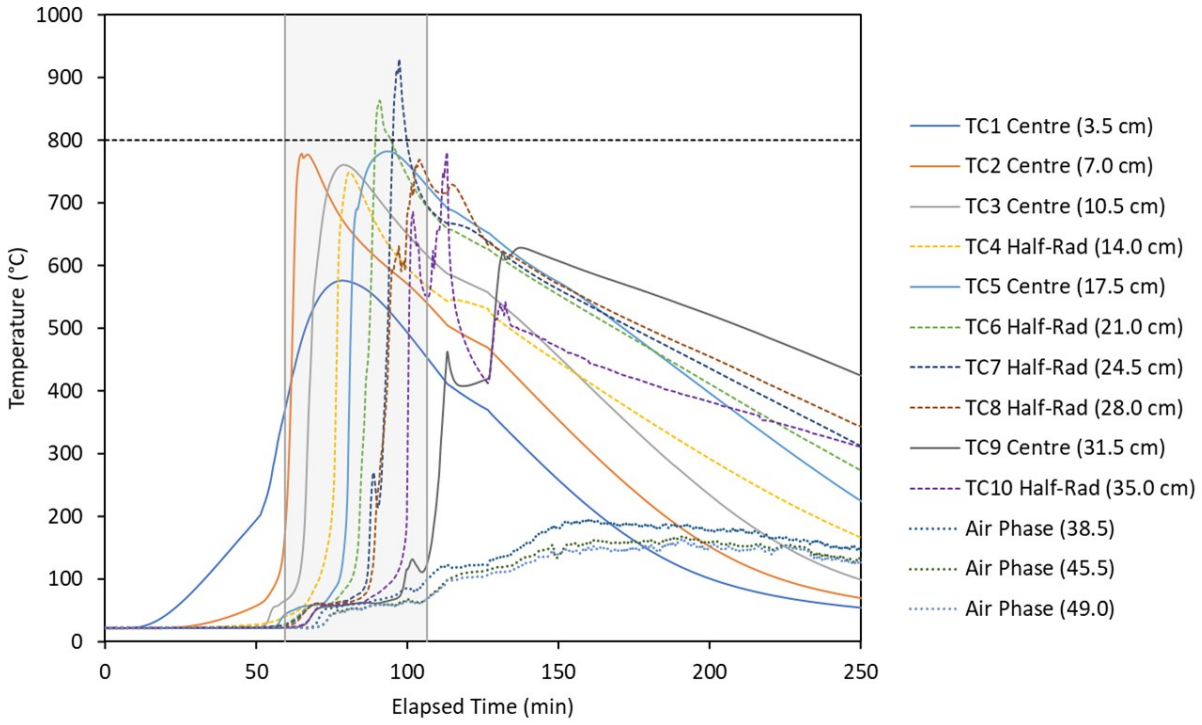

Figure S2-2: Test I-2, the second of 3 base case tests where dried sludge was mixed with sand at a ratio of 6.5:1 sand:dried sludge. The sampling period from 60 – 107 min is shaded in grey. The lower temperature range for significant PFAS degradation (as determined for incineration) is shown as a dotted line.

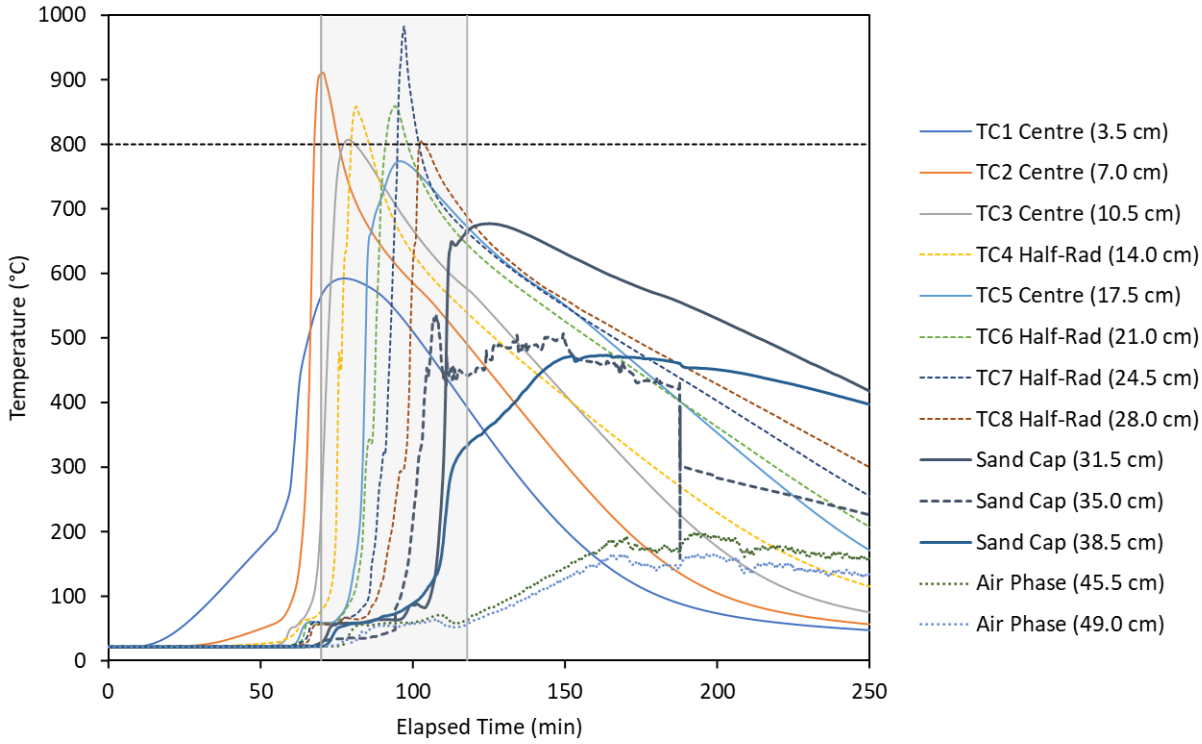

Figure S2-3: Test I-3, the third of 3 base case tests where dried sludge was mixed with sand at a ratio of 6.5:1 sand:dried sludge. The sampling period from 70 – 118 min is shaded in grey. The lower temperature range for significant PFAS degradation (as determined for incineration) is shown as a dotted line.

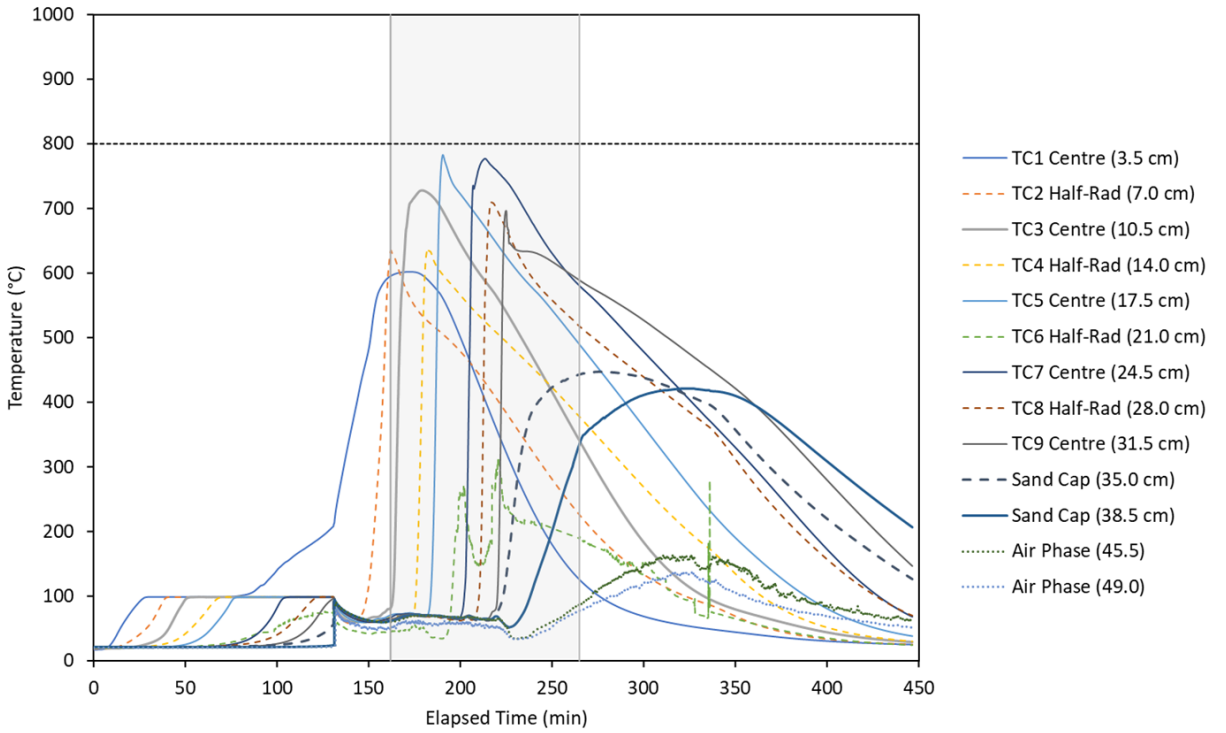

Figure S2-4: Test II-1-1, the first high MC content (75%) smouldering test where 20 g GAC / kg sand was added to supplement the fuel. The sampling period from 162 – 265 min is shaded in grey. The lower temperature range for significant PFAS degradation (as determined for incineration) is shown as a dotted line.

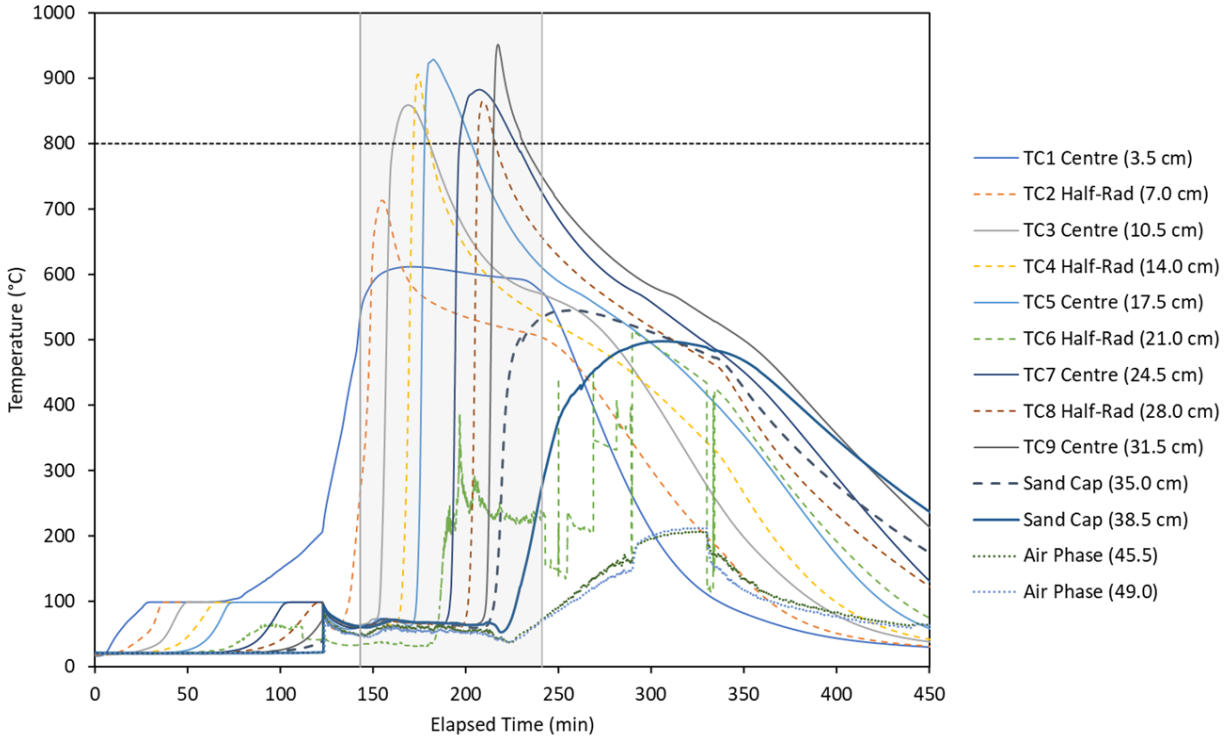

Figure S2-5: Test II-1-2, the second high MC content (75%) smouldering test where 30 g GAC / kg sand was added to supplement the fuel. The sampling period from 143 – 241 min is shaded in grey. The lower temperature range for significant PFAS degradation (as determined for incineration) is shown as a dotted line.

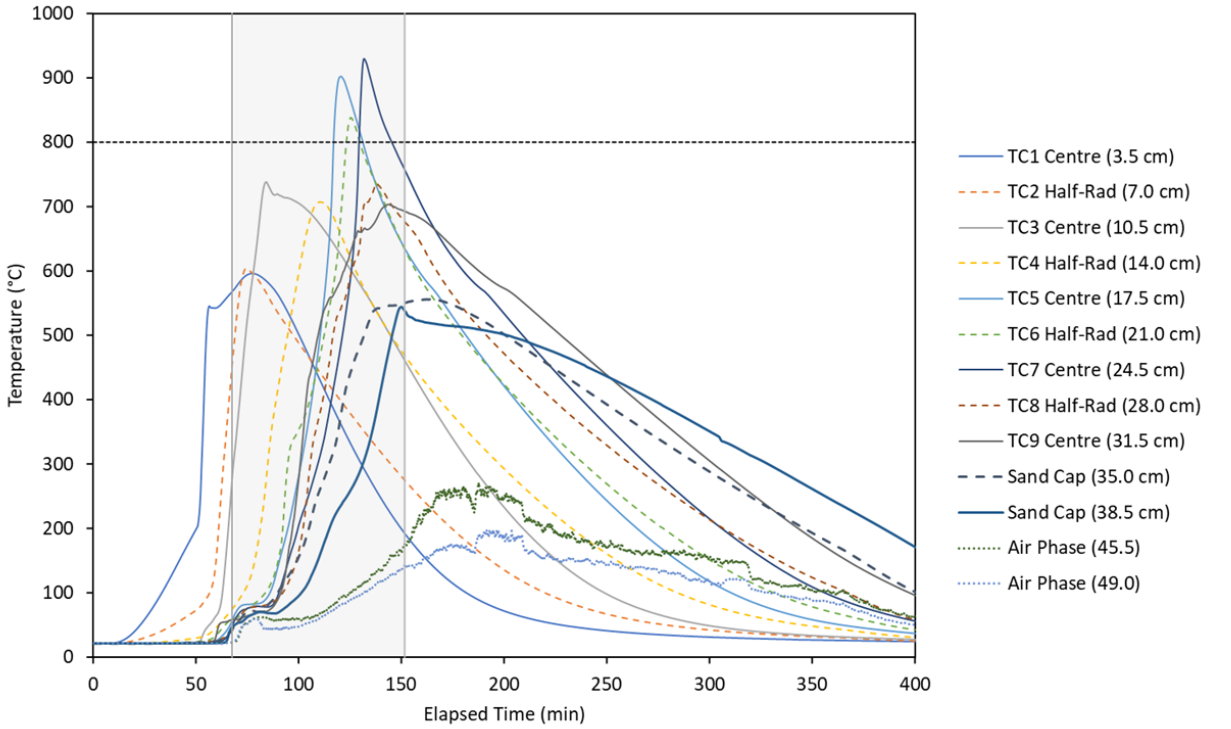

Figure S2-6: Test II-2-1, the first CaO test where 5 g CaO / kg sand was combined with dried sludge and sand at a ratio of 6.5:1 sand:dried sludge. The sampling period from 68 – 152 min is shaded in grey. The lower temperature range for significant PFAS degradation (as determined for incineration) is shown as a dotted line.

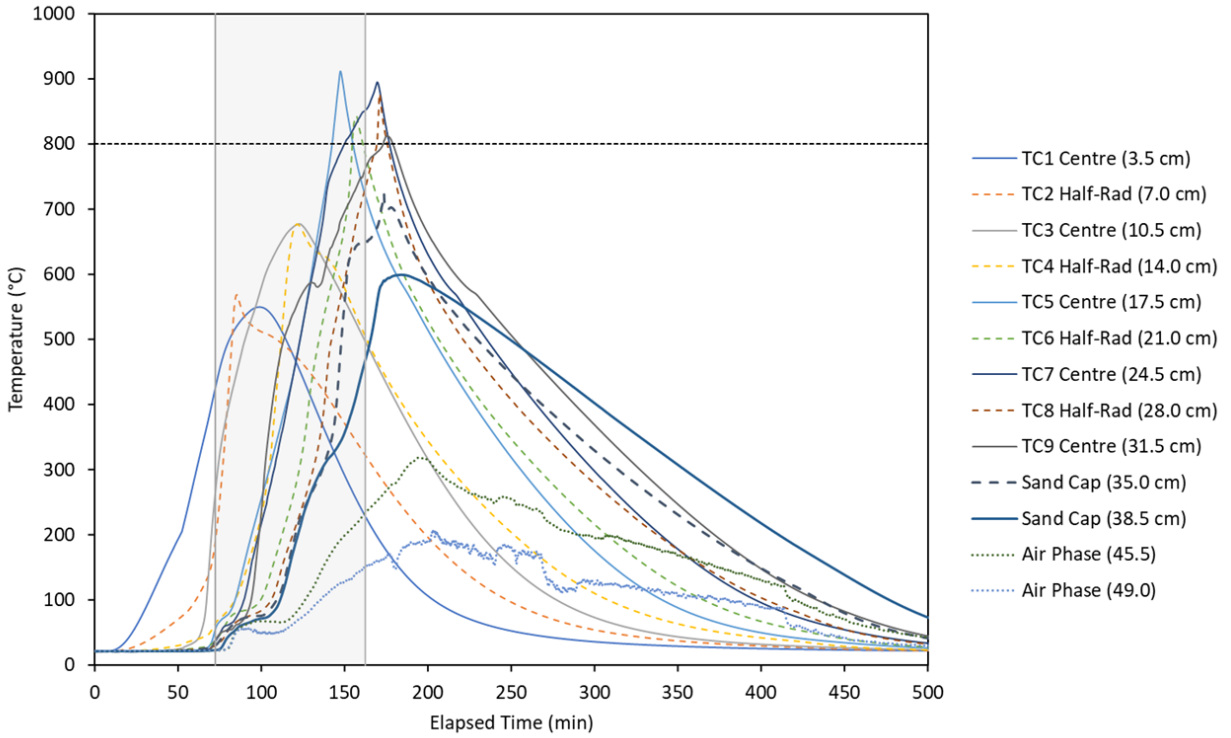

Figure S2-7: Test II-2-2, the second CaO test where 10 g CaO / kg sand was combined with dried sludge and sand at a ratio of 6.5:1 sand:dried sludge. The sampling period from 72 – 162 min is shaded in grey. The lower temperature range for significant PFAS degradation (as determined for incineration) is shown as a dotted line.

Heating Rates

The heating rates were determined using an established methodology; details can be found elsewhere (Rashwan et al., 2021).

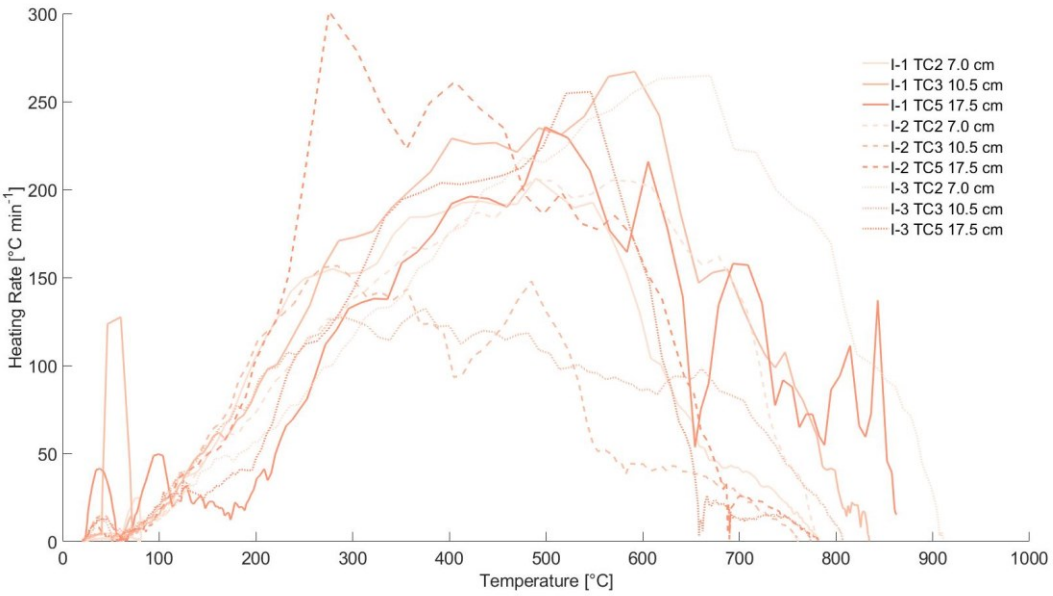

Figure S2-8: Heating rates as a function of temperature for the base case tests. I-1 is presented as a solid line, I-2 as a dashed line, and I-3 as a dotted line. Only the centreline thermocouples within the fuel bed have been included.

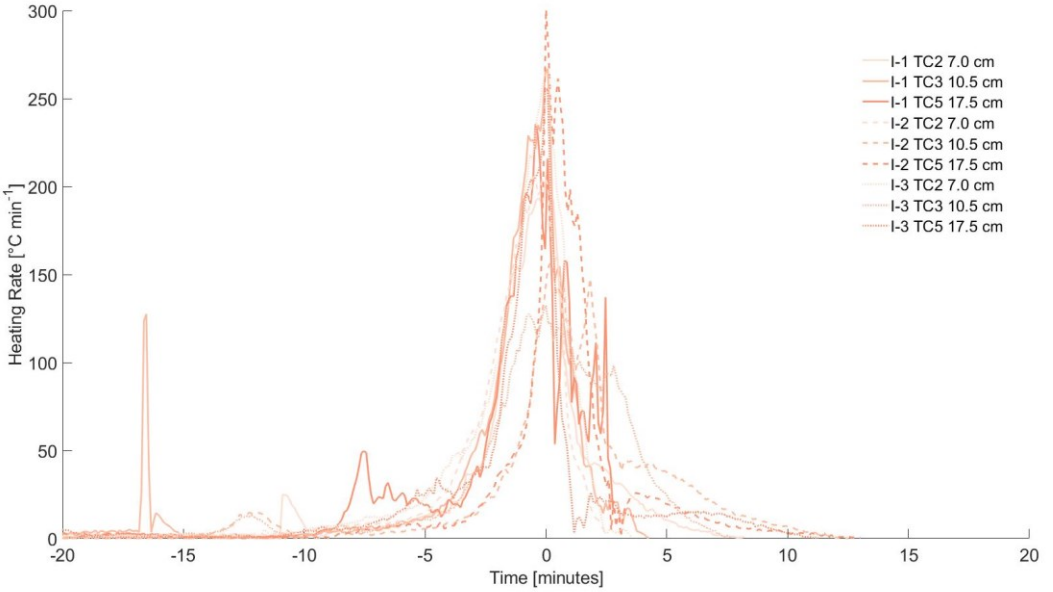

Figure S2-9: Heating rates as a function of normalized time for the base case tests. I-1 is presented as a solid line, I-2 as a dashed line, and I-3 as a dotted line. Only the centreline thermocouples within the fuel bed have been included.

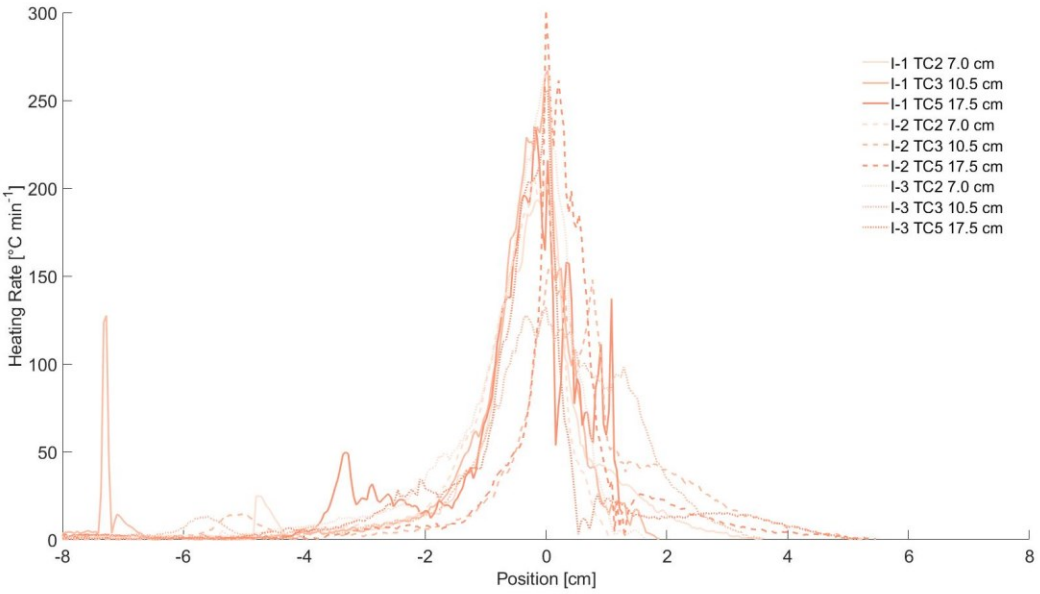

Figure S2-10: Heating rates as a function of normalized position in the reactor for the base case tests. I-1 is presented as a solid line, I-2 as a dashed line, and I-3 as a dotted line. Only the centreline thermocouples within the fuel bed have been included.

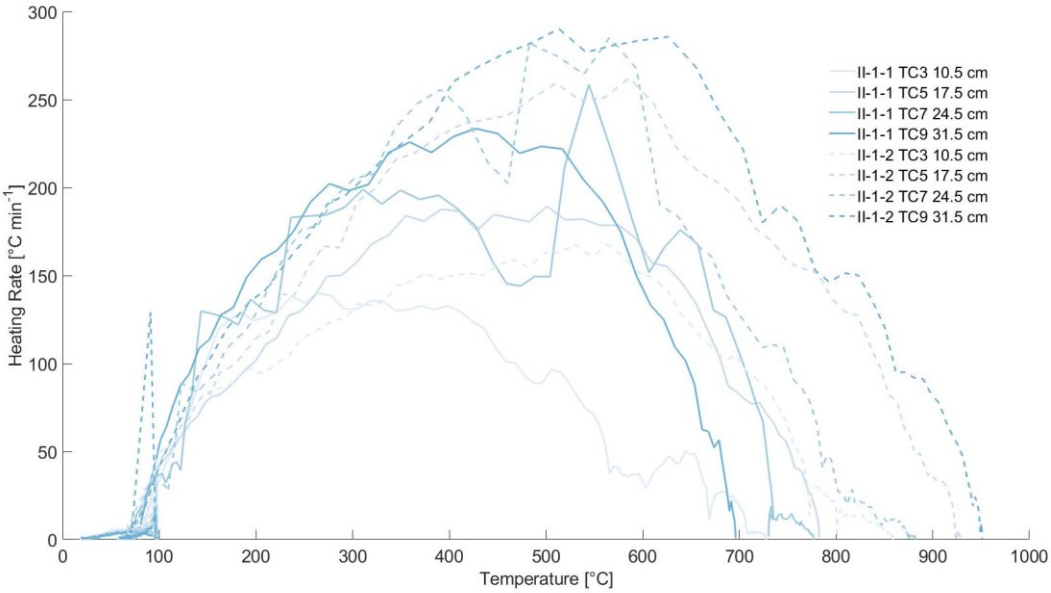

Figure S2-11: Heating rates as a function of temperature for the high MC (75%) and GAC tests. II-1-1 (20 g GAC/kg sand) is presented as a solid line, and II-1-2 (30 g GAC/kg sand) as a dashed line. Only the centreline thermocouples within the fuel bed have been included.

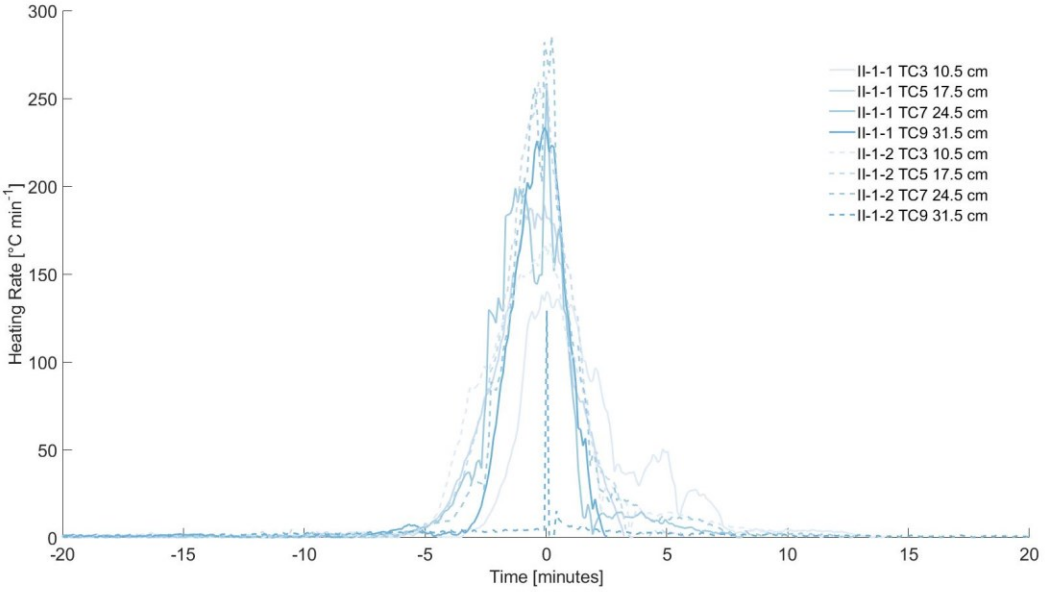

Figure S2-12: Heating rates as a function of normalized time for the high MC (75%) and GAC tests. II-1-1 (20 g GAC/kg sand) is presented as a solid line, and II-1-2 (30 g GAC/kg sand) as a dashed line. Only the centreline thermocouples within the fuel bed have been included.

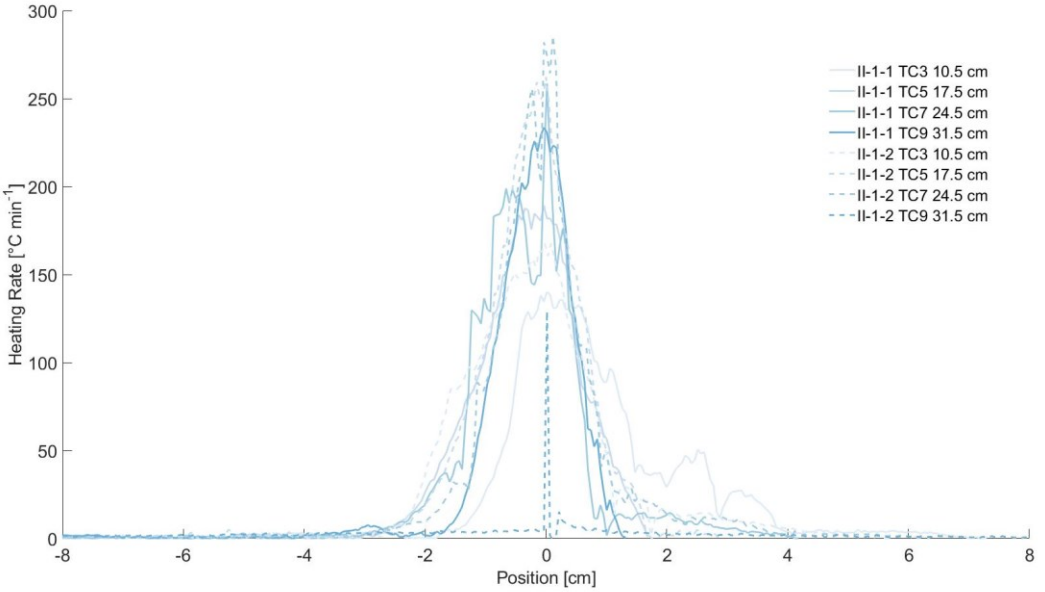

Figure S2-13: Heating rates as a function of normalized position in the reactor for the high MC (75%) and GAC tests. II-1-1 (20 g GAC/kg sand) is presented as a solid line, and II-1-2 (30 g GAC/kg sand) as a dashed line. Only the centreline thermocouples within the fuel bed have been included.

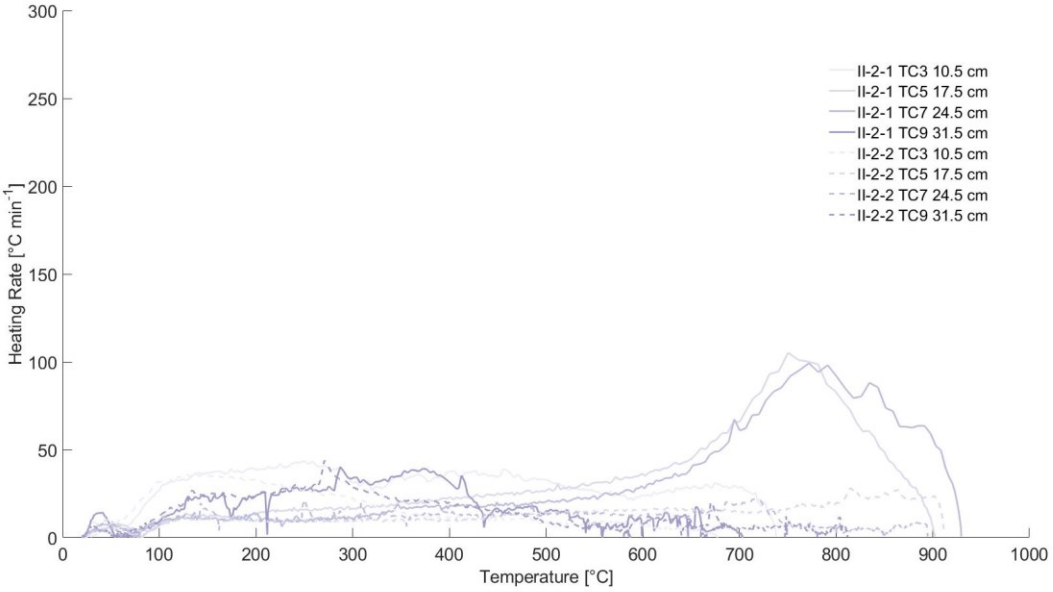

84

85 *Figure S2-14: Heating rates as a function of temperature for the CaO tests. II-2-1 (5 g CaO/kg sand) is presented as a solid line,*
86 *and II-2-2 (10 g CaO/kg sand) as a dashed line. Only the centreline thermocouples within the fuel bed have been included.*

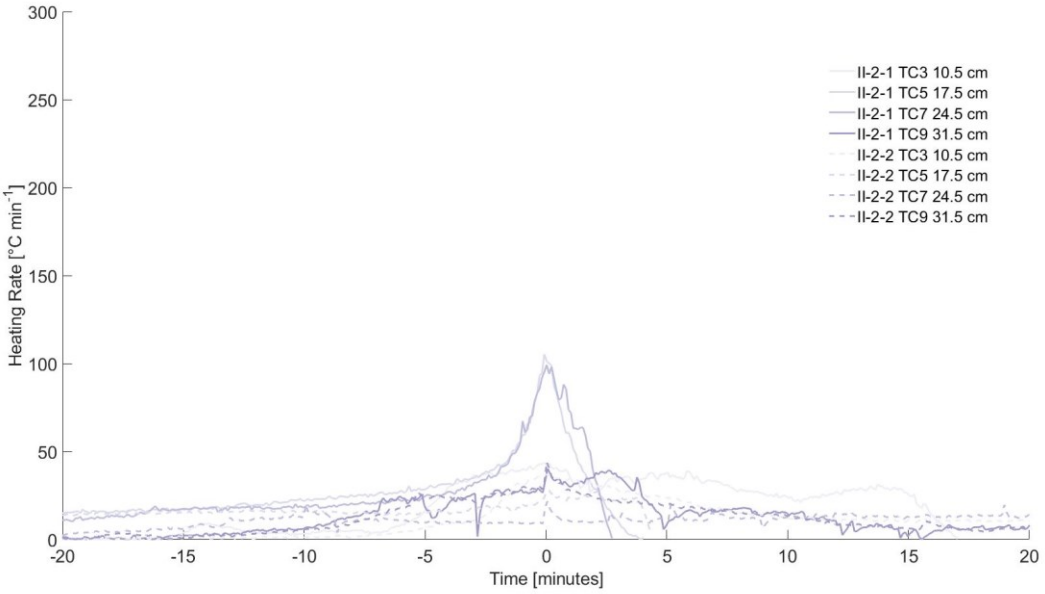

87

88 *Figure S2-15: Heating rates as a function of normalized time for the CaO tests. II-2-1 (5 g CaO/kg sand) is presented as a solid line,*
89 *and II-2-2 (10 g CaO/kg sand) as a dashed line. Only the centreline thermocouples within the fuel bed have been included.*

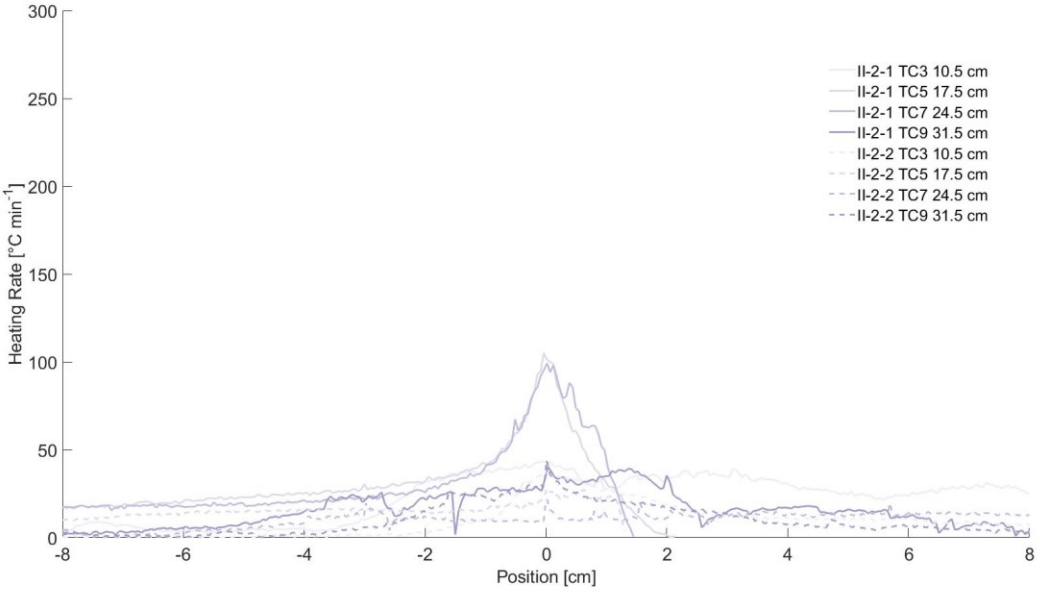

Figure S2-16: Heating rates as a function of normalized position in the reactor for the CaO tests. II-2-1 (5 g CaO/kg sand) is presented as a solid line, and II-2-2 (10 g CaO/kg sand) as a dashed line. Only the centreline thermocouples within the fuel bed have been included.

Post-Treatment Ash and Sand

Figure S2-17 shows the post-treatment samples from following the smouldering treatment of sewage sludge. The top sand cap (~38 – 48 cm from reactor base) was initially clean sand added to lower the temperature of the emissions exiting the column. During sludge smouldering, bio-oil volatilized during sludge heating and recondensed in the top sand cap. As the smouldering front exited the column, the bio-oil was pyrolyzed (Figure S2-17a.). The post-treatment materials in the top of the fuel bed (~27 – 31 cm from reactor base), and the bottom of the fuel bed (~13 – 20 cm from reactor base) were very similar with sewage sludge ash (~20% ash content) surrounded by silica sand (Figure S2-17a./b.). The silica sand used in all tests was conserved during smouldering.

Figure S2-17: Experimental photos of the post-treatment ash and sand from base case I-1 from three locations within the reactor, a. the top sand cap, b. the middle of the fuel bed, and c. the bottom of the fuel bed.

S3. Supplementary Information on Drum Reactor Experiments

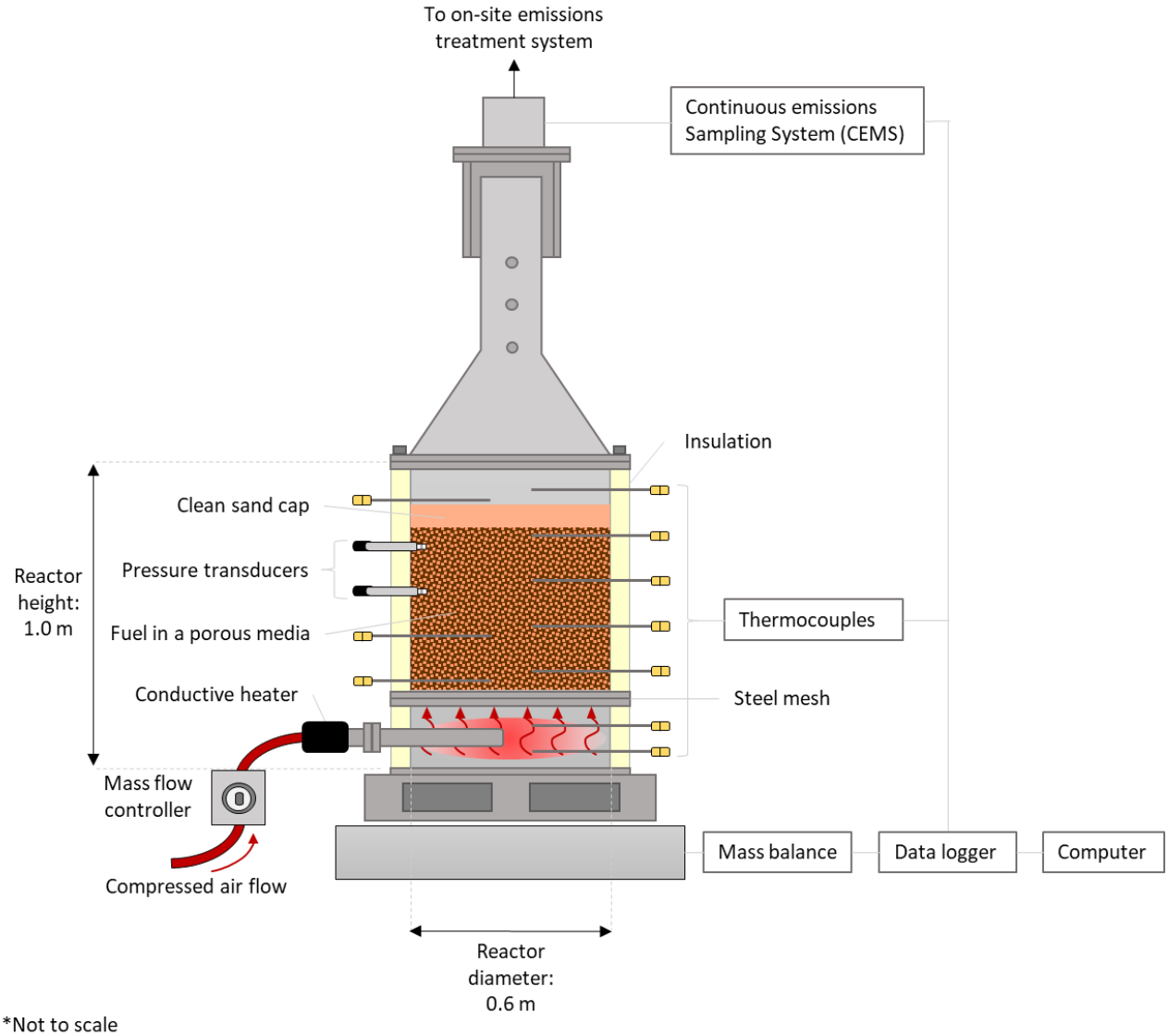

Figure S3-1: Schematic of smouldering reactor set-up.

Experimental Set-up and Procedure: DRUM Reactor

The sludge and sand used for the DRUM tests were combined using a mechanical drum mixer following established procedures (Fournie et al., 2022; Rashwan et al., 2021). Mixtures were prepared in small batches (~20 kg) before being carefully loaded into the reactor to minimize compaction.

The experimental set-up for the DRUM tests is shown in Figure S3-1. The ignition procedure is described below. Air – operated using a mass flux controller (8290B045PDB67 ASCO Numatics) – was injected into the base of the DRUM reactor from the beginning of the test. With the air on, the base of the reactor was then heated via a convective heater (F074736 36 kW SureHeat® MAX, Osram Sylvania) until ignition

occurred. Ignition was confirmed the first thermocouple in the contaminant pack peaked (i.e., 0.06 m up the column in the DRUM experiments). Following ignition, the heater was turned off and the air flow was maintained to support self-sustaining smouldering. The end of each experiment was identified when the smouldering front reached the end of the contaminant pack in the reactor. Continuous emissions monitoring systems (CEMS) measured methane, carbon dioxide, carbon monoxide, and total hydrocarbons from the DRUM tests every five seconds (ABB Ltd.).

The emissions exiting the DRUM reactors were passed through an onsite treatment system prior to release from a stack. The custom treatment system (Newterra Ltd.) consisted of two granular activated carbon vessels (with 820 and 75 kg of material in each vessel), followed by an impregnated potassium permanganate vessel (with 150 kg of material).

Representative samples, ~19 – 100L per DRUM test, of the post-treatment material (i.e., ash mixed with silica sand) were collected in 19 L buckets. These large sample volumes aimed to capture the heterogeneities throughout the reactor.

Temperature Profiles

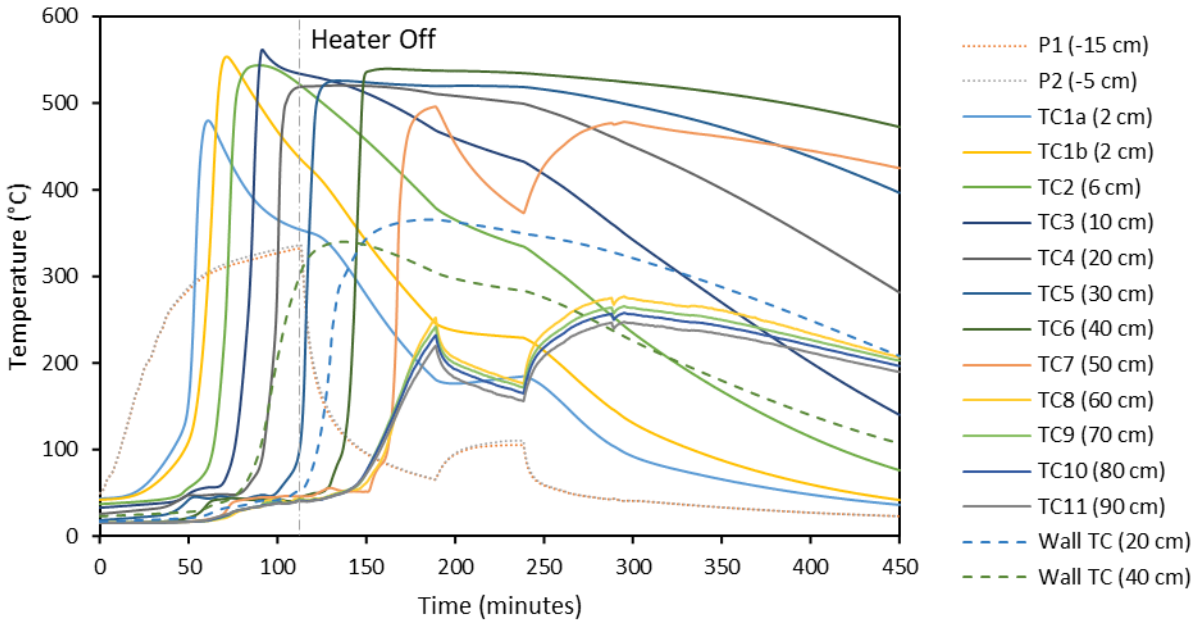

Figure S3-2: Temperature profile for Test III-1, a self-sustaining smouldering experiment with a 3.81% moisture content sludge in a fixed bed with 25.5 g/g sand/sludge mass ratio. Plenum, centreline, and wall thermocouples are presented. Note the air flux was changed at 190, 238, 288, 290, and 296 minutes.

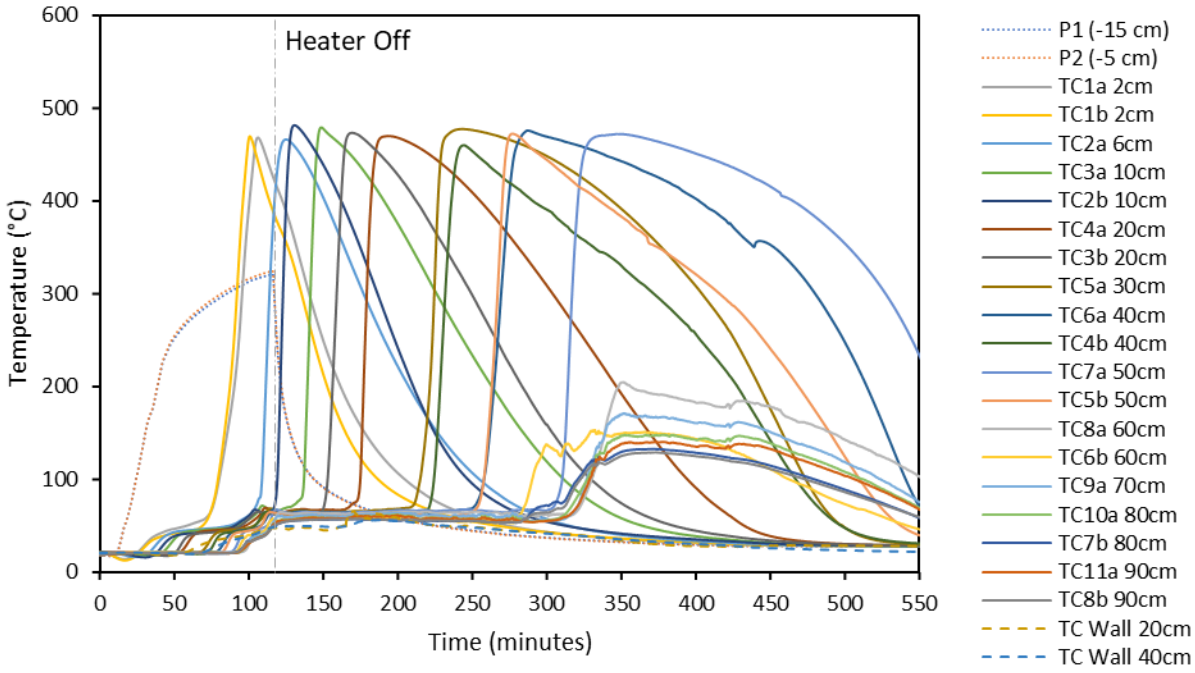

137

138 *Figure S3-3: Temperature profile for Test III-2, a self-sustaining smouldering experiment with a 72.3% moisture content sludge in*
139 *a fixed bed with 4.5 g/g sand/sludge mass ratio. Plenum, centreline, and wall thermocouples are presented.*

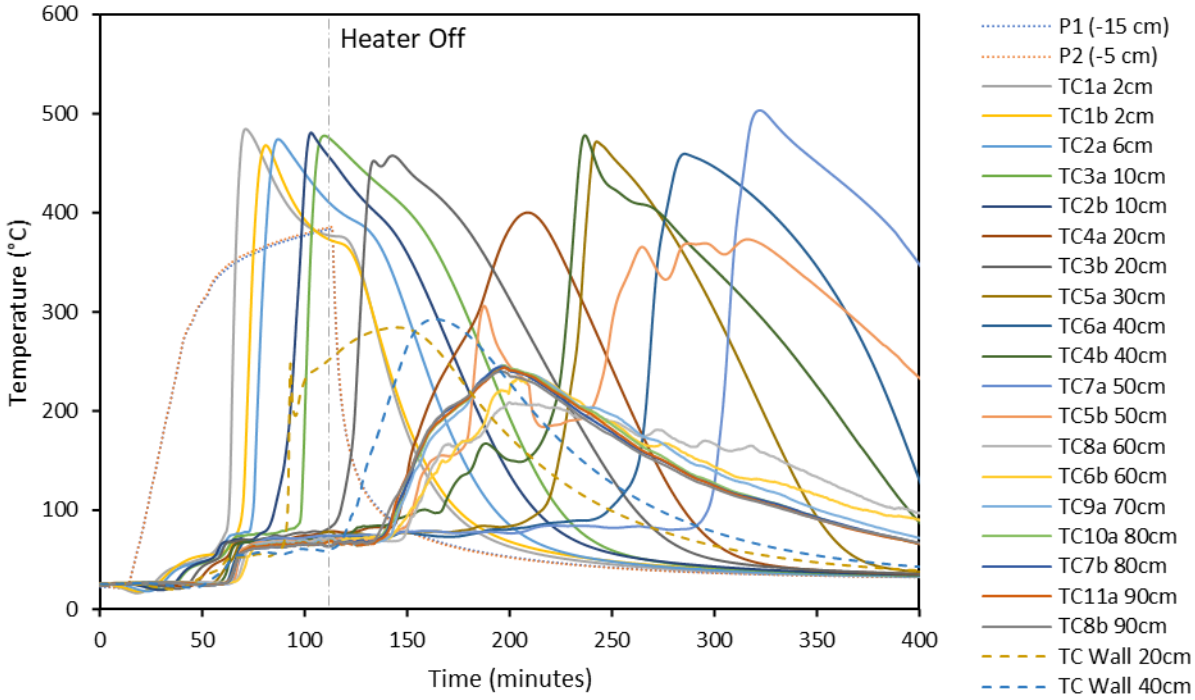

140

141 *Figure S3-4: Temperature profile for Test III-3, a self-sustaining smouldering experiment with a 74.4% moisture content sludge in*
142 *a fixed bed with 4.5 g/g sand/sludge mass ratio. Plenum, centreline, and wall thermocouples are presented.*

S4. Supplementary Information on Emissions and Solids Analyses

Solid samples were extracted with basic methanol (0.1% ammonium hydroxide (CAS: 1336-21-6, Fisher Scientific) v/v) using 5:1 extractant-to-sample (g/g). Samples were vortexed for 30 seconds, then placed on a shaker table at 30 RPM for 48 hours. Samples were then centrifuged at 4000 RPM for 10 minutes, and a sub-sample transferred to a PFAS-free HPLC vial for analysis.

All PFAS analyses were conducted by the Environmental Sciences Group at the Royal Military College of Canada. These analyses were completed following a modified EPA 8327 method using liquid chromatography with tandem mass spectrometry (LC-MS/MS). Mass-labelled internal standards of PFOA, PFOS, and PFHxS were added to solid samples before extraction to examine matrix effects. Blank samples of (1) methanol, (2) DI water, (3) sand, (4) GAC, and (5) glass wool collected during each test were analyzed to ensure no cross-contamination during experimental procedures. Blanks were included every 20 samples were analyzed and monitored to ensure no cross-contamination of samples occurred during analysis. Duplicate samples were included to ensure reproducibility of results.

Concentrations of 12 PFAS (TFA, PFPA, PFBA, PFBS, PFPeA, PFPeS, PFHxA, PFHxS, PFHpA, PFHpS, PFOA, PFOS) were determined using a seven-point calibration curve across 0.4 ppb to 100 ppb. Internal standard recoveries were found to be between 70-120% and no correction was applied for the internal standard. Two double injection blanks (basic methanol) were run before each method blank, reagent blank, calibration curve, post-treatment sample, and experimental blanks to eliminate contamination and carry-over from other samples. Sample duplicates within 30% relative percent difference (RPD) was considered acceptable according to EPA Method 531.1. The instrumental detection limit was 0.0004 ppm PFAS and the quantitation limit was 0.001 ppm PFAS.

S5. PFAS in virgin sludge and post-treatment ash

Base Case Tests

Smouldering resulted in 92 – 100% reduction in total PFAS in the post-treatment materials. The highest concentrations of PFAS in the post-treatment materials during base case tests tended to be in the top sand cap (Figure S5-1). TFA (2C) was the primary compound measured in the ash (1.1 ng/g-DS of PFPA was measured in the ash from I-2). PFPA (3C) was primarily measured in the top ash. Since neither TFA nor PFPA were measured in the dried sludge, their presence in the post-treatment materials could be from breakdown products of larger PFAS. PFOS retained in top sand cap from I-1 is 68% less than present in the dried sludge. With 100% removal of PFOS and PFOA from the ash from I-1, the presence of PFOS in the sand cap is evidence of the compound recondensing. This was also observed during test I-3 where the sand cap retained 1% of the PFOS originally present in the sludge but none was measured in the ash. The sand cap from I-2 had no PFOS or PFOA. This could be due to the flaming that occurred at the end of this test. A combination of an insufficient sand cap (required to reduce exiting temperatures), and bio-oil accumulation in the sand cap resulted in flaming occurring as the smouldering front exited the contaminant pack. The flaming significantly increased the temperatures in the sand cap, removing any PFOS or PFOA that may have recondensed there during smouldering.

High MC/GAC Tests

For both high MC/GAC tests, only TFA (2C) was measured in the ash following smouldering treatment. TFA was also the only compound measured in the sand cap from II-1-2. In comparison, the sand cap from II-1-1 also contained PFPA (3C) and PFHpS (7C) (Figure S5-2). The concentration of the three compounds were similar with 54 ng/g-DS TFA, 69 ng/g-DS PFPA, and 63 ng/g-DS PFHpS (Figure S5-1). Since neither TFA nor PFPA were measured in the virgin sludge, the presence of these compounds in the top sand cap are evidence of the breakdown of larger PFAS. Similar to the base case tests, the presence of PFAS in the sand cap demonstrate recondensation occurring.

CaO Tests

For both CaO tests, only TFA (2C) was measured in the ash and additionally PFPA (3C) in the sand cap (Figure S5-2). The concentration of TFA was higher in the sand cap than ash for both tests. The lower CaO test had a higher fraction of PFCA in the sand cap (II-2-1: 42% TFA, 58% PFCA) than the higher CaO test (II-2-2: 68% TFA, 22% PFCA). Overall, smouldering resulted in a 99% reduction in PFAS in the ash from both II-2-1 and II-2-2. Similar to the base cases and high MC/GAC tests, recondensation of PFAS occurred in the sand cap.

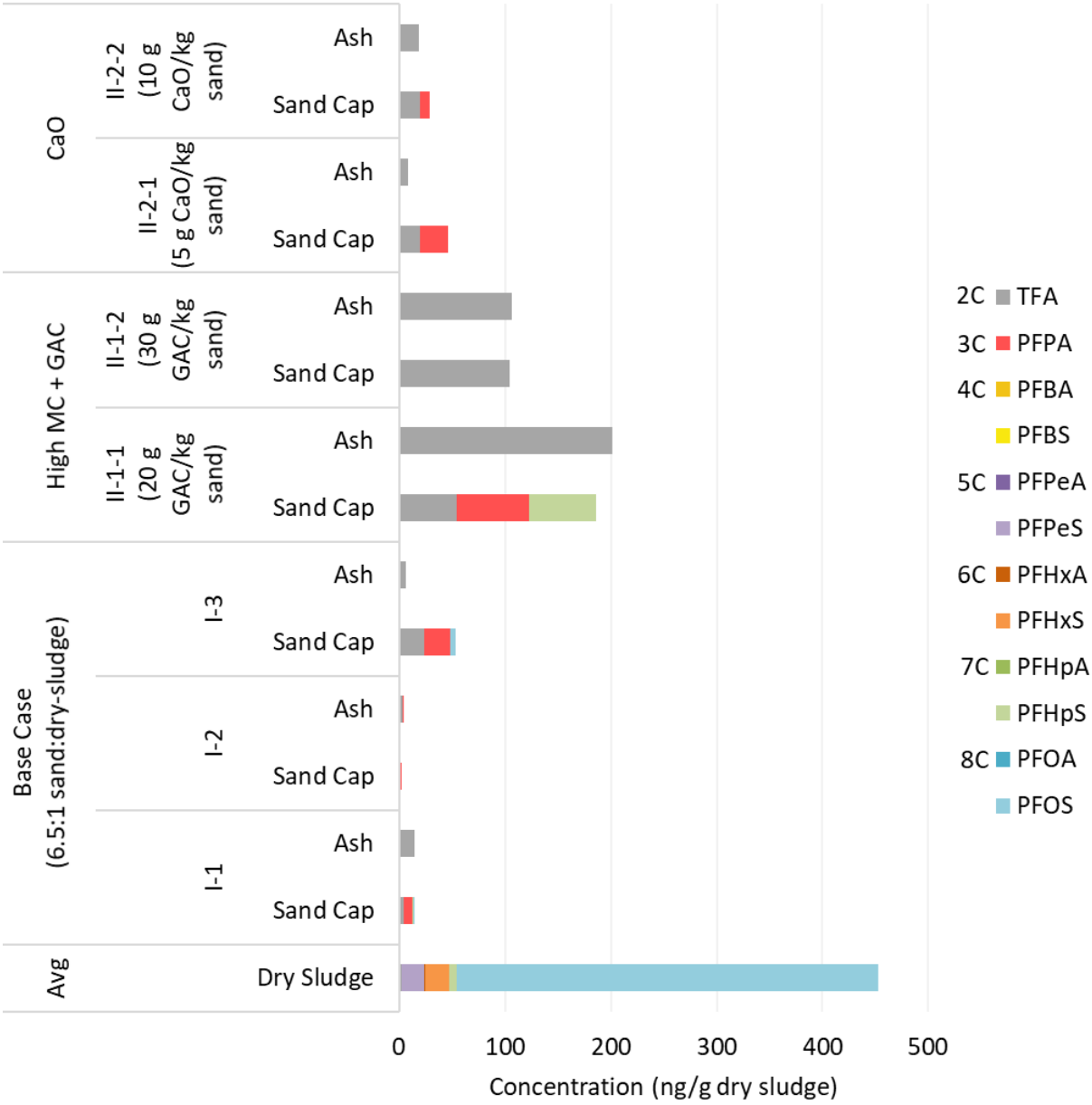

206

207 *Figure S5-1: Content of 12 PFAS originally present in the dried sludge utilized for the LAB smouldering tests and the post-treatment*
208 *ashes normalized per mass of dried sludge. The content in the top sand cap have been presented with the content in the post-*
209 *treatment ash. All base cases have been presented separately.*

210

211

212

213

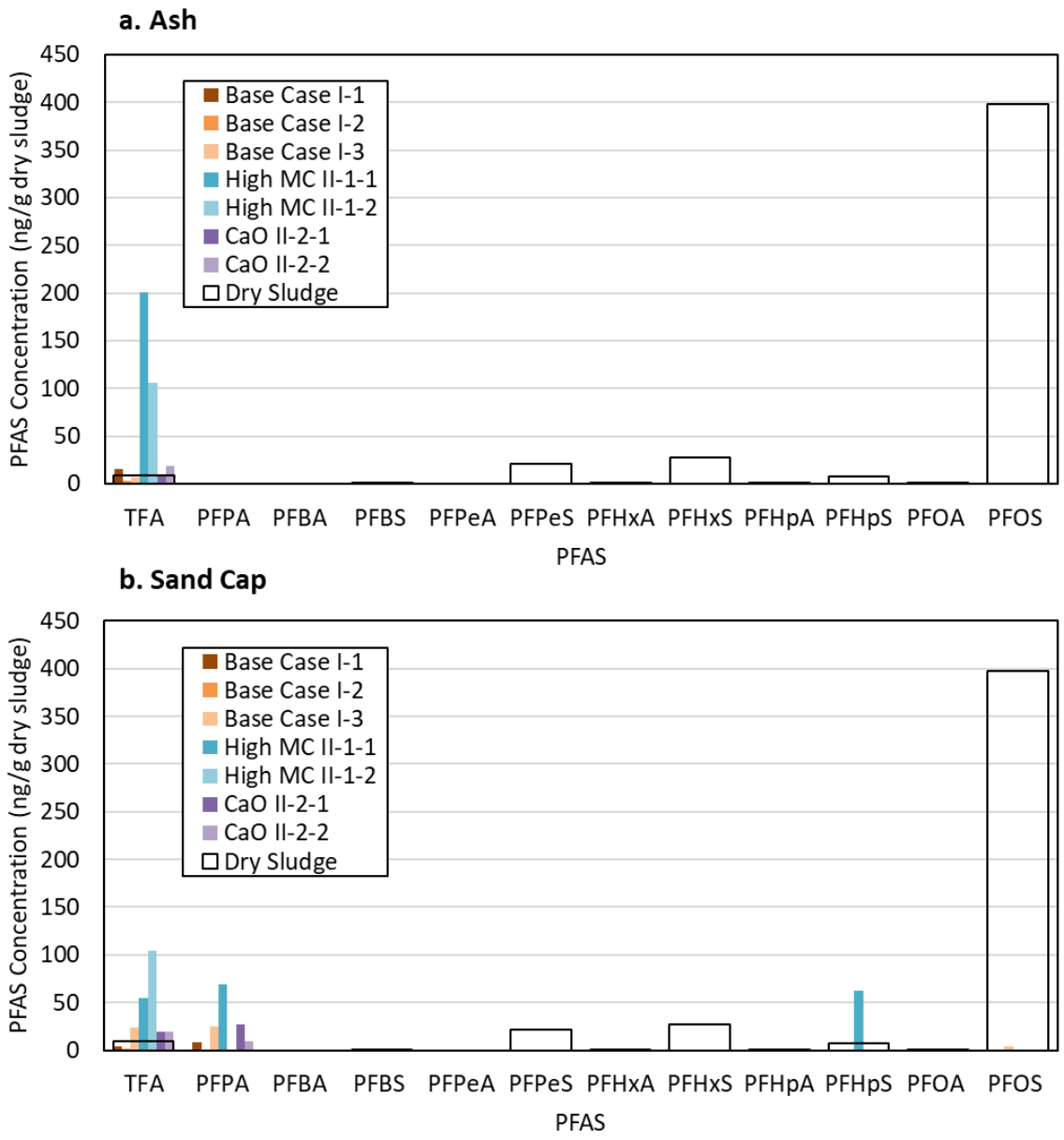

Figure S5-2: The content of 12 PFAS originally present in the sludge are compared to the content in a. the post-treatment ash, and b. the top sand cap. The solid columns present the PFAS content observed during each LAB test and the outlined columns show the original content in the sludge. All values have been normalized per mass of dried sludge.

S6. PFAS in emissions

The GAC in the second absorbent tube (XAD 2) often contained more PFAS than the first absorbent tube (XAD 1), likely due to breakthrough (Figure S6-1). Bio-oil/condensate breakthrough from XAD 1 to XAD 2 was observed during every test. This is an argument for designing a different emissions capture system especially for high MC/condensable fuels. Comparatively, the PFAS content from XAD 1 rinse was consistently higher than XAD 2. Since XAD 1 tended to capture most of the bio-oil/condensate from the tests, the rinse procedure recovered more PFAS from this absorbent tube.

The emissions from the base case tests contain the highest quantities (by mass) of PFOS and PFOA (Figure S6-3). PFOA makes up the largest mass fraction in the emissions from I-1 (68%) and I-2 (65%), while PFOS makes up the largest mass fraction in I-3 (87%) (Figure S6-2).

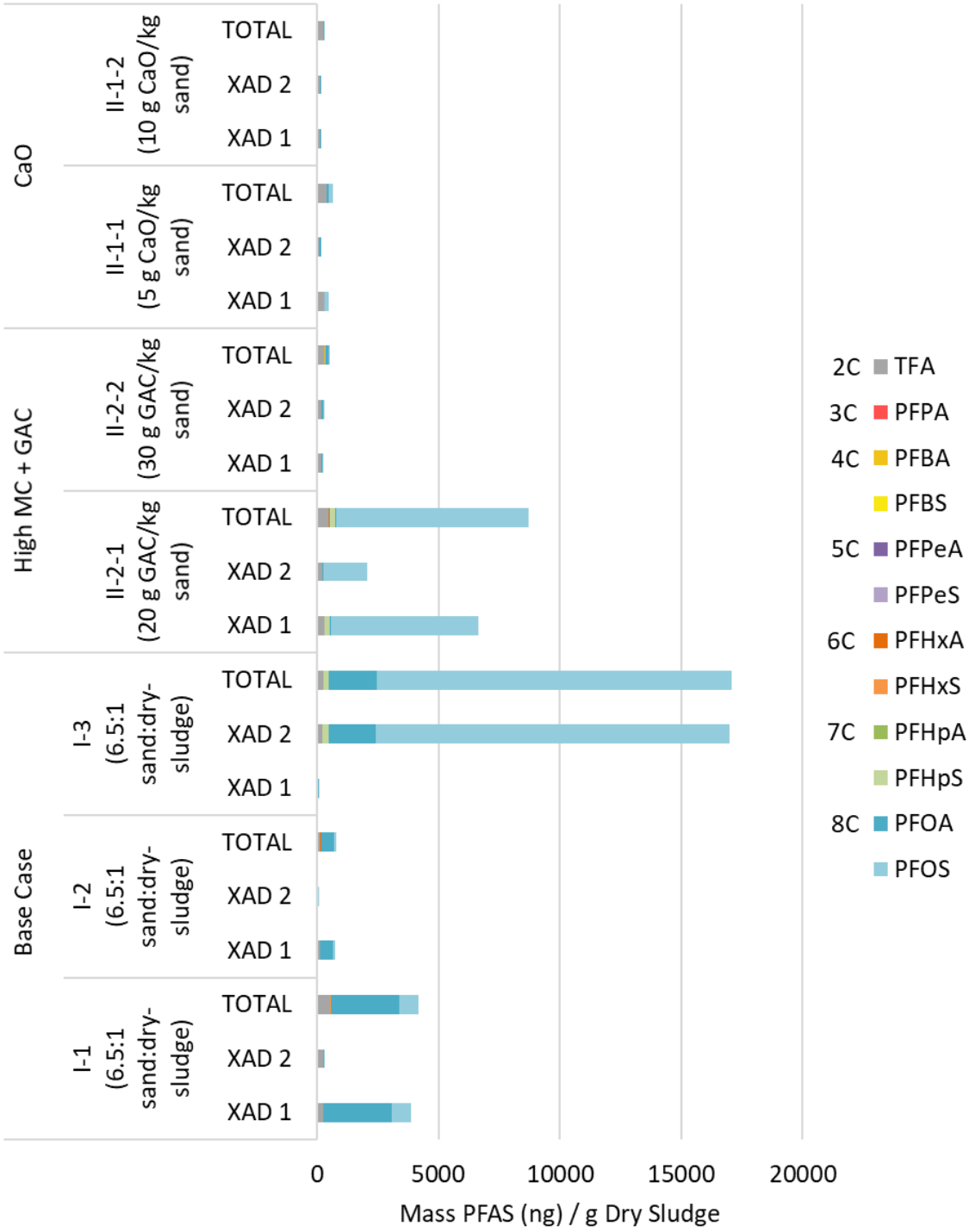

232

233 *Figure S6-1: Content of 12 PFAS in the emissions during smouldering compared to the content originally present in the dried sludge.*
234 *The PFAS content in the two XAD tubes which collected the emissions are presented in addition to the total content. The results*
235 *from the base case tests are presented separately. The contents in the emissions have been normalized to account for differences*
236 *between the experiments.*

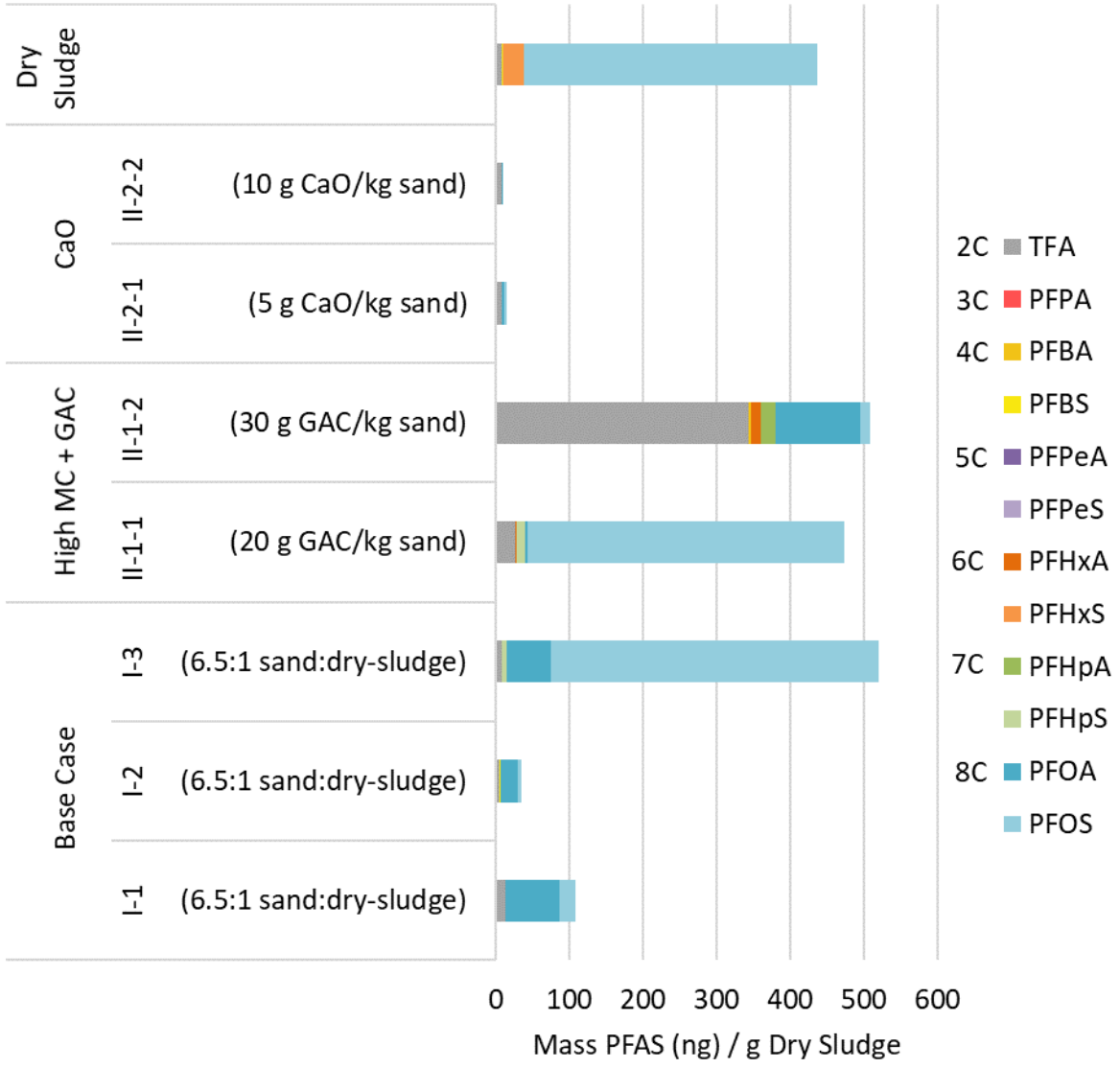

237

238 *Figure S6-2: Content of 12 PFAS in the emissions during smouldering compared to the content originally present in the dried sludge.*
239 *The contents in the emissions have been normalized to account for differences between the experiments. Results from each base*
240 *case test are presented separately.*

241

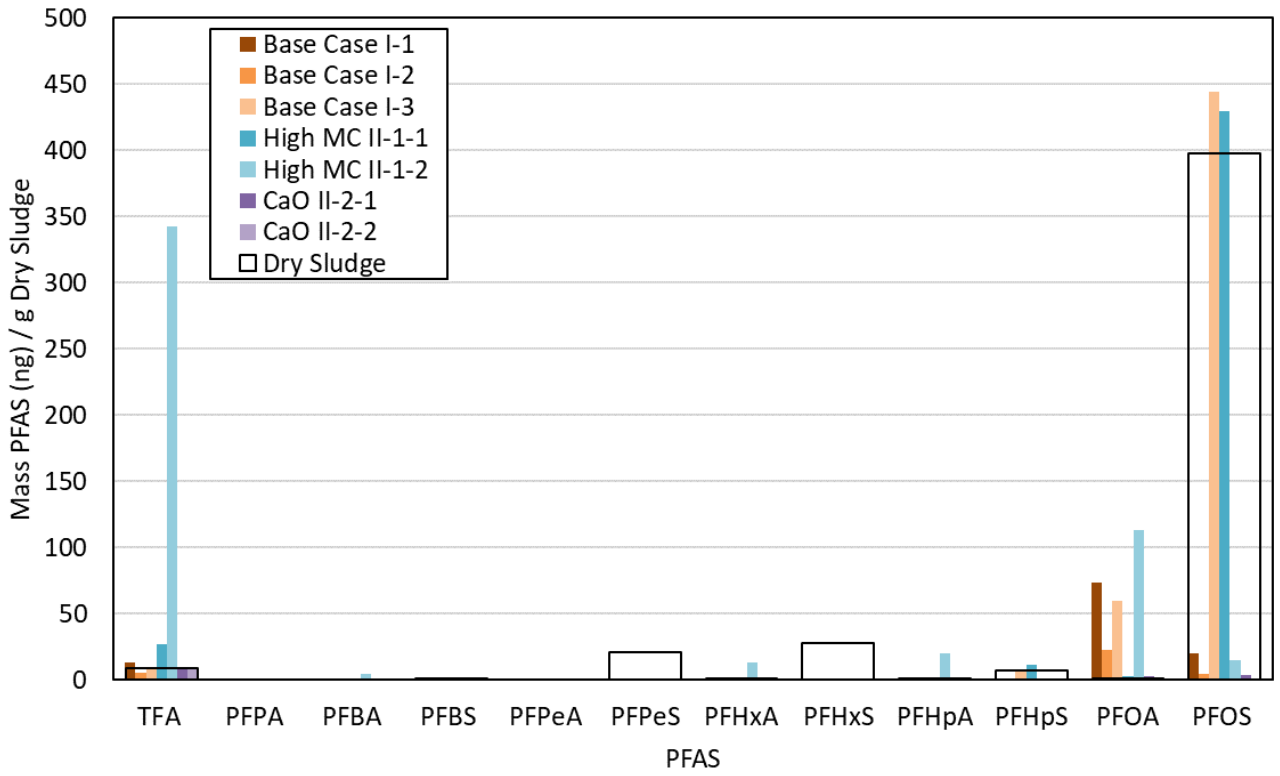

Figure S6-3: The content of 12 PFAS originally present in the sludge are compared to the content in the emissions. The solid columns present the PFAS content observed during each LAB test and the outlined columns show the original content in the sludge. The contents in the emissions have been normalized to account for differences between the experiments. Results from each base case test are shown.

S7. Defluorination

Impingers 1 and 2 contained the highest quantities of HF collected from the emissions (Figure S7-1 & Figure S7-2). There was still breakthrough and measurable amounts in impingers 3 and 4, as well as residual on the glassware (exceeding quantities in impingers 3 and 4) that was recovered by rinsing.

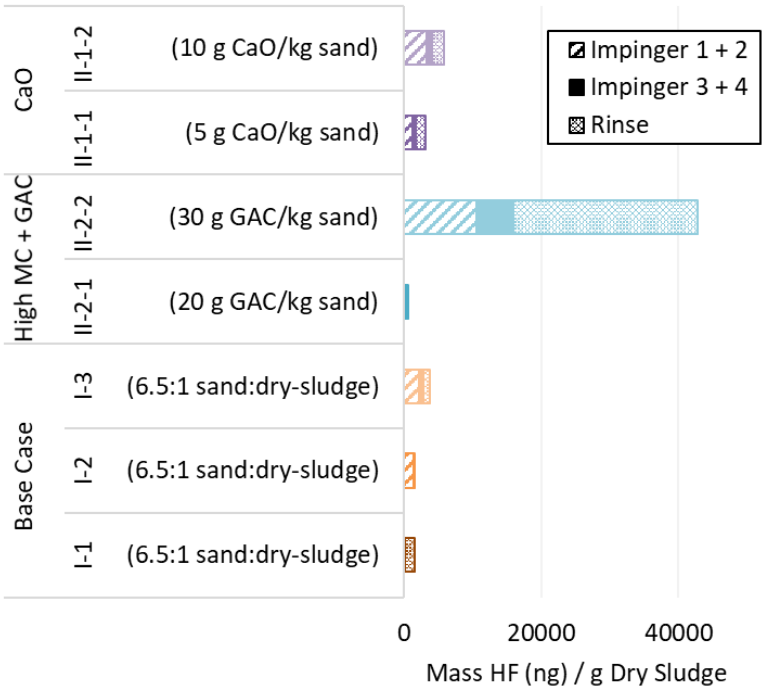

Figure S7-1: HF content measured in the emissions from each laboratory smouldering experiment. The contents collected from two sections of the glassware sampling train and additionally the glassware rinse have been presented separately. The results from each base case have also been presented. The contents in the emissions have been normalized to account for differences between the experiments.

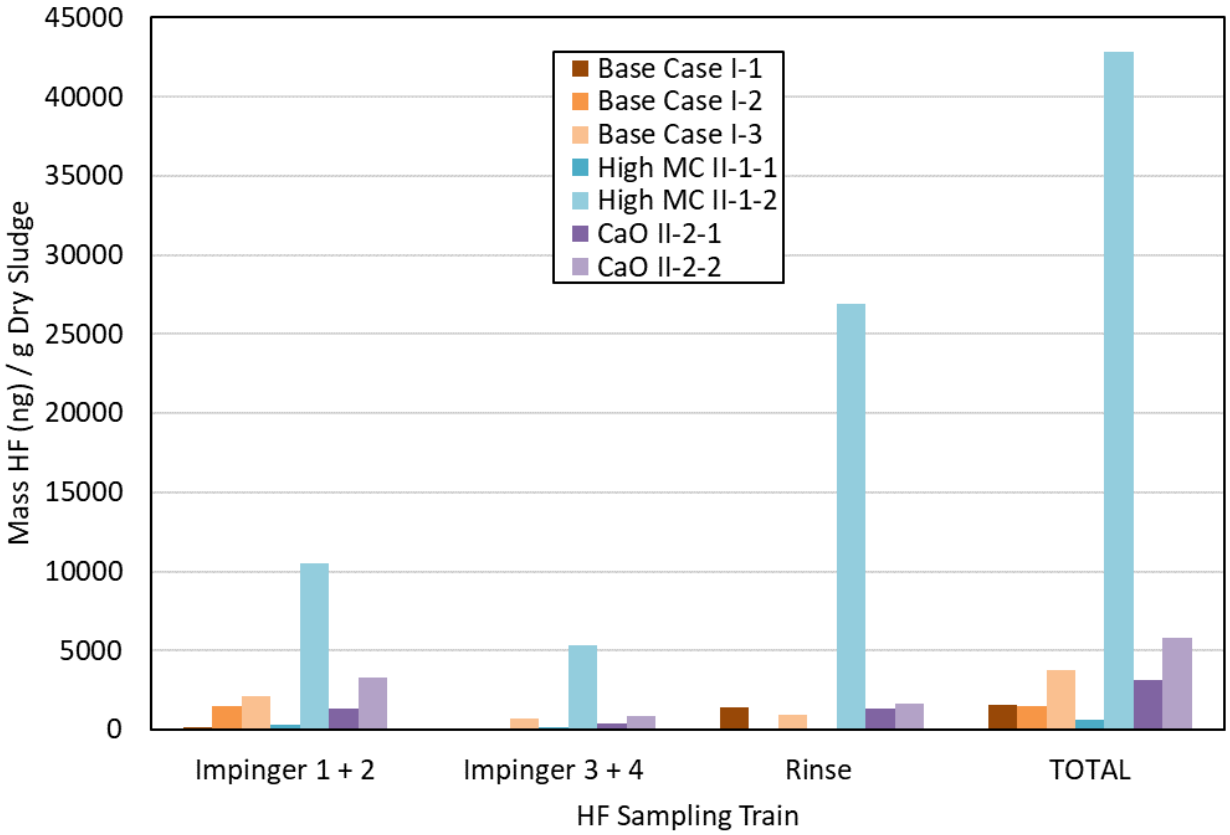

Figure S7-2: HF content measured in the emissions from each laboratory smouldering experiment. The contents collected from two sections of the glassware sampling train and the glassware rinse have been presented separately. In addition, the total content is shown. The results from each base case have also been presented. The contents in the emissions have been normalized to account for differences between the experiments.

S8. Normalization Derivation

Nomenclature

Latin Letters

A_C	Cross sectional area, m^2
Ash	Ash content, %
m/m	Mass ratio, -
$\dot{m}$	Mass flux, kg s^{-1}
m_{em}	Mass of emissions sample, ng
M_{air}	Molar mass of air, kg mol^{-1}
MC	Moisture content, %
P	Pressure, Pa
R	Universal gas constant, m^3 Pa mol^{-1} K^{-1}
T	Temperature, K
$\vec{v}$	Air flow velocity, m s^{-1}
$\vec{v}_{oxid}$	Smouldering propagation velocity, m s^{-1}
$\dot{V}$	Volumetric air flux, m^3 s^{-1}
V_{em}	Volume of emissions sample, m^3

Greek Symbols

ρ	Density, kg m^{-3}

Subscripts

$bulk$	Volume averaged
des	Destroyed fuel
dry	Dry fuel
$fuel$	Fuel
in	Into the reactor
NTP	Conditions at normal temperature and pressure
out	Out of the reactor

Mass Out:

The mass flux out of the reactor is calculated to be a conservatively high estimate of the PFAS leaving the system. The following equations assume that all sewage sludge is destroyed during smouldering, i.e., only inorganic ash and sand remains in the reactor post-treatment. The mass flux out of the system is assumed to be the sum of the mass flux into the reactor and the dry mass destroyed during smouldering, given in Equation (1):

$$\dot{m}_{out}\left[\frac{kg}{s}\right] = \dot{m}_{in}\left[\frac{kg}{s}\right] + \dot{m}_{des}\left[\frac{kg}{s}\right] \quad (1)$$

Airflow Volume Flux:

The airflow volume flux of the system is the product of the air flux and the reactor area. The size of the reactor varies from a radius of 0.3 m at the DRUM scale, to 0.075 m at the LAB scale. For the volume flux into the reactor, the air flux is based on the air flow rate into the base of the column, given in Equation (2):

$$\dot{V}_{in}\left[\frac{m^3}{s}\right] = \vec{v}\left[\frac{m}{s}\right] \cdot A_C[m^2] \quad (2)$$

The mass destroyed is related to the total mass lost per time. Therefore, the airflow volume flux is a function of the smouldering front propagation velocity upwards through the reactor, given in Equation (3):

$$\dot{V}_{des}\left[\frac{m^3}{s}\right] = \vec{v}_{oxid}\left[\frac{m}{s}\right] \cdot A_C[m^2] \quad (3)$$

Mass In:

The ideal gas law was used to determine the mass flux into the system, given in Equation (4):

$$\dot{m}_{in}\left[\frac{kg}{s}\right] = \frac{\dot{V}_{in}\left[\frac{m^3}{s}\right] P_{NTP}[Pa]}{R\left[\frac{m^3 \cdot Pa}{mol \cdot K}\right] \cdot T_{NTP}[K]} \cdot \left(M_{air}\left[\frac{kg}{mol}\right]\right) \quad (4)$$

The airflow into the reactor was assumed to be at normal temperature and pressure conditions. The molar mass of air was used to convert the ideal gas law constant from a molarity to a mass.

Substituting Equation (2) into Equation (4) gives an equation for the mass flux into the reactor in terms of the airflow rate into the reactor and the area of the column, given by Equation (5):

$$\dot{m}_{in}\left[\frac{kg}{s}\right] = \frac{\vec{v}\left[\frac{m}{s}\right] \cdot A_C[m^2] \cdot P_{NTP}[Pa]}{R\left[\frac{m^3 \cdot Pa}{mol \cdot K}\right] \cdot T_{NTP}[K]} \cdot \left(M_{air}\left[\frac{kg}{mol}\right]\right) \quad (5)$$

Dry Bulk Density:

The bulk density of each fuel mixture was determined for each test. Since the moisture content of the sewage sludge varied for each test, the bulk density was converted to dry bulk density to account for the difference and is given in Equation (6):

$$\rho_{dry\ bulk}\left[\frac{kg}{m^3}\right] = \frac{\rho_{bulk}\left[\frac{kg}{m^3}\right]}{\left(1+\frac{m_w}{m_s}\right)} = \frac{\rho_{bulk}\left[\frac{kg}{m^3}\right]}{\left(1+\frac{MC_{fuel}\,[\%]}{100\%}\right)} \quad (6)$$

Dry Mass Destroyed:

The dry mass destroyed is a function of the rate that the smouldering front moves up the column and the dry bulk density of the fuel, given in Equation (7):

$$\dot{m}_{des}\left[\frac{kg}{s}\right] = \dot{V}_{des}\left[\frac{m^3}{s}\right] \cdot \rho_{dry\ bulk}\left[\frac{kg}{m^3}\right] \quad (7)$$

Substituting Equation (3) and Equation (7) into Equation (8) gives an equation for the dry mass destroyed in terms of the smouldering velocity, area of the reactor, bulk density and moisture content of the fuel, given by Equation (8):

$$\dot{m}_{des}\left[\frac{kg}{s}\right] = \vec{v}_{oxid}\left[\frac{m}{s}\right] \cdot A_C[m^2] \cdot \frac{\rho_{bulk}\left[\frac{kg}{m^3}\right]}{\left(1+\frac{MC_{fuel}\,[\%]}{100\%}\right)} \quad (8)$$

Considering Sand-to-Sludge Ratio and Ash Content:

The dry bulk density of the fuel considers the mixture of silica sand with sewage sludge. Since only the sewage sludge is destroyed during smouldering, the mass destroyed should be normalized to the sewage sludge content by considering the sand-to-sludge ratio (on a dry mass basis) for each test. Furthermore, since not all the sewage sludge is destroyed during smouldering, i.e., some amount of ash remains, the dry mass destroyed should also be normalized to the ash content of the sewage sludge. Equation (8) can therefore be rewritten to include the sand-to-sludge ratio, and the ash content of the sewage sludge, given in Equation (9):

$$\dot{m}_{des}\left[\frac{kg}{s}\right] = \vec{v}_{oxid}\left[\frac{m}{s}\right] \cdot (A_C)[m^2] \cdot \frac{\rho_{bulk}\left[\frac{kg}{m^3}\right]}{\left(1+\frac{MC_{Fuel}\,[\%]}{100\%}\right)} \cdot \left(m/m\left[\frac{kg}{kg}\right]\right)_{dry} \cdot \left(\frac{Ash_{fuel}[\%]}{100\%}\right) \quad (9)$$

Volume Out of Reactor:

The air volume flux out of the reactor can be determined by rearranging the ideal gas law, given by Equation (10):

$$\dot{V}_{out}\left[\frac{m^3}{s}\right] = \frac{\dot{m}_{out}\left[\frac{kg}{s}\right] \cdot R\left[\frac{m^3 \cdot Pa}{mol \cdot K}\right] \cdot T_{out}\ [K]}{P_{out}[Pa]} \cdot \left(\frac{1}{M_{air}}\left[\frac{mol}{kg}\right]\right) \quad (10)$$

The temperature of emissions leaving the column is taken from the highest thermocouple measurement within the column, above the fuel pack i.e., the closest thermocouple to the PFAS and HF sampling trains. An average temperature is used. The pressure of the emissions is corrected to the temperature leaving the column. Again, the molar mass of air is used to convert the ideal gas constant from a molarity to mass.

Normalized PFAS Measurement:

Finally, the PFAS and HF samples collected from the emissions leaving the reactor can be scaled to approximate the total mass of PFAS and HF released from smouldering sewage sludge. The mass quantity of both PFAS and HF in the emissions, m_{PFAS} [ng] and m_{HF} [ng], respectively, were quantified per volume of emissions sample, V_{PFAS} [m^3] and V_{HF} [m^3], for each test. Multiplying this concentration by the volume flux out of the reactor provides an approximation of the PFAS and HF released from the system, given by Equation (11):

$$\dot{m}_{PFAS,Total}\left[\frac{ng}{s}\right] = \frac{m_{PFAS}\ [pg]}{\dot{V}_{em}\ [m^3]} \cdot \dot{V}_{out}\left[\frac{m^3}{s}\right] \quad (11)$$

The PFAS and HF flux can then be normalized to the dry mass destroyed during smouldering to approximate the mass of both PFAS and HF leaving the system per mass of dry sludge, given in Equation (12):

$$m_{em,Total}\left[\frac{ng}{g_{dry\ fuel}}\right] = \frac{m_{em}\ [pg]}{\dot{V}_{em}\ [m^3]} \cdot \frac{\dot{V}_{out}\left[\frac{m^3}{s}\right]}{\dot{m}_{des}\left[\frac{kg}{s}\right]} \frac{[kg]}{1000\ [g]} \quad (12)$$

S9. Mineral Analyses

X-ray diffractometer (XRD) analysis was performed on the post-treatment ash from I-1, II-2-1, II-2-2, and III-1 tests to evaluate the use of calcium to mineralize fluorine from the sludge. A powder XRD technique was utilized. Scanning Electron Microscopy coupled with Energy Dispersive X-ray (SEM/EDX) Spectroscopy was performed in addition to XRD analysis, to assist in results interpretation. This analysis was performed by Surface Science Western using The Rigaku SmartLab.

X-ray diffractometer (XRD)

Table S9-1: Instrument Specifications and Operating Conditions for XRD Analysis

Instrumentation	
X-ray Diffractometer (XRD)	Rigaku SmartLab
X-ray Detector	2D HyPix-3000 (Horizontal)
X-ray Tube	2.2 kW long-fine focus Cu- X-ray
Goniometer	Inplane Goniometer
Attachment	Standard Attachment Head
Filter	Kβ Filter for Cu
Operating Conditions	
X-Ray Generator	40 kV 40 mA
Scan Speed	4.00° /min
Step Width	0.02°
Scan Axis	θ/2θ
Scan Range	8° to 90°
Incident Slit Box	2/3°
Length-Limiting Slit	10 mm
Analysis Tools	
Analysis Software	Crystallinity determination module
Databases	1) PDF-4+ Database 2) Crystallography Open Database (COD) 3) FIZ/NIST Inorganic Crystal Structure Database (ICSD)

Scanning Electron Microscopy Coupled with Energy Dispersive X-ray (SEM/EDX) Spectroscopy

Table S9-2: Instrument Specifications and Operating Conditions for SEM/EDX Analysis

Hitachi SU8230 Regulus Ultra High-Resolution Field Emission SEM	
Resolution	3 nm at 30 kV (high vacuum mode) 4 nm at 30 kV (low vacuum mode)
Pressure	Variable (~6 – 650 Pa)
Imaging Modes	1) secondary electron (SE) detector 2) multi-segment solid-state backscattered electron (BSE) detector 3) SE equivalent variable pressure (UVD) detector
Drift Detector	X-Max 50mm2 Silicon Drift Detector with 127 eV resolution (Peltier cooling)
Analysis Software	AZtecFeature Automated Analysis
Detection Limit	~0.5 weight % (*for most elements)
Bruker X-Flash FQ5060 Annular Quad EDX detector	
Solid Angle	1.1 sr
Detector	Annular four channel detector with 60 mm^2 active area
Energy Resolution	127 eV
Analysis Software	ESPRIT
Bruker X-Flash 6160 EDX detector	
Active Area	60 mm^2
Energy Resolution	125 eV
Analysis Software	ESPRIT

XRD Results: I-1

Table S9-3: XRD Peak List for Test I-1 showing only major phases detected.

No.	2θ, °	d, Å	Height, counts	FWHM, °	Int. I., counts°	Int. W., °	Asymmetry	Decay(ηL/mL)	Decay(ηH/mH)	Size, Å
1	10.92(2)	8.093(15)	255(3)	0.15(3)	57(6)	0.23(3)	1.6(11)	1.3(4)	0.0(8)	561(106)
2	13.717(15)	6.450(7)	413(5)	0.96(6)	714(23)	1.73(8)	0.50(10)	0.2(2)	1.55(7)	87(5)
3	17.126(19)	5.173(6)	457(5)	0.64(5)	619(24)	1.35(7)	3.0(5)	1.55(10)	1.5(2)	132(11)
4	19.41(17)	4.57(4)	200(3)	3.61(16)	771(48)	3.9(3)	1.4(3)	0.0(3)	0.0(3)	23.3(10)
5	20.270(12)	4.377(3)	609(7)	0.46(3)	377(22)	0.62(4)	1.48(15)	0.70(5)	0.51(12)	181(10)

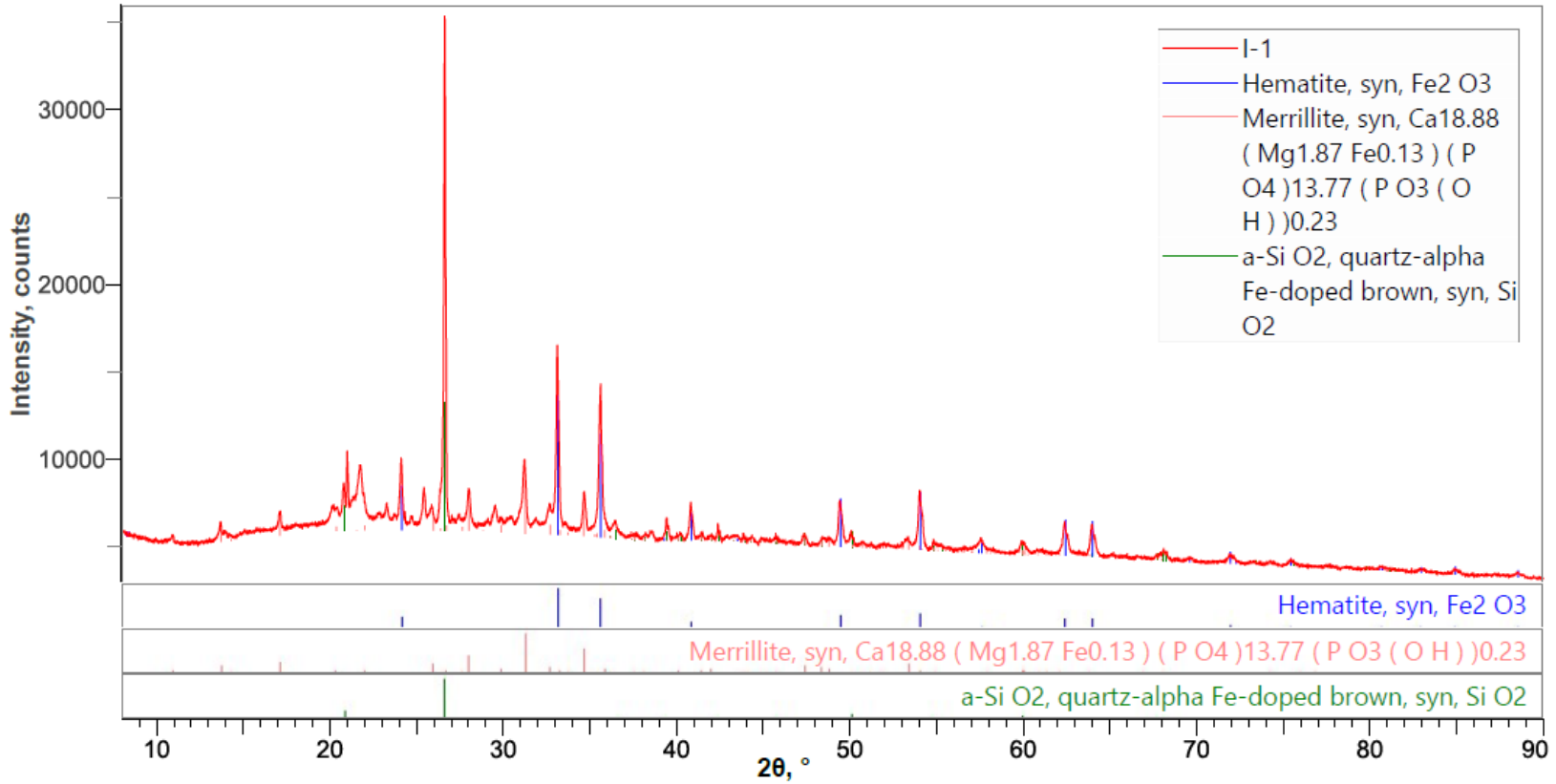

Figure S9-1: XRD Phase Data View for Test I-1 showing only major phases detected.

XRD Results: II-2-1

Table S9-4: XRD Peak List for Test II-2-1 showing only major phases detected.

No.	2θ, °	d, Å	Height, counts	FWHM, °	Int. I., counts°	Int. W., °	Asymmetry	Decay(ηL/mL)	Decay(ηH/mH)	Size, Å
1	13.66(4)	6.480(18)	318(5)	0.66(7)	413(18)	1.30(8)	0.6(2)	1.54(19)	1.34(19)	126(14)
2	17.111(8)	5.178(3)	270(4)	0.14(3)	49(8)	0.18(3)	1.13(2)	0.66(2)	0.559(16)	609(121)
3	17.950(3)	4.9376(8)	8120(66)	0.563(3)	6066(22)	0.747(9)	1.13(2)	0.66(2)	0.559(16)	149.3(7)
4	20.32(2)	4.367(4)	168(3)	0.19(5)	53(9)	0.31(6)	0.9(2)	1.55(15)	0.4(2)	445(112)
5	20.822(5)	4.2626(9)	1705(24)	0.086(7)	244(8)	0.143(7)	0.9(2)	1.55(15)	0.4(2)	976(77)

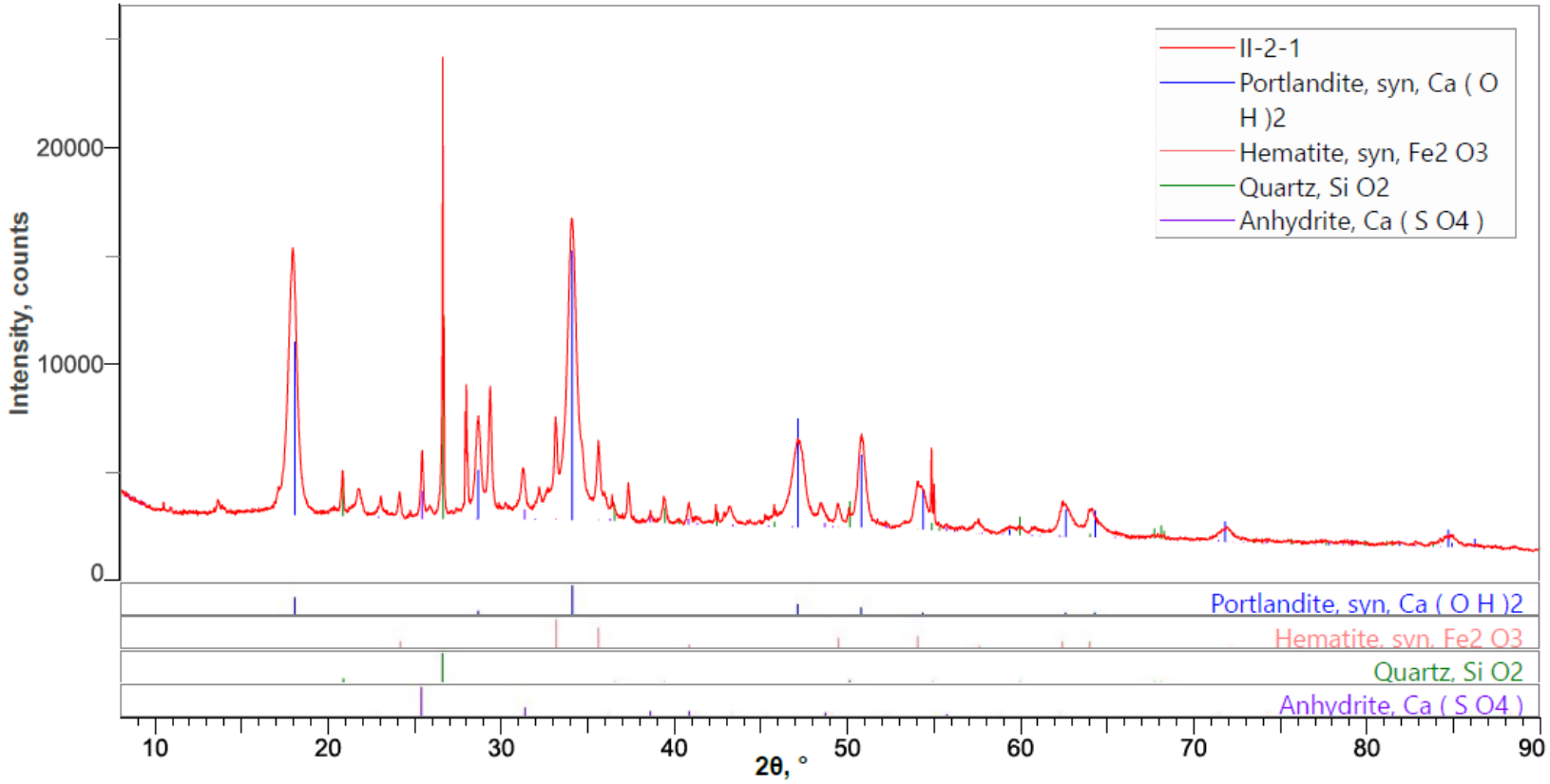

Figure S9-2: XRD Phase Data View for Test II-2-1 showing only major phases detected.

XRD Results: II-2-2

Table S9-5: XRD Peak List for Test II-2-2 showing only major phases detected.

No.	2θ, °	d, Å	Height, counts	FWHM, °	Int. I., counts°	Int. W., °	Asymmetry	Decay(ηL/mL)	Decay(ηH/mH)	Size, Å
1	15.60(5)	5.68(2)	104(3)	0.63(11)	138(11)	1.33(14)	1.5(8)	1.5(2)	1.5(3)	133(24)
2	17.946(2)	4.9387(6)	5728(58)	0.574(2)	4427(10)	0.773(10)	1.083(17)	0.726(11)	0.564(11)	146.4(5)
3	20.825(17)	4.262(3)	127(3)	0.111(18)	17(2)	0.13(2)	2.6(18)	0.5(5)	0.0(10)	758(123)
4	21.79(2)	4.076(4)	218(6)	0.356(19)	110(4)	0.50(3)	1.4(4)	0.72(18)	0.8(2)	237(13)
5	23.032(10)	3.8585(16)	435(11)	0.210(11)	135(3)	0.312(14)	1.9(5)	0.73(11)	1.1(2)	404(21)

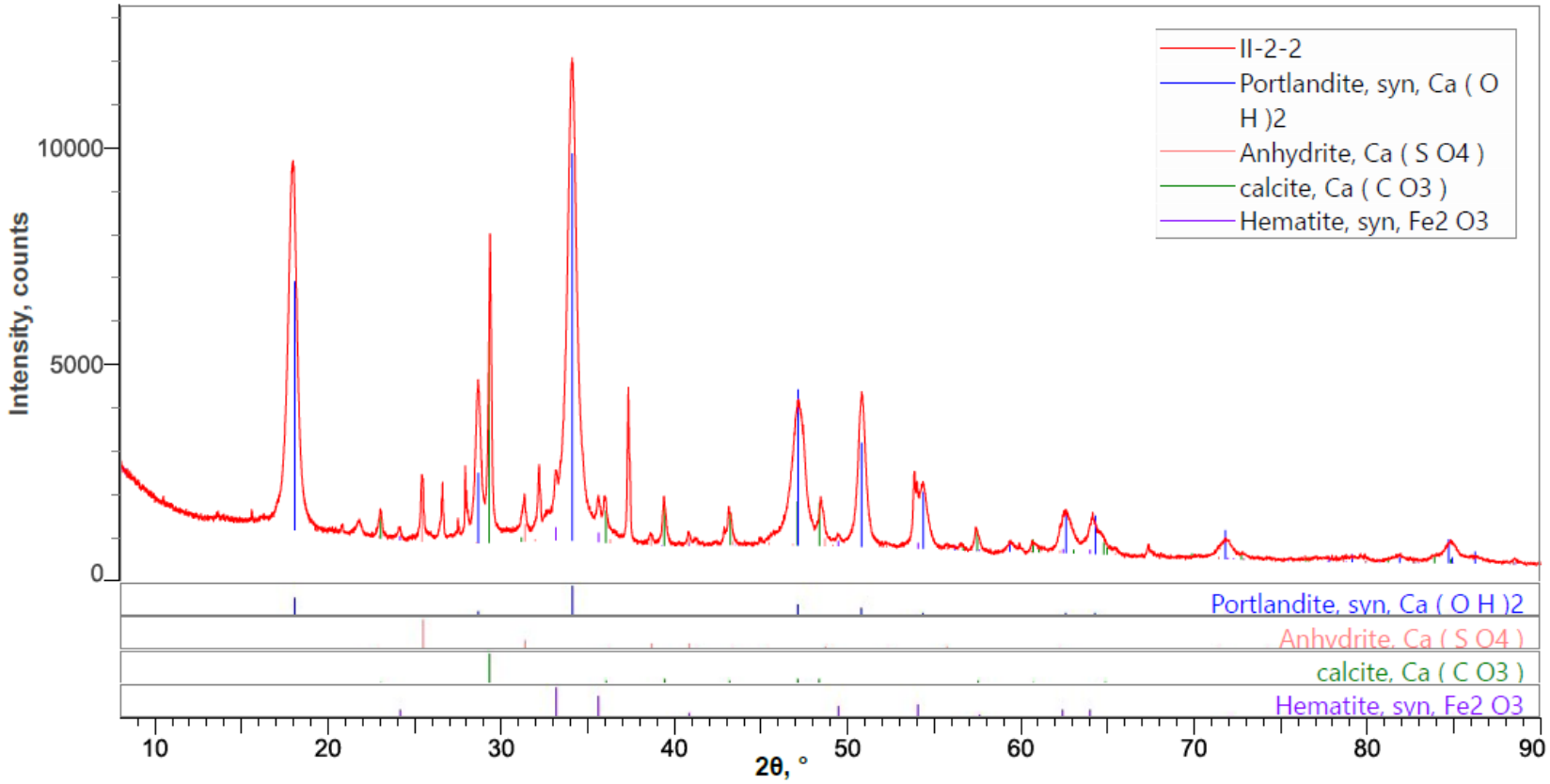

Figure S9-3: XRD Phase Data View for Test II-2-2 showing only major phases detected.

XRD Results: III-1

Table S9-6: XRD Peak List for Test III-1 showing only major phases detected.

No.	2θ, °	d, Å	Height, counts	FWHM, °	Int. I., counts°	Int. W., °	Asymmetry	Decay(ηL/mL)	Decay(ηH/mH)	Size, Å
1	9.415(19)	9.386(19)	430(6)	0.17(3)	115(10)	0.27(3)	4(3)	1.1(3)	0.1(9)	487(80)
2	18.775(12)	4.723(3)	177(3)	0.12(4)	43(6)	0.24(4)	1.3(17)	1.3(4)	1.5(6)	675(192)
3	20.6288(9)	4.30215(18)	3592(37)	0.046(2)	227(10)	0.063(3)	2.05(10)	0.68(3)	0.74(4)	1837(99)
4	20.7995(8)	4.26722(17)	30544(148)	0.0854(9)	3587(19)	0.1174(12)	2.05(10)	0.68(3)	0.74(4)	988(10)
5	21.82(2)	4.070(4)	256(4)	0.82(7)	288(18)	1.12(9)	2.05(10)	0.68(3)	0.74(4)	104(9)

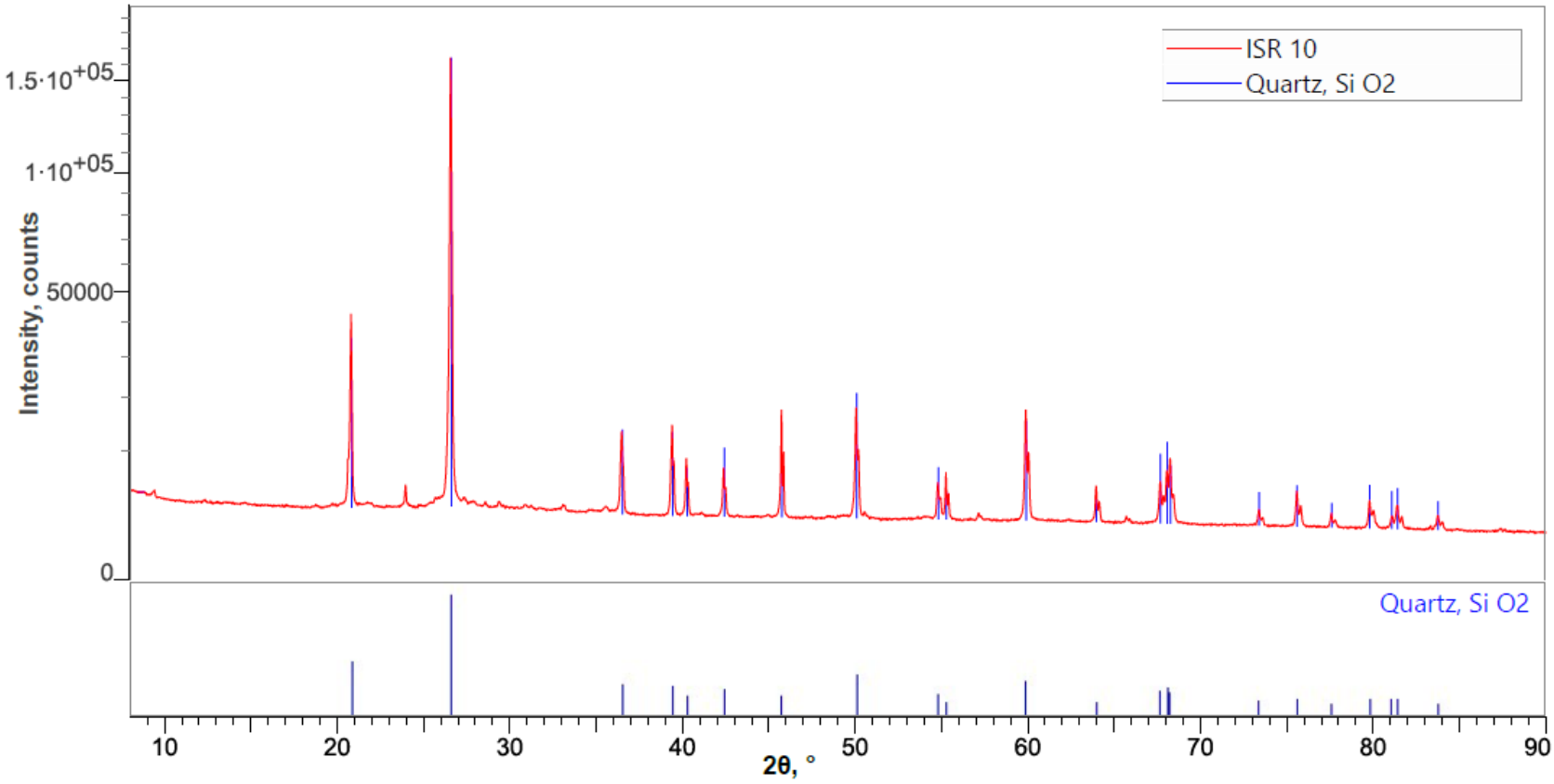

Figure S9-4: XRD Phase Data View for Test III-1 showing only major phases detected.

EDX Results

Table S9-7: SEM/EDX Results in Weight Percent

Sample	Elemental Concentration (weight %)															
	C	O	Na	Mg	Al	Si	P	S	Cl	K	Ca	Ti	Mn	Fe	Cu	F
I-1																
1	11.7	44.2	0.6	0.8	1.7	9.0	7.0	0.5	*B.D.L.*	0.6	7.1	0.5	*B.D.L.*	16.3	0.2	*B.D.L.*
2	7.9	39.4	*B.D.L.*[1]	1.2	1.7	4.8	5.7	*B.D.L.*	*B.D.L.*	0.7	5.5	0.9	*B.D.L.*	32.3	*B.D.L.*	*B.D.L.*
3	8.3	43.7	0.5	1.1	1.9	6.3	7.7	0.5	*B.D.L.*	0.7	6.8	0.5	*B.D.L.*	22.0	*B.D.L.*	*B.D.L.*
4	11.5	54.3	0.3	0.2	0.8	26.0	1.3	*B.D.L.*	*B.D.L.*	0.4	1.5	0.1	*B.D.L.*	3.6	*B.D.L.*	*B.D.L.*
5	10.6	53.3	0.2	0.3	0.5	24.9	1.7	*B.D.L.*	*B.D.L.*	0.3	1.9	0.1	*B.D.L.*	6.3	*B.D.L.*	*B.D.L.*
6	7.2	31.5	*B.D.L.*	0.5	0.9	4.0	7.8	*B.D.L.*	*B.D.L.*	1.1	6.7	0.3	*B.D.L.*	40.0	*B.D.L.*	*B.D.L.*
7	10.4	43.7	0.9	1.1	3.0	8.6	6.6	0.6	*B.D.L.*	0.9	7.9	0.7	*B.D.L.*	15.6	*B.D.L.*	*B.D.L.*
II-2-1																
1	7.4	48.8	*B.D.L.*	0.4	0.3	0.6	0.4	0.2	*B.D.L.*	*B.D.L.*	40.7	*B.D.L.*	*B.D.L.*	1.2	*B.D.L.*	*B.D.L.*
2	6.7	30.6	0.4	1.1	1.5	5.0	6.5	*B.D.L.*	*B.D.L.*	1.2	17.4	0.9	0.4	28.5	*B.D.L.*	*B.D.L.*
3	11.4	42.6	*B.D.L.*	*B.D.L.*	*B.D.L.*	39.0	*B.D.L.*	0.5	*B.D.L.*	*B.D.L.*	5.2	*B.D.L.*	*B.D.L.*	1.3	*B.D.L.*	*B.D.L.*
4	7.5	42.7	*B.D.L.*	0.7	1.1	3.1	2.3	0.6	0.1	0.4	29.8	0.3	*B.D.L.*	11.4	*B.D.L.*	*B.D.L.*
II-2-2																
1	5.9	44.4	*B.D.L.*	0.2	0.1	0.2	0.3	0.8	0.2	*B.D.L.*	47.4	*B.D.L.*	*B.D.L.*	0.6	*B.D.L.*	*B.D.L.*
2	13.6	44.6	0.6	0.7	1.5	8.1	5.6	1.1	0.1	1.0	9.1	0.5	*B.D.L.*	13.5	*B.D.L.*	*B.D.L.*
3	7.4	49.7	*B.D.L.*	0.5	0.2	0.3	0.3	0.3	0.1	*B.D.L.*	40.6	*B.D.L.*	*B.D.L.*	0.8	*B.D.L.*	*B.D.L.*
4	7.7	44.8	*B.D.L.*	0.4	0.4	1.0	1.0	0.6	0.1	0.2	41.4	*B.D.L.*	*B.D.L.*	2.5	*B.D.L.*	*B.D.L.*
III-1																
1	10.5	52.6	0.1	0.3	1.0	32.7	0.4	0.2	*B.D.L.*	0.3	0.5	*B.D.L.*	*B.D.L.*	1.4	*B.D.L.*	*B.D.L.*
2	11.7	53.5	*B.D.L.*	0.3	1.7	30.5	0.2	0.2	*B.D.L.*	0.4	0.4	0.2	*B.D.L.*	1.0	*B.D.L.*	*B.D.L.*
3	10.2	46.2	0.4	1.0	2.0	19.4	3.3	1.2	0.2	0.8	4.9	0.2	*B.D.L.*	10.2	*B.D.L.*	*B.D.L.*
4	10.9	46.7	0.3	0.9	2.1	17.9	3.2	0.9	0.2	0.9	4.3	0.3	*B.D.L.*	11.2	*B.D.L.*	*B.D.L.*
5	10.7	44.7	0.4	0.9	2.3	17.2	3.8	1.0	0.2	1.0	5.3	0.3	*B.D.L.*	12.3	*B.D.L.*	*B.D.L.*
6	20.8	44.8	0.4	0.8	1.8	15.8	2.9	0.6	*B.D.L.*	0.9	3.5	0.1	*B.D.L.*	7.6	*B.D.L.*	*B.D.L.*

[1] Below instrument detection limit

414 *Table S9-8: SEM/EDX Results in Atomic Percent*

Sample	Elemental Concentration (atomic %)															
	C	O	Na	Mg	Al	Si	P	S	Cl	K	Ca	Ti	Mn	Fe	Cu	F
I-1																
1	1.0	2.8	0.03	0.03	0.06	0.3	0.2	0.01	*B.D.L.*	0.01	0.2	0.01	*B.D.L.*	0.3	0.003	*B.D.L.*
2	0.7	2.5	*B.D.L.*[1]	0.05	0.06	0.2	0.2	*B.D.L.*	*B.D.L.*	0.02	0.1	0.02	*B.D.L.*	0.6	*B.D.L.*	*B.D.L.*
3	0.7	2.7	0.02	0.04	0.07	0.2	0.2	0.02	*B.D.L.*	0.02	0.2	0.01	*B.D.L.*	0.4	*B.D.L.*	*B.D.L.*
4	1.0	3.4	0.01	0.01	0.03	0.9	0.04	*B.D.L.*	*B.D.L.*	0.01	0.04	0.003	*B.D.L.*	0.1	*B.D.L.*	*B.D.L.*
5	0.9	3.3	0.01	0.01	0.02	0.9	0.1	*B.D.L.*	*B.D.L.*	0.01	0.05	0.002	*B.D.L.*	0.1	*B.D.L.*	*B.D.L.*
6	0.6	2.0	*B.D.L.*	0.02	0.03	0.1	0.3	*B.D.L.*	*B.D.L.*	0.03	0.2	0.01	*B.D.L.*	0.7	*B.D.L.*	*B.D.L.*
7	0.9	2.7	0.04	0.05	0.11	0.3	0.2	0.02	*B.D.L.*	0.02	0.2	0.01	*B.D.L.*	0.3	*B.D.L.*	*B.D.L.*
II-2-1																
1	0.6	3.1	*B.D.L.*	0.02	0.01	0.02	0.01	0.01	*B.D.L.*	*B.D.L.*	1.0	*B.D.L.*	*B.D.L.*	0.02	*B.D.L.*	*B.D.L.*
2	0.6	1.9	0.02	0.05	0.06	0.2	0.2	*B.D.L.*	*B.D.L.*	0.03	0.4	0.02	0.01	0.5	*B.D.L.*	*B.D.L.*
3	0.9	2.7	*B.D.L.*	*B.D.L.*	*B.D.L.*	1.4	*B.D.L.*	0.02	*B.D.L.*	*B.D.L.*	0.1	*B.D.L.*	*B.D.L.*	0.02	*B.D.L.*	*B.D.L.*
4	0.6	2.7	*B.D.L.*	0.03	0.04	0.1	0.1	0.02	0.003	0.01	0.7	0.01	*B.D.L.*	0.2	*B.D.L.*	*B.D.L.*
II-2-2																
1	0.5	2.8	*B.D.L.*	0.01	0.004	0.01	0.01	0.03	0.004	*B.D.L.*	1.2	*B.D.L.*	*B.D.L.*	0.01	*B.D.L.*	*B.D.L.*
2	1.1	2.8	0.03	0.03	0.05	0.3	0.2	0.03	0.002	0.03	0.2	0.01	*B.D.L.*	0.2	*B.D.L.*	*B.D.L.*
3	0.6	3.1	*B.D.L.*	0.02	0.01	0.01	0.01	0.01	0.002	*B.D.L.*	1.0	*B.D.L.*	*B.D.L.*	0.01	*B.D.L.*	*B.D.L.*
4	0.6	2.8	*B.D.L.*	0.02	0.01	0.03	0.03	0.02	0.003	0.00	1.0	*B.D.L.*	*B.D.L.*	0.05	*B.D.L.*	*B.D.L.*
III-1																
1	0.9	3.3	*B.D.L.*	0.01	0.04	1.2	*B.D.L.*	0.01	*B.D.L.*	0.01	0.01	*B.D.L.*	*B.D.L.*	0.03	*B.D.L.*	*B.D.L.*
2	1.0	3.3	*B.D.L.*	0.01	0.06	1.1	*B.D.L.*	0.01	*B.D.L.*	0.01	0.01	0.004	*B.D.L.*	0.02	*B.D.L.*	*B.D.L.*
3	0.9	2.9	0.02	0.04	0.07	0.7	0.1	0.04	0.01	0.02	0.1	0.005	*B.D.L.*	0.2	*B.D.L.*	*B.D.L.*
4	0.9	2.9	0.01	0.04	0.08	0.6	0.1	0.03	0.01	0.02	0.1	0.01	*B.D.L.*	0.2	*B.D.L.*	*B.D.L.*
5	0.9	2.8	0.02	0.04	0.09	0.6	0.1	0.03	0.01	0.02	0.1	0.01	*B.D.L.*	0.2	*B.D.L.*	*B.D.L.*
6	1.7	2.8	0.02	0.03	0.07	0.6	0.1	0.02	*B.D.L.*	0.02	0.1	0.003	*B.D.L.*	0.1	*B.D.L.*	*B.D.L.*

415 [1] Below instrument detection limit

SEM Results: I-1

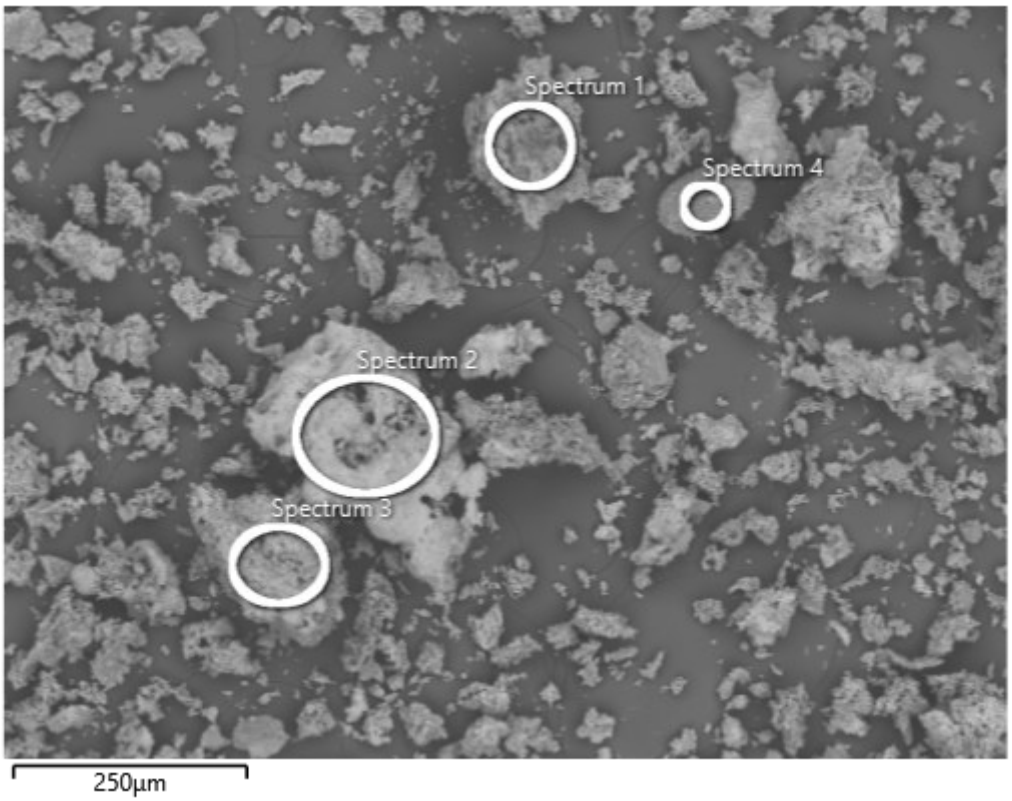

Figure S9-5: The first of two SEM images for Test I-1, taken at the resolution of x120 magnification with a scale of 250 µm.

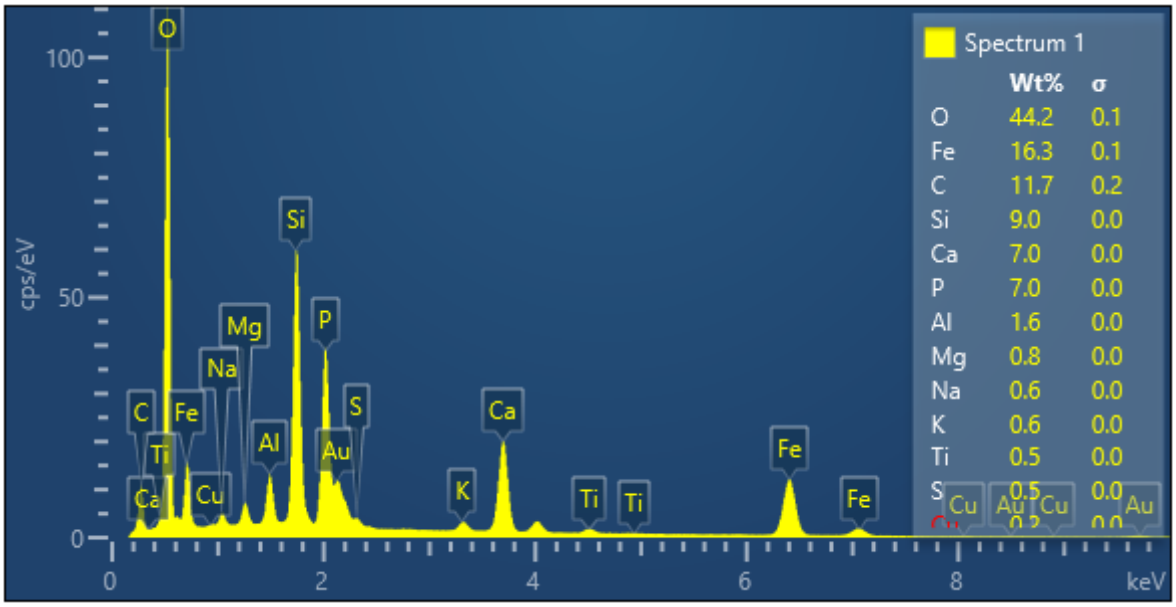

Figure S9-6: The elemental weight percentages for Spectrum 1 of the first SEM image for Test I-1 (Figure S9-5).

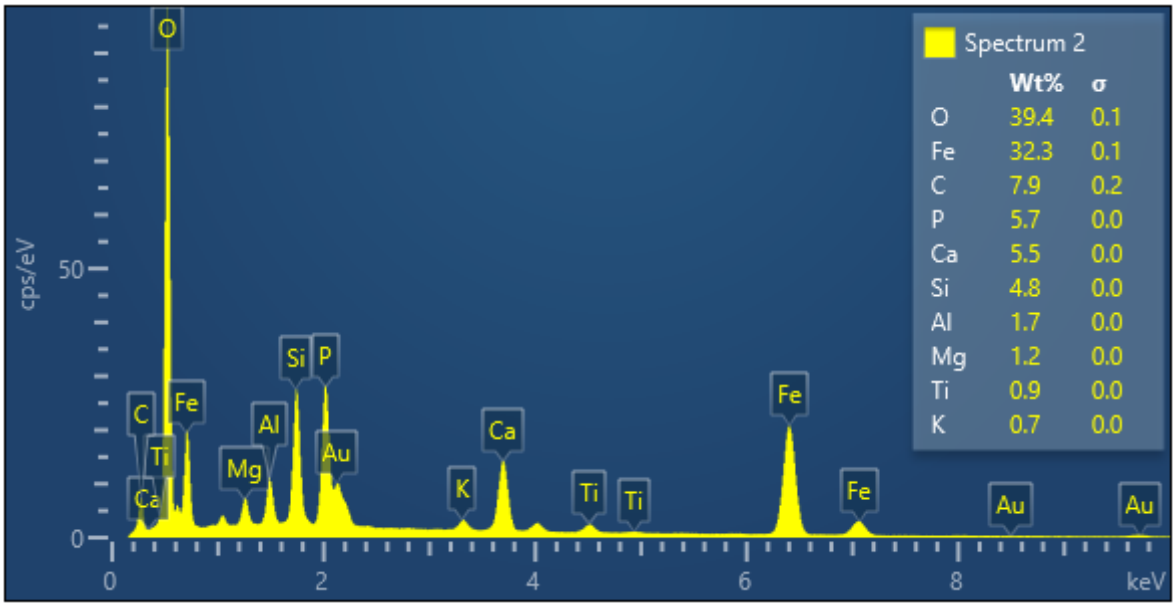

Figure S9-7: The elemental weight percentages for Spectrum 2 of the first SEM image for Test I-1 (Figure S9-5).

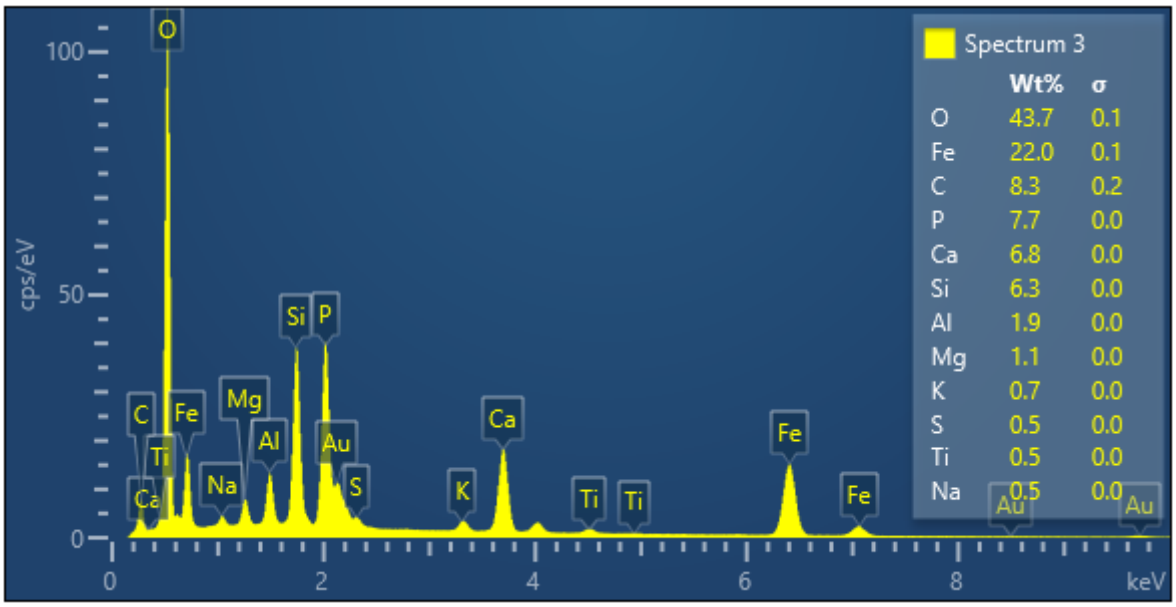

Figure S9-8: The elemental weight percentages for Spectrum 3 of the first SEM image for Test I-1 (Figure S9-5).

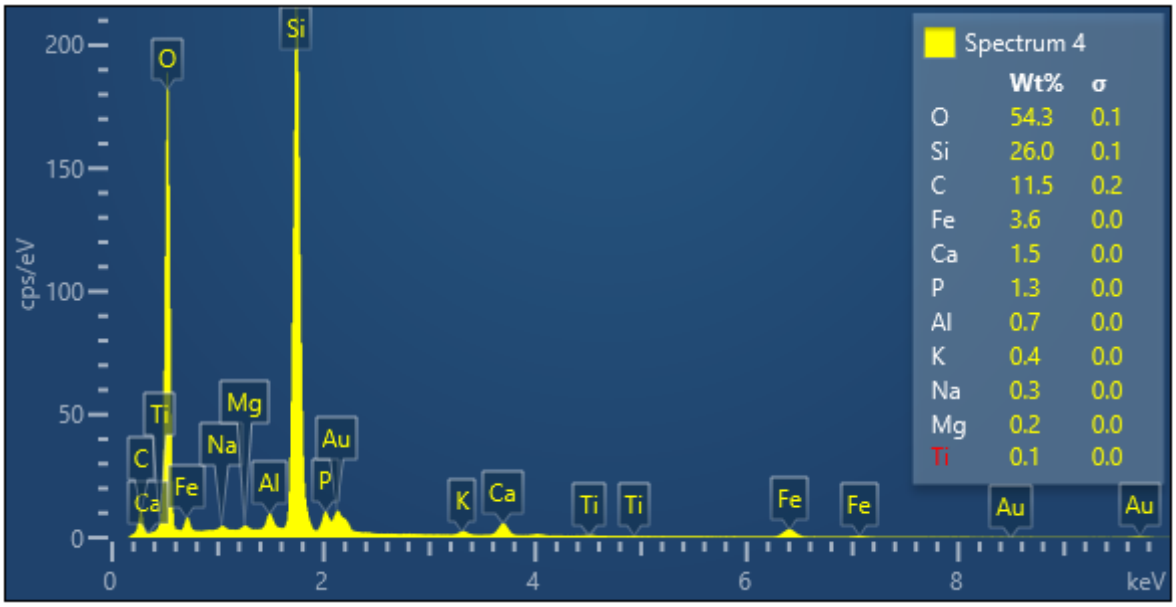

Figure S9-9: The elemental weight percentages for Spectrum 4 of the first SEM image for Test I-1 (Figure S9-5).

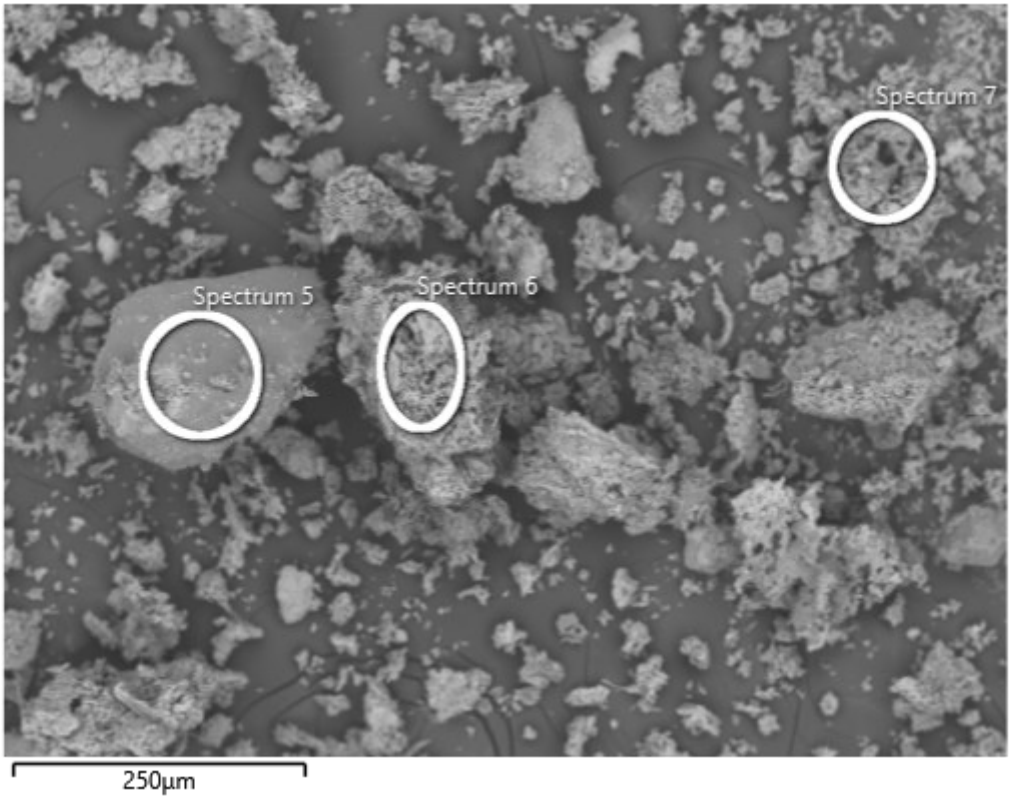

Figure S9-10: The second of two SEM images for Test I-1, taken at the resolution of x150 magnification with a scale of 250 µm.

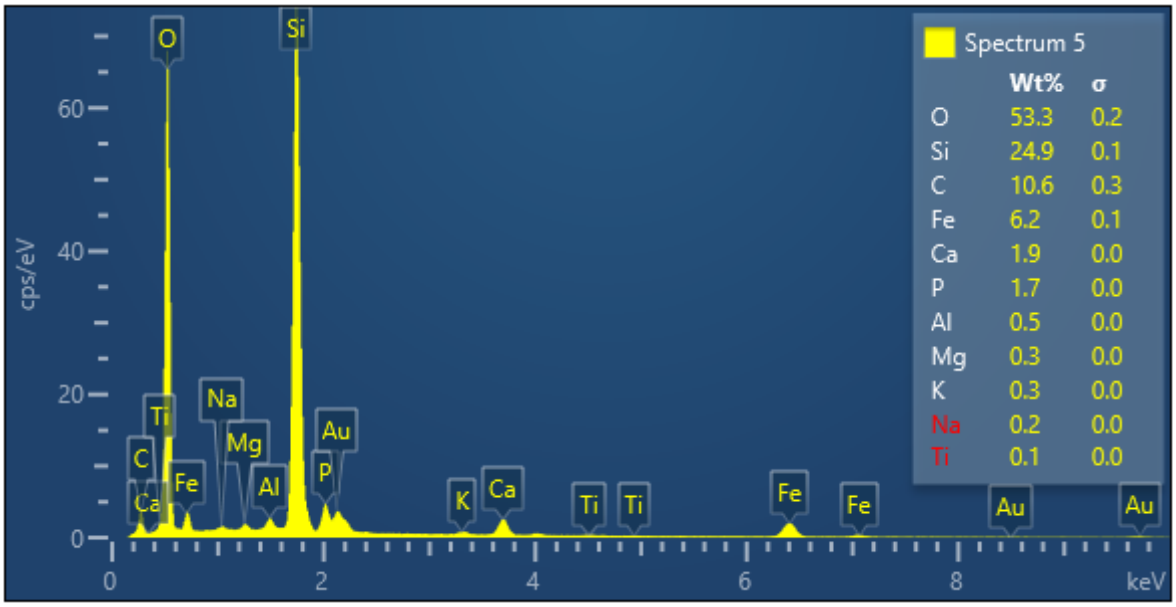

Figure S9-11: The elemental weight percentages for Spectrum 5 of the second SEM image for Test I-1 (Figure S9-10).

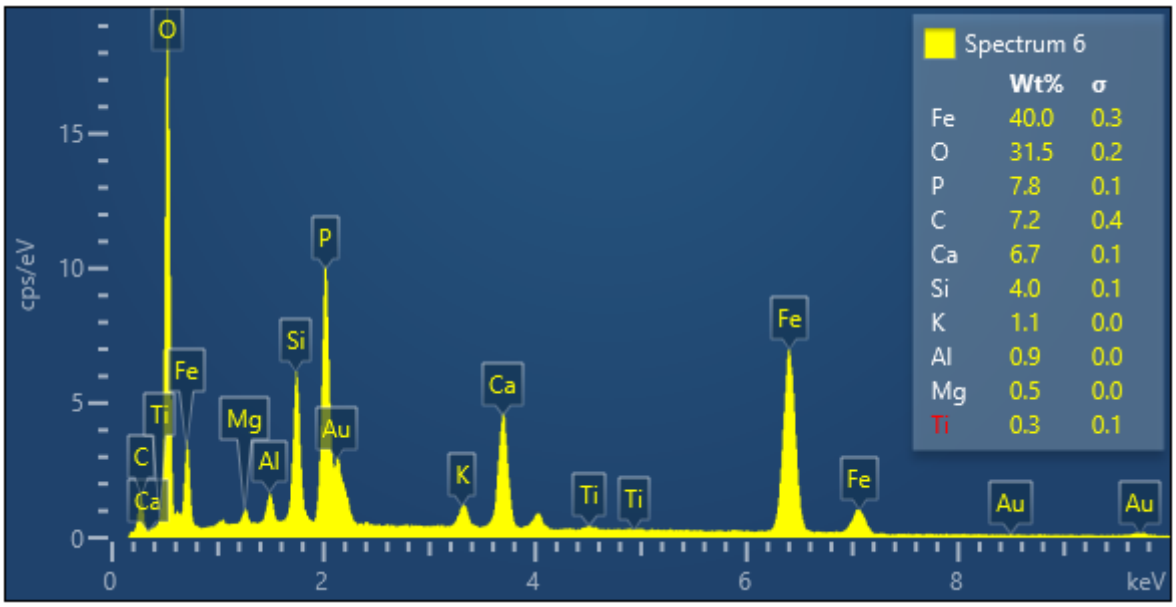

Figure S9-12: The elemental weight percentages for Spectrum 6 of the second SEM image for Test I-1 (Figure S9-10).

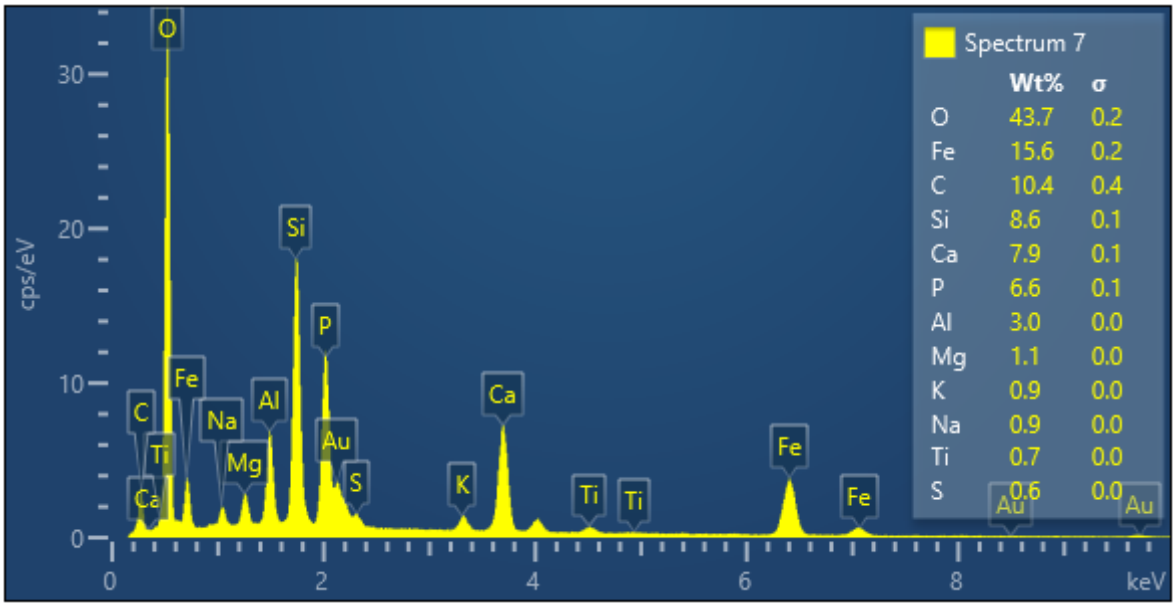

Figure S9-13: The elemental weight percentages for Spectrum 7 of the second SEM image for Test I-1 (Figure S9-10).

SEM Results: II-2-1

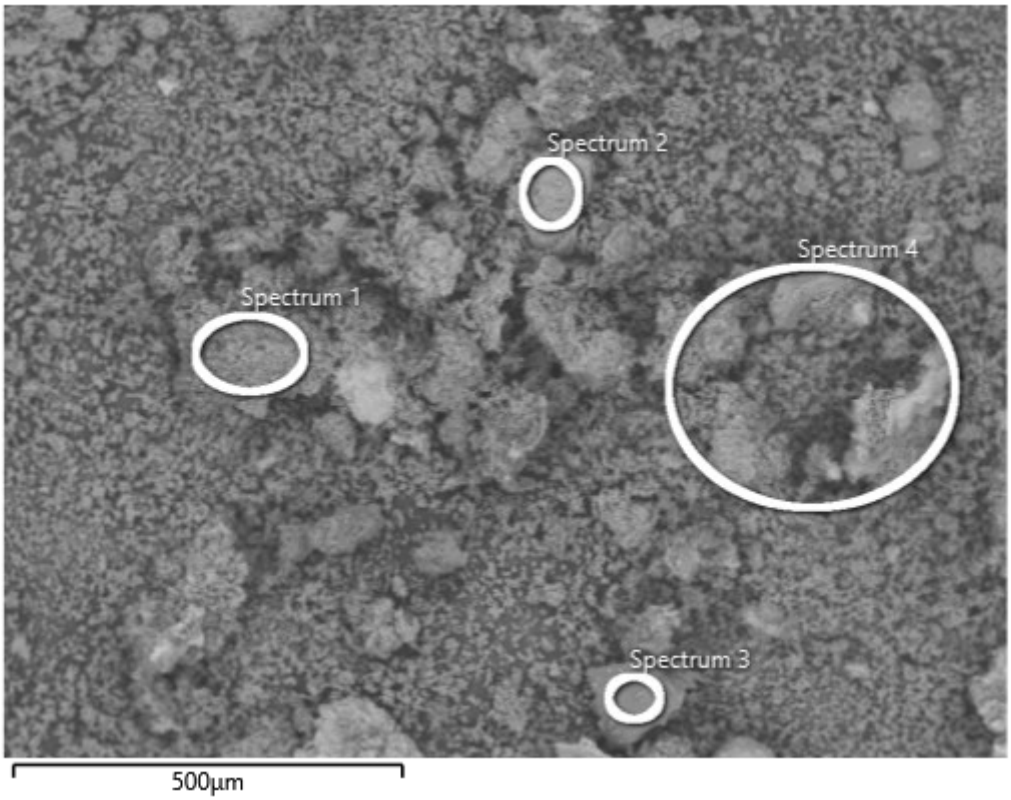

Figure S9-14: The SEM image for Test II-2-1, taken at the resolution of x100 magnification with a scale of 500 µm.

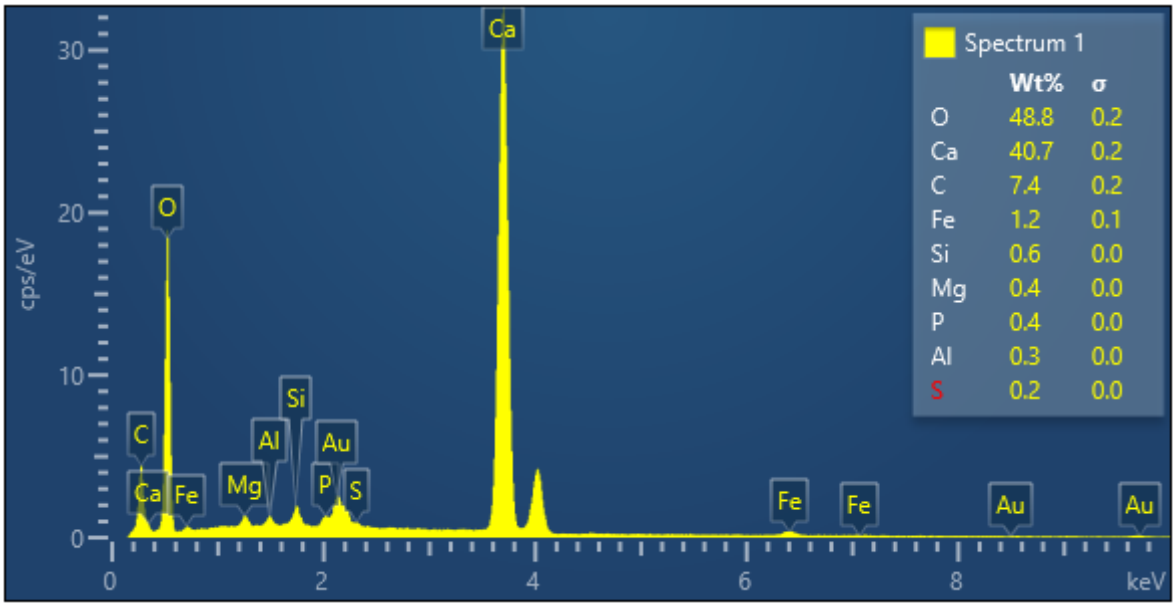

Figure S9-15: The elemental weight percentages for Spectrum 1 of the SEM image for Test II-2-1 (Figure S9-14).

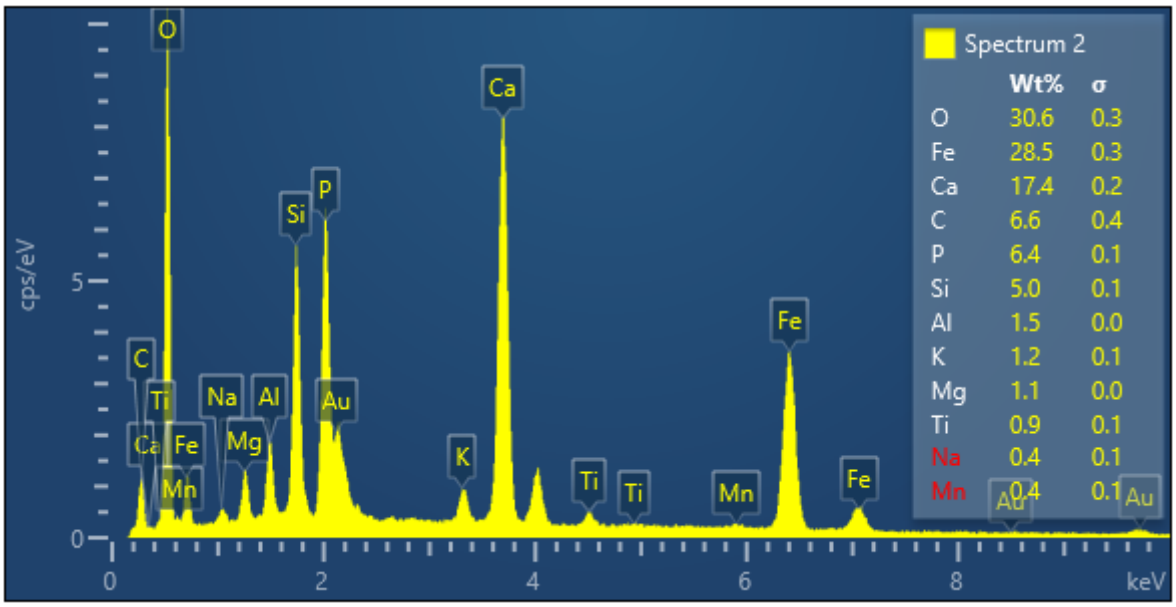

Figure S9-16: The elemental weight percentages for Spectrum 2 of the SEM image for Test II-2-1 (Figure S9-14).

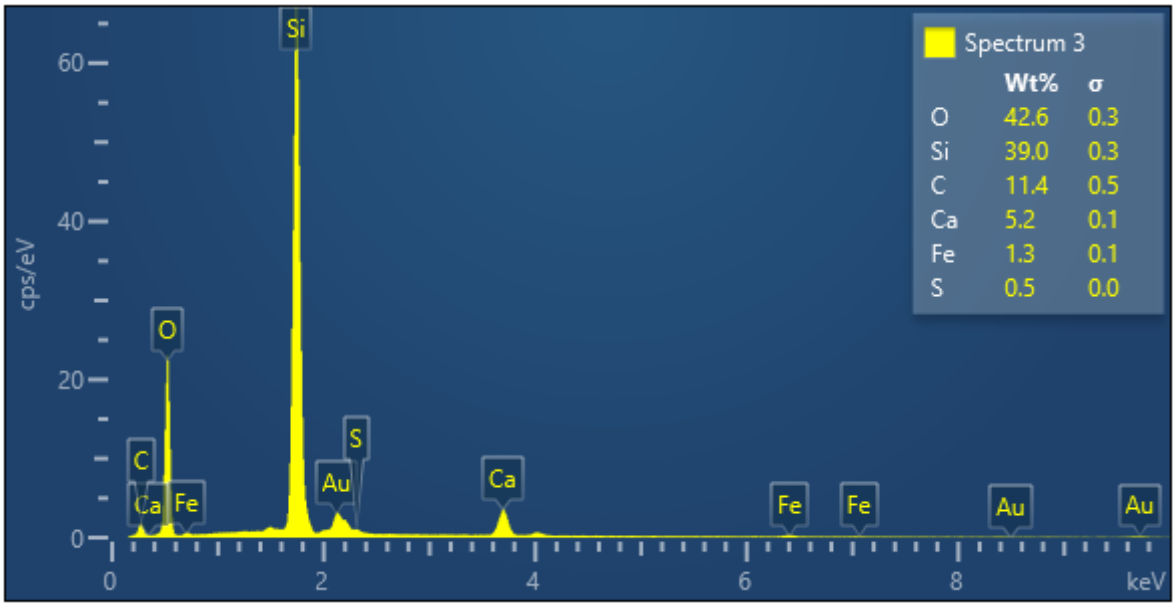

Figure S9-17: The elemental weight percentages for Spectrum 3 of the SEM image for Test II-2-1 (Figure S9-14).

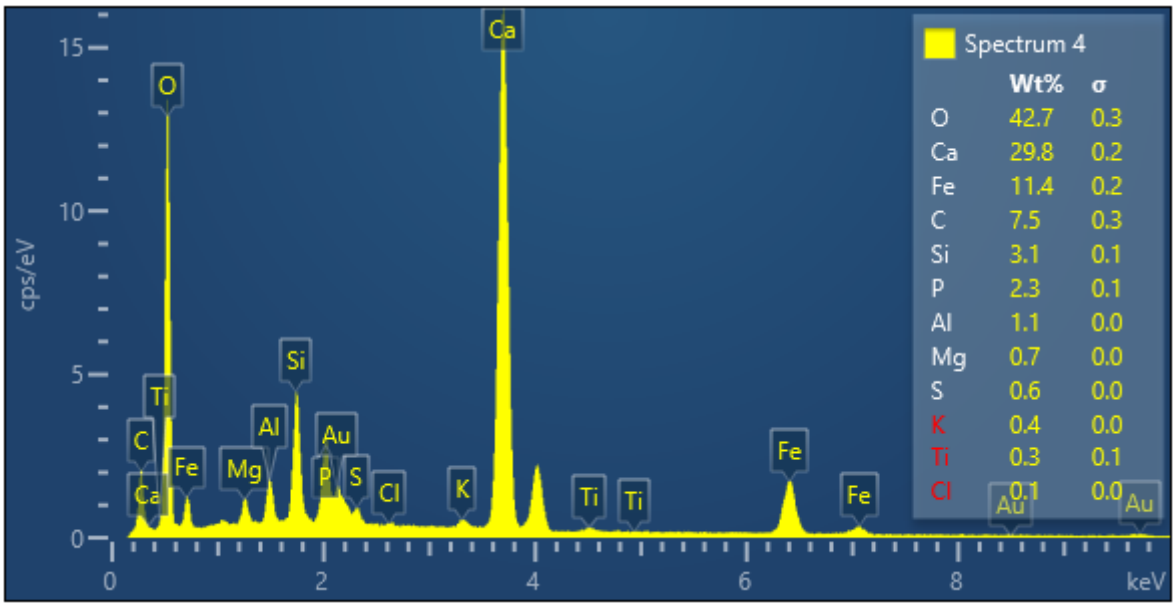

Figure S9-18: The elemental weight percentages for Spectrum 4 of the SEM image for Test II-2-1 (Figure S9-14).

SEM Results: II-2-2

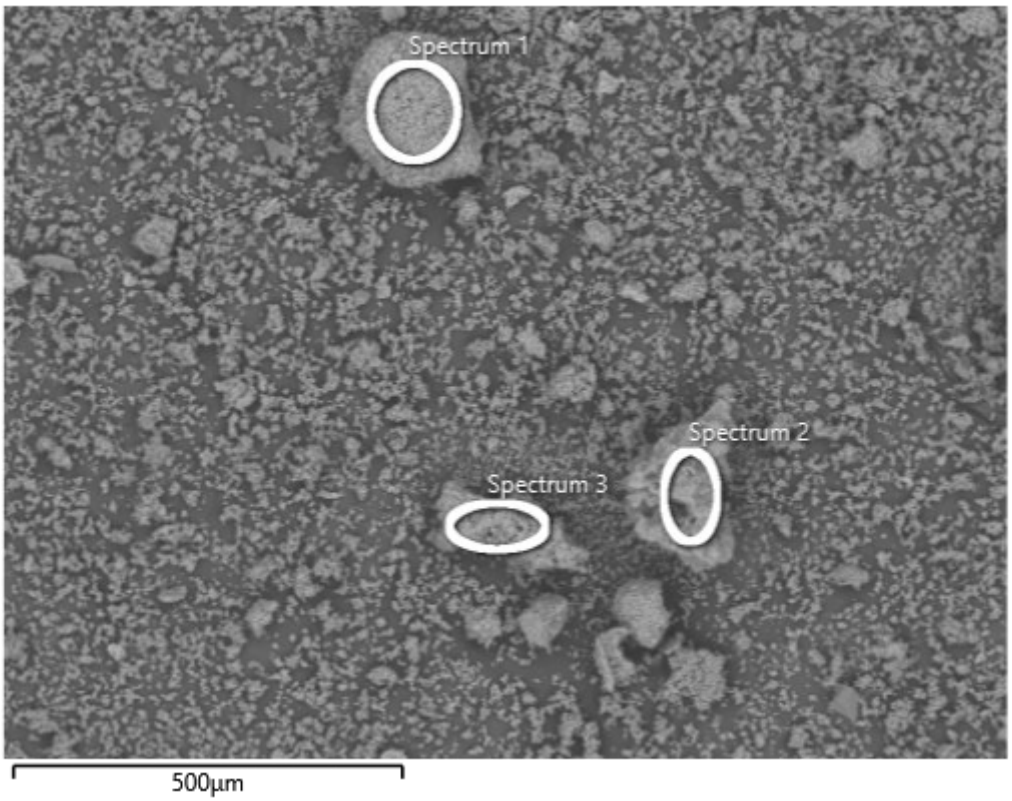

Figure S9-19: The first of two SEM images for Test II-2-2, taken at the resolution of x100 magnification with a scale of 500 µm.

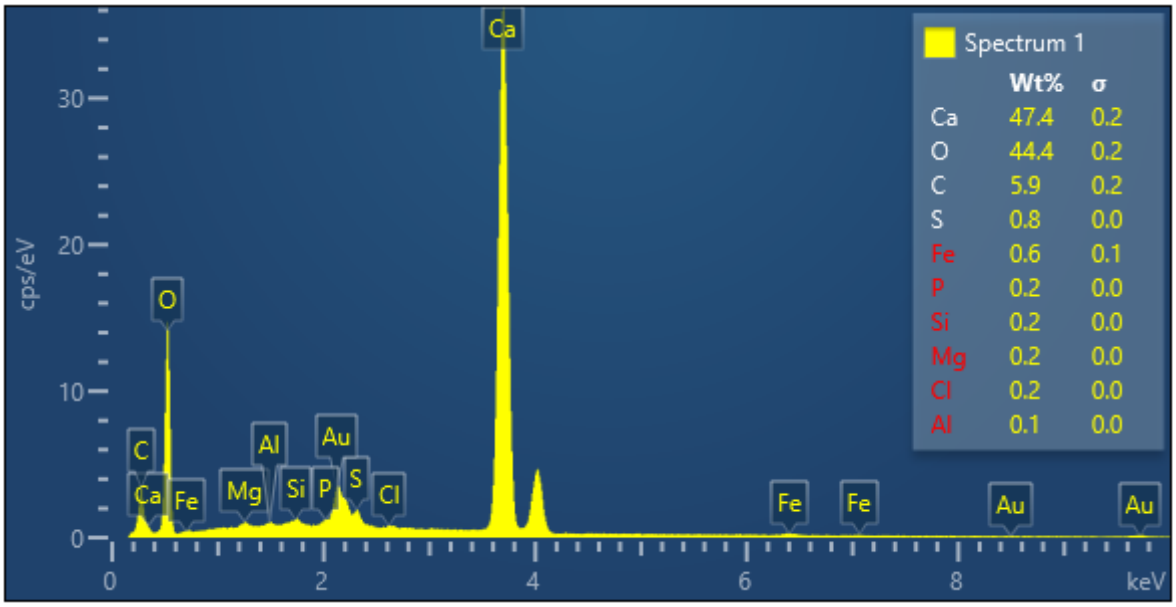

Figure S9-20: The elemental weight percentages for Spectrum 1 of the first SEM image for Test II-2-2 (Figure S9-19).

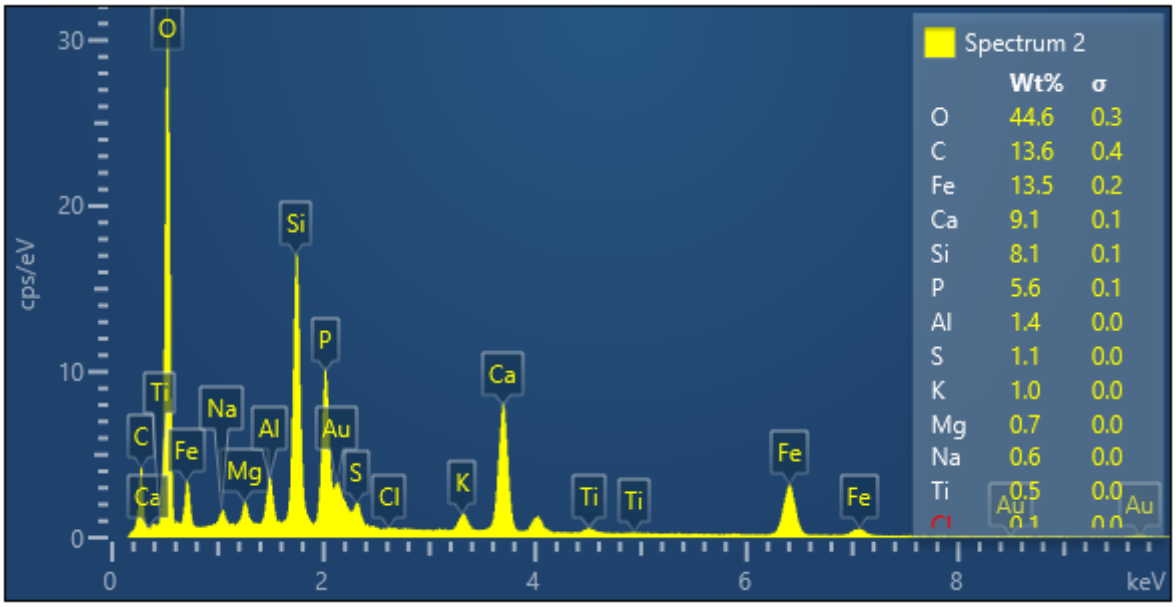

Figure S9-21: The elemental weight percentages for Spectrum 2 of the first SEM image for Test II-2-2 (Figure S9-19).

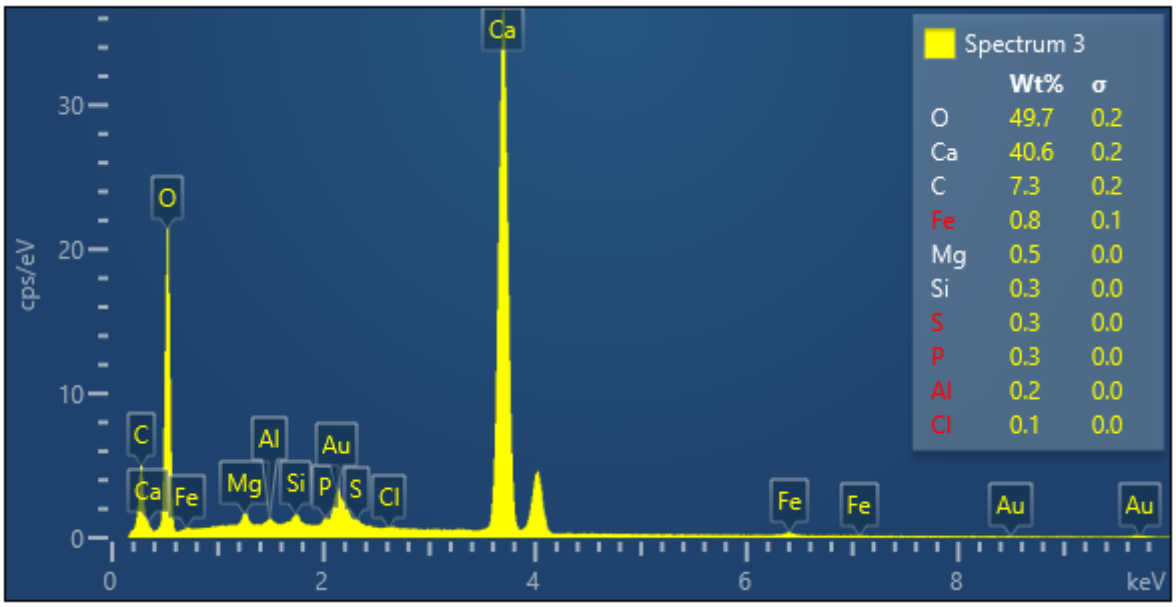

Figure S9-22: The elemental weight percentages for Spectrum 3 of the first SEM image for Test II-2-2 (Figure S9-19).

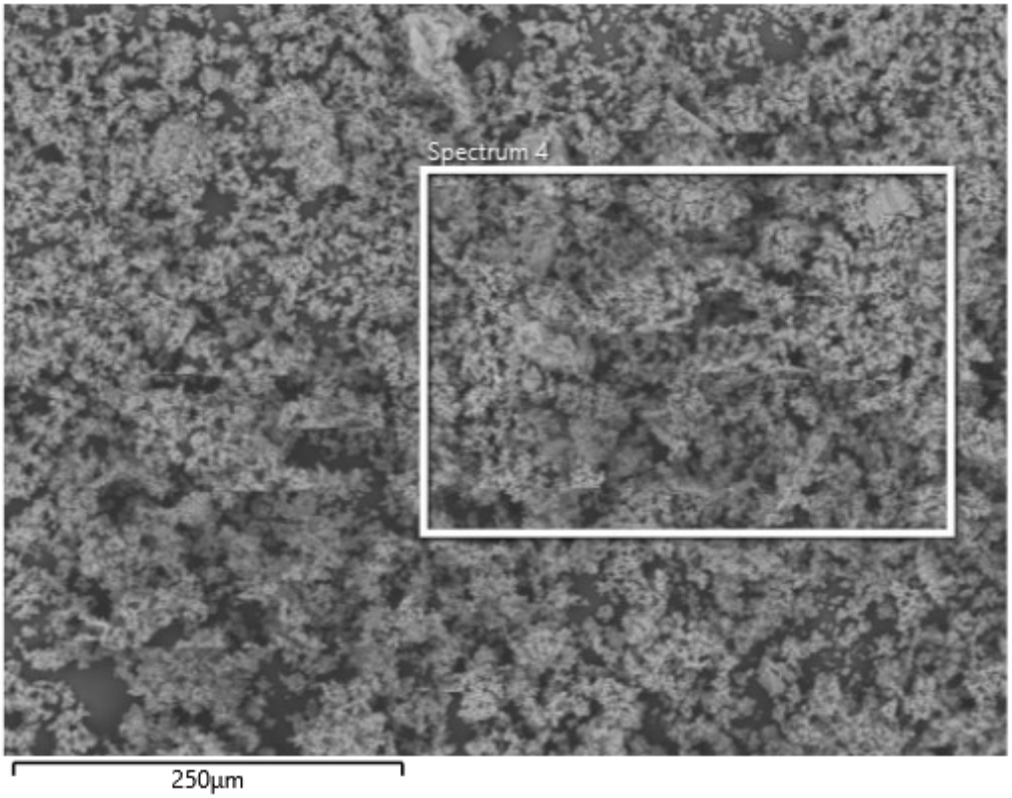

Figure S9-23: The second of two SEM images for Test II-2-2, taken at the resolution of x200 magnification with a scale of 250 µm.

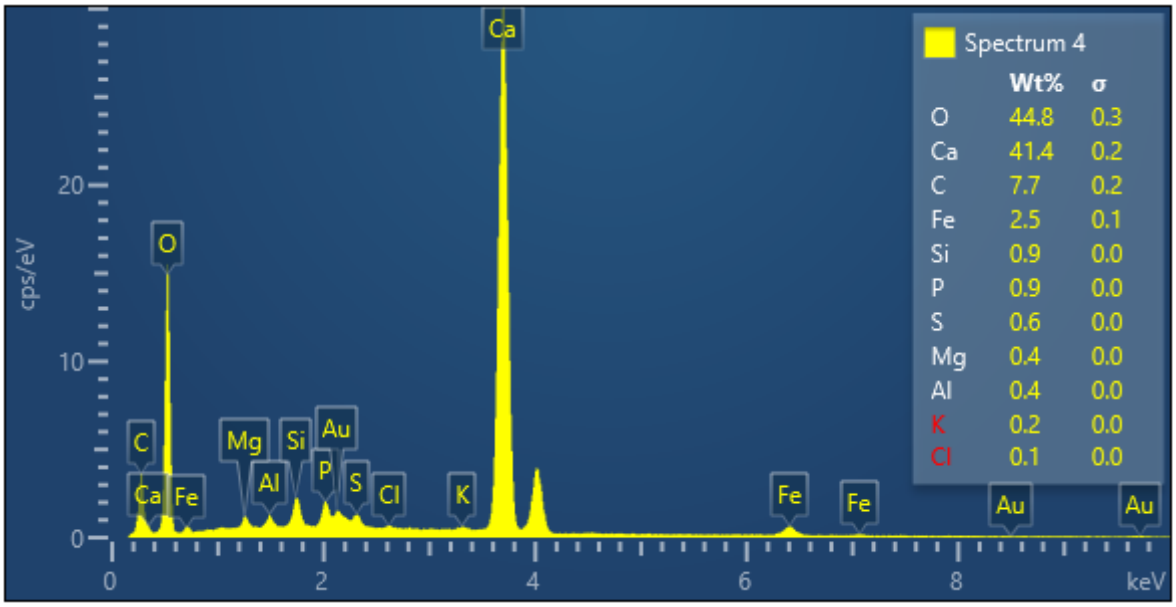

Figure S9-24: The elemental weight percentages for Spectrum 4 of the second SEM image for Test II-2-2 (Figure S9-23).

SEM Results: III-1

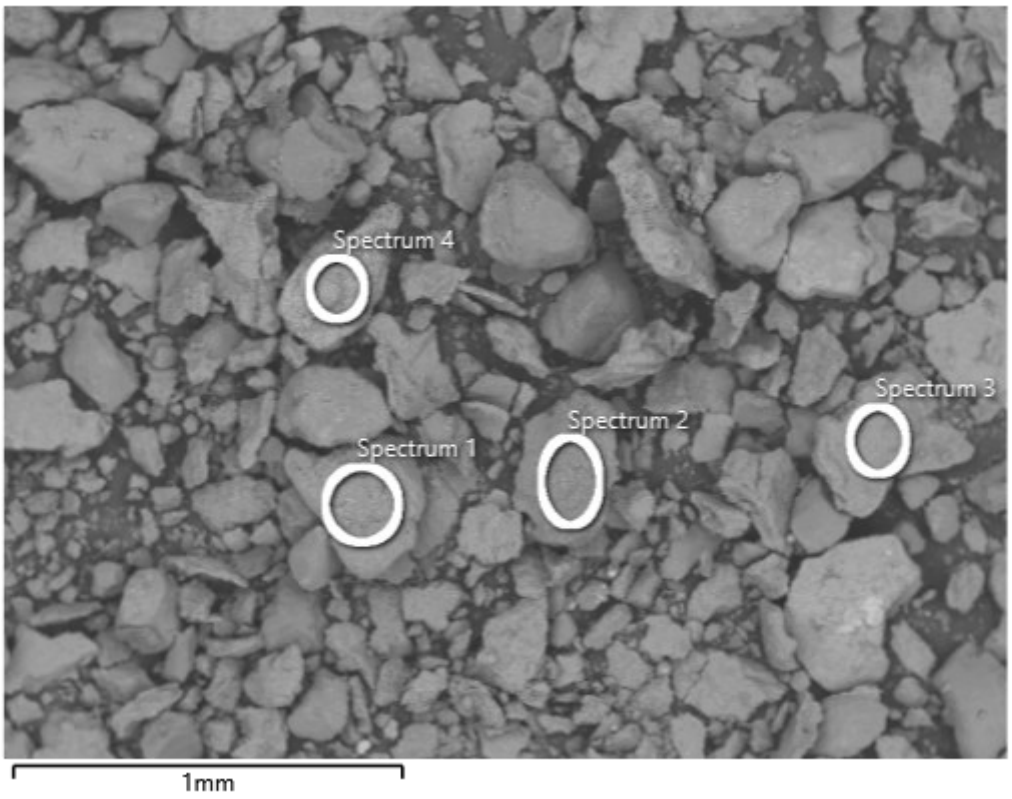

Figure S9-25: The first of two SEM images for Test III-1, taken at the resolution of x50 magnification with a scale of 1 mm.

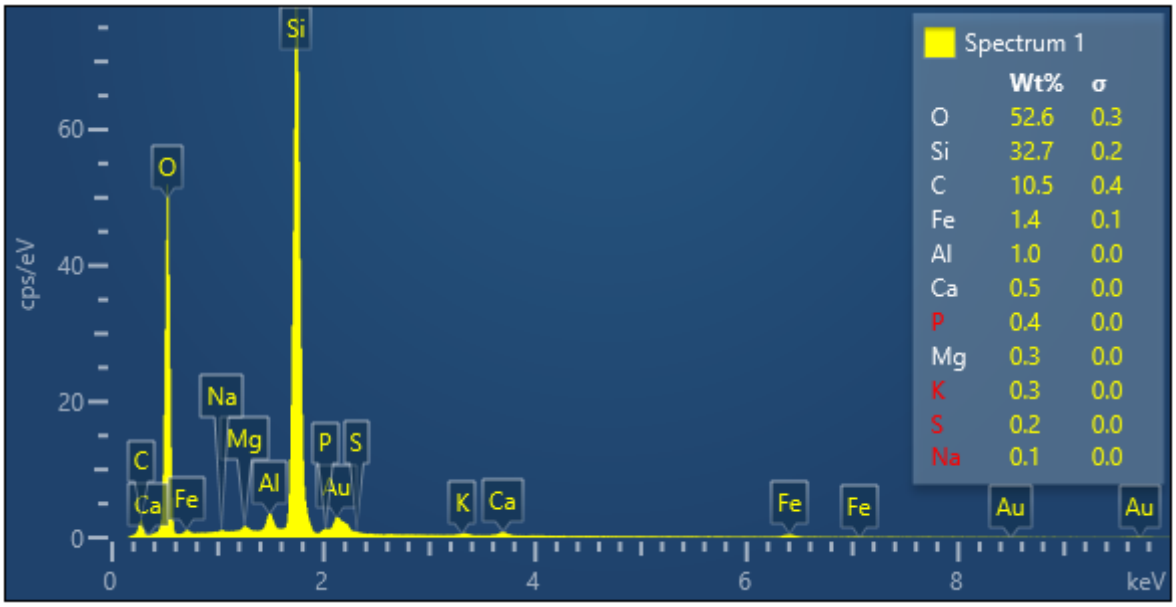

Figure S9-26: The elemental weight percentages for Spectrum 1 of the first SEM image for Test III-1 (Figure S9-25).

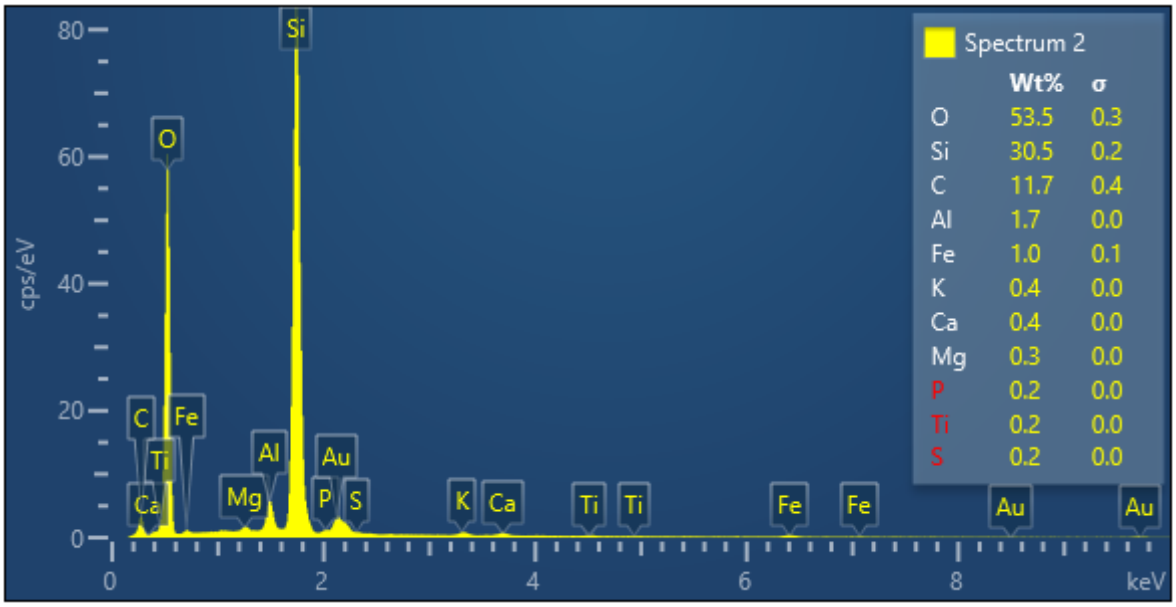

Figure S9-27: The elemental weight percentages for Spectrum 2 of the first SEM image for Test III-1 (Figure S9-25).

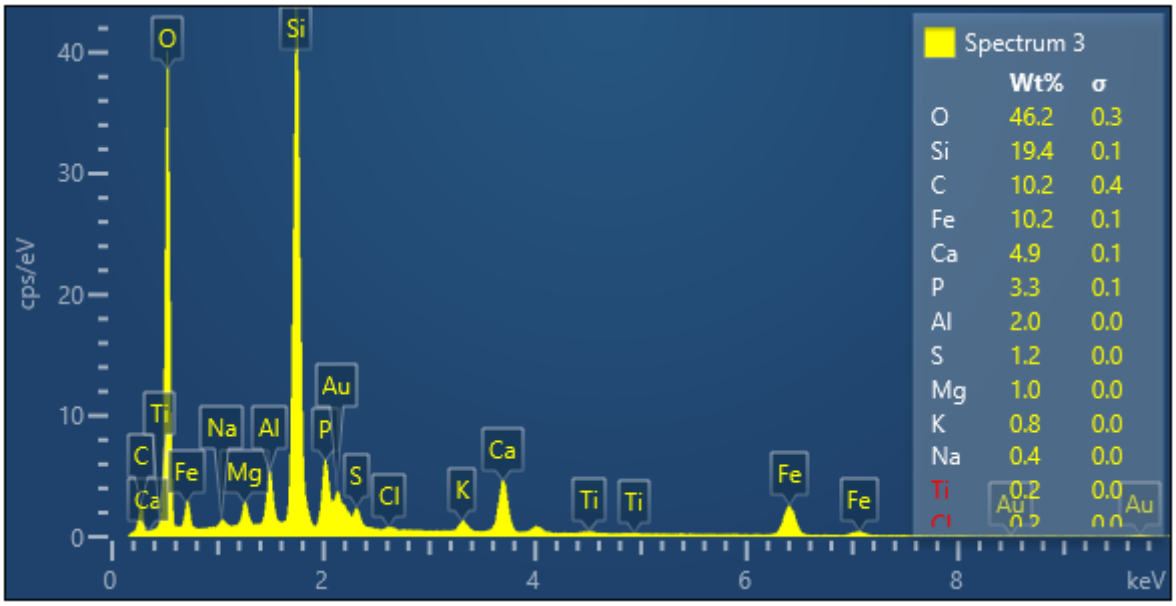

Figure S9-27: The elemental weight percentages for Spectrum 3 of the first SEM image for Test III-1 (Figure S9-25).

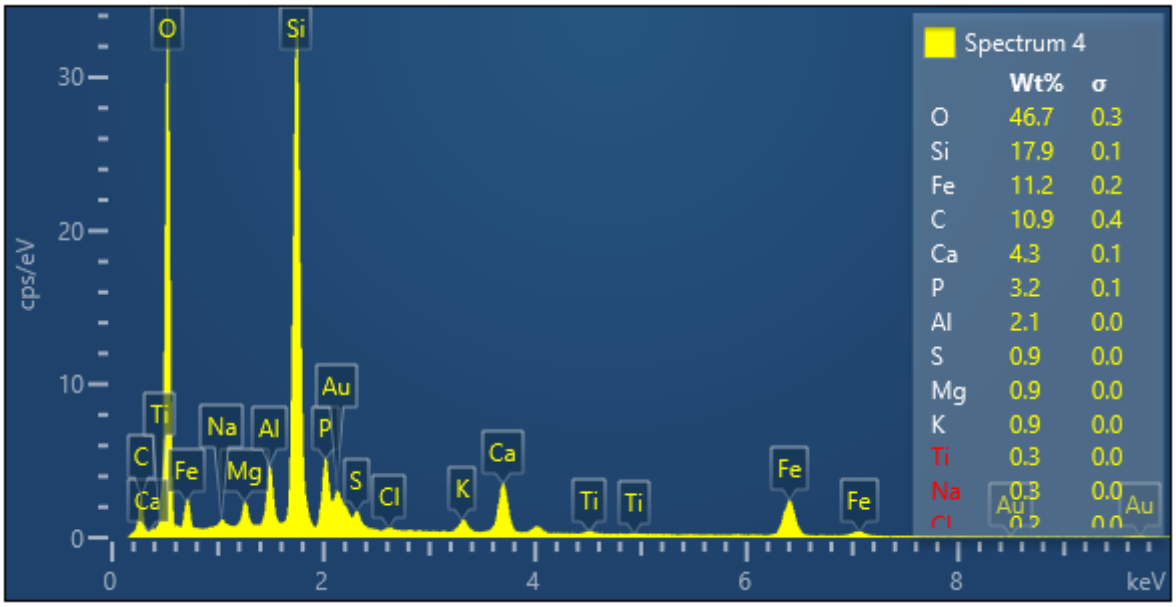

Figure S9-28: The elemental weight percentages for Spectrum 4 of the first SEM image for Test III-1 (Figure S9-25).

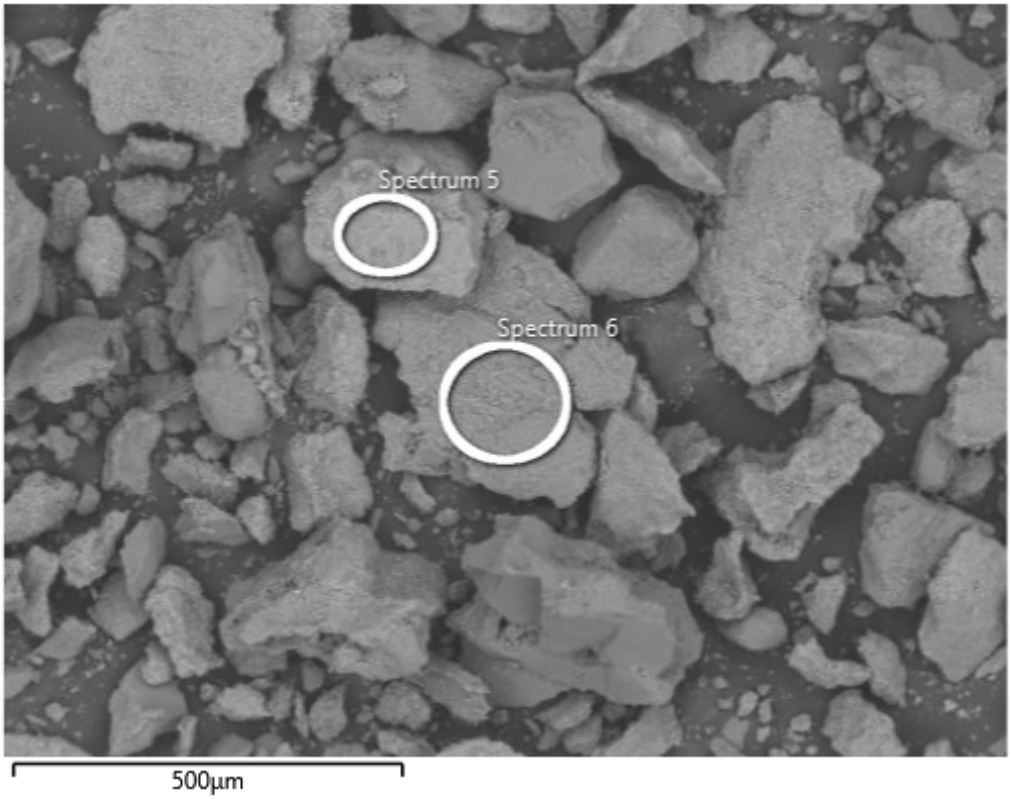

Figure S9-29: The second of two SEM images for Test III-1, taken at the resolution of x100 magnification with a scale of 500 µm.

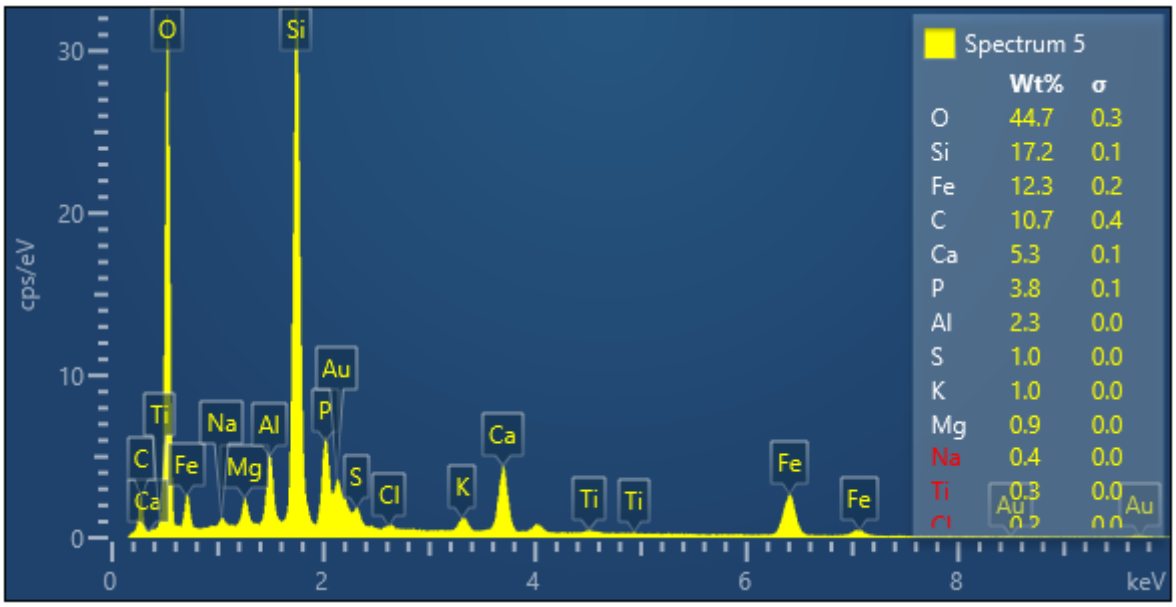

Figure S9-30: The elemental weight percentages for Spectrum 5 of the second SEM image for Test III-1 (Figure S9-29).

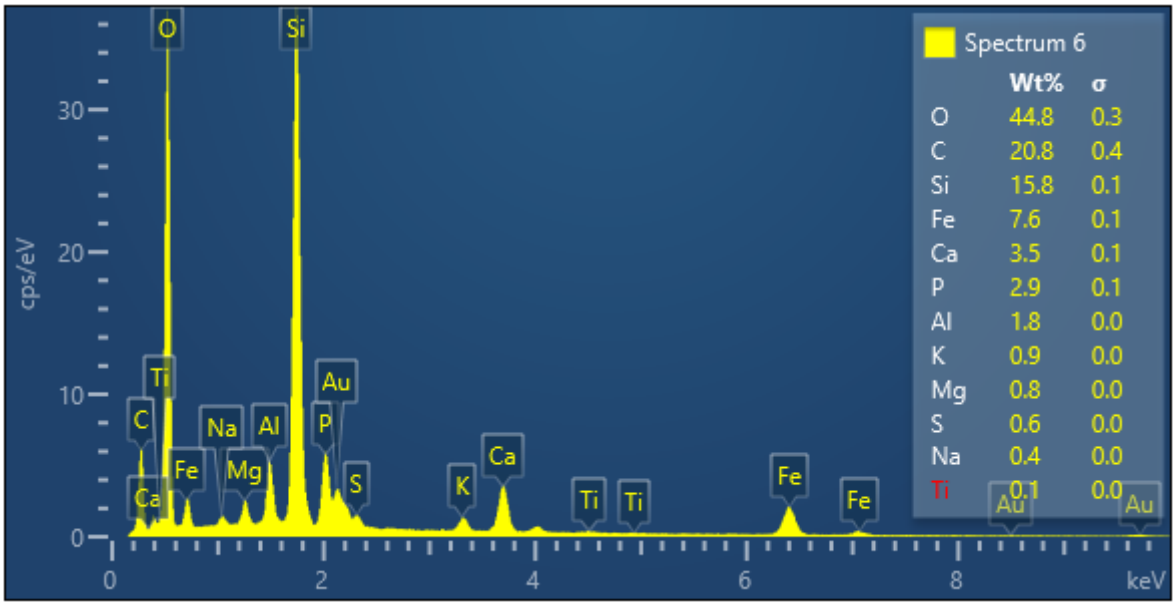

Figure S9-31: The elemental weight percentages for Spectrum 6 of the second SEM image for Test III-1 (Figure S9-29).

S10. References

Fournie, T., Rashwan, T.L., Switzer, C., Gerhard, J.I., 2022. Phosphorus recovery and reuse potential from smouldered sewage sludge ash. Waste Manag. 137, 241–252. https://doi.org/10.1016/J.WASMAN.2021.11.001

Rashwan, T.L., Fournie, T., Torero, J.L., Grant, G.P., Gerhard, J.I., 2021. Scaling up self-sustained smouldering of sewage sludge for waste-to-energy. Waste Manag. 135, 298–308. https://doi.org/10.1016/J.WASMAN.2021.09.004